EFFECTS OF CONTACT LOAD ON FRETTING FATIGUE
BEHAVIOR OF IN-100 AT ELEVATED TEMPERATURE

THESIS

Alfred G. Traylor II, 1st Lieutenant, USAF

AFIT/GMS/ENY/09-M04

DEPARTMENT OF THE AIR FORCE
AIR UNIVERSITY

AIR FORCE INSTITUTE OF TECHNOLOGY

Wright-Patterson Air Force Base, Ohio

AFIT/GMS/ENY/09-M04

Effects of Contact Load on Fretting Fatigue Behavior of IN-100 at Elevated Temperature

Thesis

Presented to the Faculty

Department of Aeronautics and Astronautics

Graduate School of Engineering and Management

Air Force Institute of Technology

Air University

Air Education and Training Command

In Partial Fulfillment of the Requirements for the

Degree of Master of Science (Materials Science & Engineering)

Alfred Traylor II AFIT, BS

1st Lieutenant, USAF

March 2009

Effects of Contact Load on Fretting Fatigue Behavior of IN-100 at Elevated Temperature

Alfred Traylor II AFIT, BS

1st Lieutenant, USAF

Approved: Date:

_____//signed//_____   _____
Dr. Shankar Mall (Chairman)

_____//signed//_____   _____
Dr. Som Soni (Member)

_____//signed//_____   _____
Dr. Vinod K. Jain (Member)

AFIT/GMS/ENY/09-M04

Abstract

This thesis studied the effects of contact load of 8006 N on the fretting fatigue behavior of IN-100 at an elevated temperature of 600˚C . First, S-N curves were created for a range of applied axial stresses at an identical stress ratio of 0.03 at 8006 N. A condition of partial slip condition necessary to fretting fatigue was verified by generating hysteresis loops, plotting shear force against axial stress. The half-contact width and the crack initiation location were determined for all of the fretting specimens using optical and scanning electron microscopes. The contact widths were consistent with expected analytical values and the crack initiation location was at the trailing edge of contact for all fretting specimens at a mean angle of 45˚. This study compared the fretting results at higher contact load (8006 N) to similar results from previous studies of IN-100 at lower contact load (4003 N) with an identical microstructure at an elevated temperature of 600 ˚C as well as to previous room temperature testing. It was found that fretting fatigue at higher contact load drastically reduces the cycles to failure compared to fretting fatigue at elevated temperature with a lesser contact load. While the higher temperature environment allowed a longer initiation and crack propagation time, this was quickly negated by the increase in the contact load. The development of glaze oxide films and temperature induced softening or plasticity were both found to act as crack closure mechanisms in another nickel-based superalloy, IN-718, when fatigued in the high temperature environment. This glaze oxide reduces the coefficient of friction between contact surfaces, an important factor in fretting fatigue, and is also observed to be present in high temperature studies of IN-100. It was also found that a difference exists between the fretting fatigue lives of specimens that were annealed when compared to those specimens that were not annealed. These findings were slightly different than other studies at increased contact load which used various alloys of aluminum and steels.

Acknowledgements

       I would like to thank my thesis advisor, Dr. Mall, for his patient and supportive assistance in every step of this thesis project. His wealth of knowledge served as an inspiration and motivation. I would not have been able to complete my research without the support of Barry Page and the rest of the ENY lab staff who helped me tremendously in the laboratory, from equipment familiarization to correcting my mistakes. I would also like to thank my parents for their constant support and encouragement of my education from an early age, throughout the U.S. Naval Academy, and now at AFIT. Most of all, I would like to thank my wife for her continued and unconditional support and patience during my pursuit of two Master's degrees. I know that it was not always convenient, but your support means the world to me. Finally, I would like to thank the U.S. Air Force for extending me the opportunity to further my education at AFIT.

       Alfred Traylor II, 1Lt, USAF

Table of Contents

List of Figures

List of Tables

List of Symbols

a	Half contact width
b	Specimen half thickness
c	Stick zone boundary
d	Tensile bar thickness
E	Modulus of elasticity
f	Coefficient of friction
K_1	First Ruiz parameter
K_2	Second Ruiz parameter
N	Number of cycles
N_f	Number of cycles to failure
P	Normal load
p_o	Maximum pressure in the contact zone
Q	Shear load
Q_{max}	Maximum shear load
Q_{min}	Minimum shear load
r	Radius of curvature
R	Stress ratio
σ	Stress
δ	Slip at interface
σ_{axial}	Axial stress applied to tensile bar
σ_{max}	Maximum applied axial stress
σ_{min}	Minimum applied axial stress

σ_{xx}	Axial stress in the contact zone
σ_{yy}	Transverse stress in the contact zone
$\Delta\sigma$	Stress range
τ	Surface shear stress
τ_{max}	Maximum shear
τ_{min}	Minimum shear
τ_{xy}	Shear stress in contact zone
$\Delta\tau$	Shear stress range
$\Delta\tau_{crit}$	Shear range in the critical range
υ	Possion's ratio

EFFECTS OF CONTACT LOAD ON FRETTING FATIGUE

BEHAVIOR OF IN-100 AT ELEVATED TEMPERATURE

I. Introduction

1.1 Fretting Fatigue

Fretting is the term that describes the physical phenomenon that occurs when two surfaces are in contact with one another, subject to some oscillating force and, though not rigidly attached, rub against one another to the point that material is damaged. Despite the fact that these surfaces are not rigidly attached they are also not free to move very large distances as they are forced to remain in close contact. It is under this condition that an extremely small amount of movement between these two surfaces is observed. This motion is referred to as microslip and is of an extremely small amplitude, usually between 5 and 50 microns, [1]. While the two surfaces are in fact slipping against each other, the displacements are microscopic as they are bound from slipping further by the surrounding environment. Microslip, and therefore fretting damage, occurs only where the materials are in direct contact and causes stress concentrations to develop in the material.

As stated above, fretting initiates when this microslip conditions begin to damage the outermost region of the two surfaces at the contact location. This damage then creates stress concentrations on the affected surface near the edge of the fretting zone. These fretting-induced stress concentrations then aid in crack initiation originating somewhere near the edge of the fretting region which will then propagate through the thickness of the material in four distinct stages. The first stage is that of crack initiation, which occurs relatively soon after the fretting condition is established. This stage is also

called nucleation. In the second stage, the bulk and contact stresses on the material combine to propagate the initiated crack. The bulk stress dominates the third stage as the crack continues to propagate further. The fourth and final stage occurs when either the crack propagates all the way to the edge of the affected part or when the critical stress intensity factor, K_{Ic}, is reached and fracture of the material occurs. As stresses develop within the material and they reach a level high enough to permit cracks that have initiated to grow and propagate throughout the thickness of the materials, fretting fatigue is observed and the cracks will allow for a quicker fracture of the component. The aforementioned microslip and stress conditions in material components are commonly found in mechanical joints where materials are kept in constant contact and are subject to a cyclic loading. This can occur in places such as bolt and rivet connections or in geometrically locking joints, such as are common in turbine engine dovetail joints.

A very relevant example where fretting fatigue effects are easily observed is the dovetail joints in modern turbine engines. It is here where surface to surface contact between similar materials is found, where the numerous turbine blades are held in place in the collar of the turbine through a geometrically locking joint only (Figure 1.1 and Figure 1.2). Though the blades are held in place and constrained to their intended location through the geometry of the joint, they are not firmly bound and extremely small relative displacements occur. As technology increases and more capable aircraft are developed, higher performance engines will be needed that are able to meet the demands of engineers as well as endure higher stresses and harsher conditions. In order to optimize performance and minimize engine and aircraft downtime due to repair or malfunction, it is in the best interests of engineers to develop components in a way that will reduce untimely wear. This includes wear due to fretting fatigue in mechanical components such

as turbine blades. In order to accomplish this objective, the fundamentals of fretting fatigue need to be better understood so that any undue wear from fretting in mechanical systems, particularly high performance turbines, can be avoided. It is the goal of this study to provide insight into and further the knowledge of the phenomenon of fretting fatigue for use in improving the design of turbine engines and mechanical components.

1.2 Relevance and Applications of Nickel Alloys

Though fretting fatigue is seen in many locations in mechanical systems such as aircraft, the most common, as mentioned above, is in the turbine section of the engine. It is here that the individual turbine blades are in contact with the disk that contains them within the turbine (Figure 1.2). As a turbine engine is a type of combustion engine, the temperatures that any given engine component experiences will vary greatly and can often reach extremely high values. In order to perform effectively at these extreme temperature ranges and maxima, new materials and alloys have been developed, to include many alloys of nickel.

Nickel is the 24th element in relative abundance and has an average content of 0.016% in the outer 10 miles of the Earth's crust. It has an atomic number of 28 and is one of the transition elements located in the fourth series of the periodic table [2]. Although the majority of mined nickel is used as an alloying agent in products of ferrous metals, nickel can also be used as the majority element in alloys which have a very wide range of outstanding properties. The face centered cubic lattice of nickel gives adequate ductility near cryogenic temperatures as well as good strength up to 70% of melting point. This makes nickel a great base for creep-resistance metals. Pure nickel has very high corrosion resistance to non-oxidizing media and this property can be enhanced

3

through the addition of copper, chromium, and molybdenum. Nickel alloys are also known for very low thermal expansion coefficients and almost constant elastic moduli over limited ranges of temperatures [3]. This study will use the nickel alloy called IN-100. Inconels are alloys of nickel which contain high concentrations of cobalt, chromium, and molybdenum. They are very well suited for high temperature applications and have exceptional resistance to stress corrosion.

Previous work on fretting fatigue has focused on a variety of materials vital to the aerospace industry such as titanium alloys, steel alloys and aluminum alloys [4-10]. Although research has been done on the fretting fatigue behavior of nickel based alloys in the past, there are only a few studies which incorporate elevated temperature. It is extremely important to ensure that experimental conditions represent, as closely as possible, the applications in which the material will be used. Ownby [11] has previously studied the effect of fretting fatigue on IN-100 at an elevated temperature of 600 ˚C. It is the goal of this study to build on this and other previous research studies with IN-100 [12, 13] by studying the effect of increased contact load on the fretting fatigue behavior on IN-100 at 600 ˚C.

1.3 Factors Affecting Fretting

There are numerous factors which can contribute to the phenomenon of fretting fatigue; many are known and there may be more that are not yet known. Of the known contributing factors, the most important are contact conditions such as contact loads and shapes, surface treatments, and the applied cyclic stress conditions [14-17]. Each of these factors are thought to have various influences on how fretting fatigue causes premature crack initiation, crack propagation, and fracture of the component. The previously

referenced studies on fretting fatigue that have used IN-100 or other nickel-based alloys have investigated the effects of contact geometry and microstructure and did not include an investigation into elevated temperature [12, 13, 18-24]. For this reason, these studies, though very important in furthering the knowledge of fretting fatigue, do not fully represent the use of these nickel-based alloys in their actual environments. It has been shown in previous studies that elevated temperatures have an effect on how materials fatigue when compared to the same materials at lower temperatures [25, 26]. Ownby showed that temperature is a contributing factor in fretting fatigue by comparing fretting fatigue behavior of IN-100 at 600 °C to that of the behavior at room temperature as well as to previous studies of fretting fatigue behavior in IN-100. It is also the goal of this study to continue to examine the effect of elevated temperature on the fretting fatigue behavior of IN-100 but specific emphasis will be placed on the effect of contact load on the fretting fatigue behavior. The experimental conditions (contact geometry, loading conditions) of this study will be similar to the previous studies at AFIT by Ownby [11], Mahdi [12], and Saladin [13]. As such, the data provided by these studies will serve as control points for comparison in order to isolate the effect of contact load on the fretting fatigue behavior in IN-100 at elevated temperature.

1.4 Purpose and Objectives

It is the ultimate purpose of this study to determine the extent to which increase in contact load has on the fretting fatigue behavior of the nickel-based alloy IN-100. To a lesser extent, this study will also investigate whether a difference exists in the fretting behavior in the virgin (i.e. as processed) material when compared to the annealed material used in previous AFIT studies. In order to accomplish this, several experiments

5

will be conducted in order to generate a set of applied stress versus number of cycles to failure (S-N) curves. These curves will present a relationship between the fretting fatigue behavior at an increased contact load and previously observed fretting fatigue behavior under similar conditions. Each specimen will be analyzed by optical and scanning electron microscopy to determine crack initiation points, fretting contact area and the micro-slip regions and crack propagation regions and mechanisms. These observations will then be compared to previous fretting experiments [11-13] conducted at both room temperature and at elevated temperature to determine the likely causes for differences in fretting fatigue behavior.

1.5 Methodology

The successful recreation of an accurate and functioning model of a turbine environment, specifically the dovetail joint which is critical in fretting fatigue, to include operational loading conditions and temperatures in a laboratory would be extremely difficult and expensive to operate. Fortunately, a much simpler experimental setup can successfully model the fretting phenomenon and an unnecessarily complicated turbine model is not needed and will be discussed in detail in Chapter III. Using a cylinder-on-flat contact method, in which two fretting pads of IN-100 with cylindrically shaped contact regions are placed in contact with the flat dogbone specimen under a known cyclic axial load, and a known contact area derived from Hertizian geometric conditions, fretting conditions can be successfully simulated. The axial loading in the experimental setup provides the frictional motion that will produce the fretting effects. The specimen and the fretting pads are heated in place by four ceramic electric heating elements which surround the contact region. The temperature is closely controlled by thermocouples

through the software provided by the manufacturer of the MTS material test system and will be discussed and detailed later. Experimental data is collected throughout each experiment, until the fracture of the specimen, through the previously mentioned software. The collected data is then gathered, processed, analyzed and presented in Chapter IV.
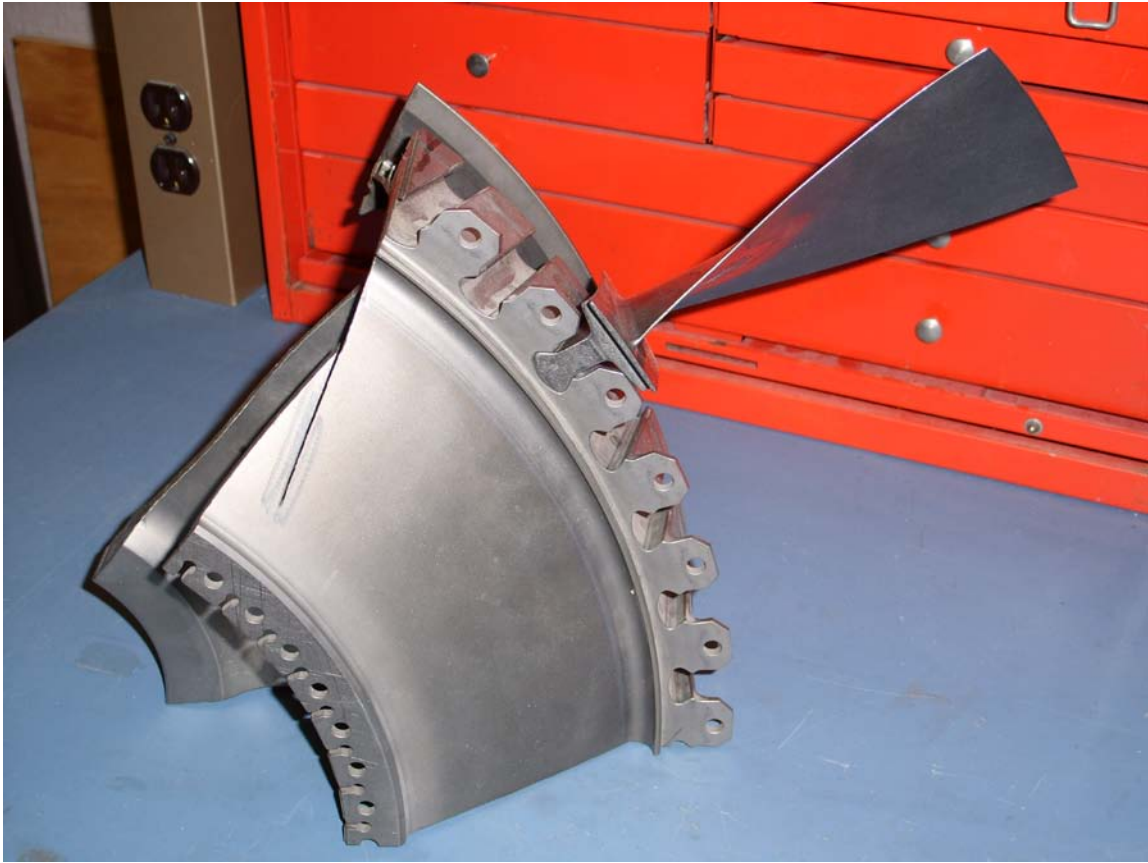
Figure 1.1 – Photograph of a turbine disk and blade

Figure 1.2 – Photograph of a turbine dovetail joint [13]
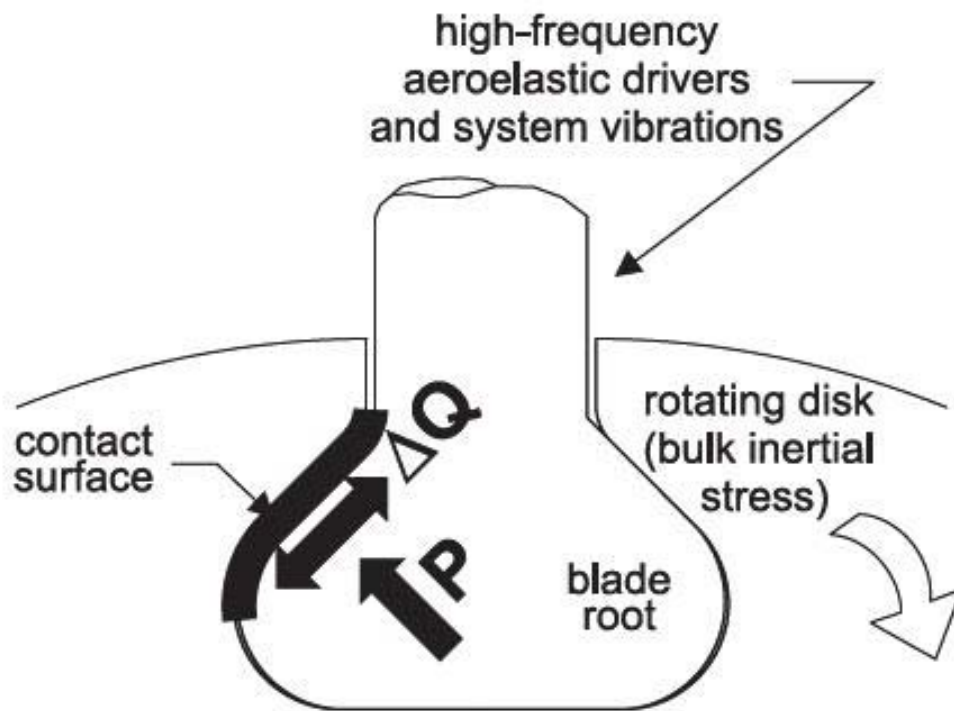
Figure 1.3 – Typical fretting fatigue contact configuration [10]

II. Background

This chapter will provide a basis for the remainder of this work by reviewing the fundamental concepts of fretting fatigue as developed through research on metals and alloys other than nickel and nickel-based alloys. As not much research has been conducted on fretting fatigue of nickel-based alloys, a look into the effects of fretting on other alloys will provide great insight into the behavior of IN-100. This chapter will begin with a discussion of the contact mechanics that govern the chosen fretting fatigue model for this and previous experiments. This will be followed by a discussion of crack nucleation, a poorly understood concept, and gross and partial slip. Then several leading parameters that have been developed to predict fretting fatigue life will be presented and discussed. Finally, a brief review of fretting studies completed with both titanium and nickel based alloys under various conditions will be presented for completeness.

2.1 Contact Mechanics of Fretting

As mentioned in the previous chapter, this study utilizes a cylindrical-on-flat contact geometry. This section will discuss the test sample, fretting pads, and general configuration of the experimental setup. Each test sample is a 19 cm long, with the gauge section being of length 11.4 cm (Figure 2.1). The thickness of each specimen is 3.8 mm. The surface on each specimen was finely ground to produce a smooth finish without any visible surface defects. The fretting pads are of the same material and have a 9.5 mm square cross-section with a radius of 50.8 mm (Figure 2.2). The contact surface of each fretting pad has a ground finish and this surface is refinished after each use before any further use. The specimen is loaded into a uni-axial servo-hydraulic machine and is loaded in order to produce a known stress, σ_{axial}, in the specimen. This machine also

provides the contact load, P, of the fretting pads on the specimen. The applied cyclic load provides for stretching and relaxing of the specimen and the normal contact load arrests a portion of the stretching. This difference is called the shear load, Q. This configuration can be seen in Figure 2.3. Here, σ_{axial} is the applied stress, P is the applied contact load, Q is the shear load, A is the specimen cross-sectional area, a is the contact half-width, b is the specimen half-thickness, and r is the radius of curvature of the fretting pad. Hills and Nowell [27] and Fellows et al. [28] have studied the cylinder-on-flat contact configuration in great detail and have provided a detailed analytical solution to this scenario. The analytical solution for this type of fretting condition comes from solving the displacements of the two contacting bodies. The following equation governs the contact region:

$$\frac{1}{A*}\frac{\delta h(x)}{\delta x} = \frac{1}{\pi}\int\frac{p(\varsigma)}{x-\varsigma}d\varsigma - \beta q(x) \tag{2.1}$$

where $h(x) = v_1(x) - v_2(x)$ represents the displacements in the y direction if the two surfaces could penetrate each other freely, p is the pressure in the contact zone and q is the surface shear stress. The two other parameters in the previous equation are defined as:

$$A* = 2\left(\frac{1-\upsilon_1^2}{E_1} + \frac{1-\upsilon_2^2}{E_2}\right) \tag{2.2}$$

$$\beta = \frac{1}{2A*}\left(\frac{1-2\upsilon_1}{E_1} - \frac{1-2\upsilon_2}{E_2}\right) \tag{2.3}$$

where E_i and υ_i are the modulus of elasticity and Poisson's ratio of the two contact bodies respectively. The determination of the Young's modulus for this experimental setup is discussed in Appendix C. Based on the assumption that the tangential displacements can

be defined as $g(x) = u_1(x) - u_2(x)$, the following equation can be derived from Equation 2.1.

$$\frac{1}{A^*}\frac{\delta g(x)}{\delta x} = \frac{1}{\pi}\int\frac{q(\varsigma)}{x-\varsigma}d\varsigma - \beta p(x)$$ (2.4)

Now, since both the specimen and fretting pads are of the same material, $\beta=0$ and Equations 2.1 and 2.5 can be simplified. Further, because the specimen and the fretting pads are both IN-100, the two contact bodies of interest have the same material properties, $\upsilon_1 = \upsilon_2$ and $E_1 = E_2$, and Equations 2.2 and 2.3 then reduce to:

$$A^* = 4\left(\frac{1-\upsilon_1^2}{E_1}\right)$$ (2.2a)

$$\beta = 0$$ (2.3a)

As fretting begins in the contacting region of the specimen and the fretting pads, after the application of the contact load and axial load, the displacements of adjoining points in the stick zone on the specimen and the pad will be exactly the same (Figure 2.4). Once the contact load is applied to the specimen by each fretting pad, a Hertizian applied pressure distribution, p(x), will develop and can be represented by:

$$p(x) = p_o\sqrt{1-\left(\frac{x}{a}\right)^2}$$ (2.5)

where p_o is the peak pressure which is given by either of the following equations, assuming that the two contact bodies are elastically similar:

$$p_o = \frac{2P}{\pi a}$$ (2.6)

$$p_o = \sqrt{\frac{PE}{2\pi(1-\upsilon^2)R}}$$ (2.7)

13

In equation 2.7, R is defined as:

$$R = \frac{\sigma_{min}}{\sigma_{max}} \tag{2.7a}$$

In order to calculate the half-width of the contact zone, a, the following equation is used:

$$P = \frac{(\pi k a^2)}{2A*} \tag{2.8}$$

which becomes:

$$a = \sqrt{\frac{2PA*}{\pi k}} \tag{2.8a}$$

where the parameter k, the radius of curvature, is defined as:

$$k = \frac{1}{R_1} + \frac{1}{R_2} \tag{2.9}$$

and R_1 and R_2 are the radii of the fretting pad and the specimen, respectively. As the specimen is a flat body, the radius can be approximated as infinite and the second term reduces to zero.

Now the axial stress, σ_{xx}, resulting from the applied contact load P can be defined in Cartesian coordinates in terms of x, a, and peak pressure, p_o:

$$\sigma_{xx} = -p_o \left(\frac{\sqrt{a^2 - x^2}}{a} \right) \tag{2.10}$$

The shear stress distribution along the contact surface can now be expressed in terms of x, a, and Q:

$$q(x) = \frac{Q}{\pi\sqrt{a^2 - x^2}} \tag{2.11}$$

14

Also, the total shear stress distribution along the contact length, Q, can be calculated by integrating Equation (2.11) and is defined in terms of a, c, and p_o by integrating the shear stress distribution:

$$Q = \frac{fp_o\pi}{2a}\left(a^2 - c^2\right)$$ (2.12)

Using Equation (2.13), the sick zone size can be calculated as a ratio of $\frac{c}{a}$ in terms Q, P, and the coefficient of friction, f:

$$\frac{c}{a} = \sqrt{\left(1 - \left|\frac{Q}{fP}\right|\right)}$$ (2.13)

2.2 Analytical Model

In order to calculate the numerical solutions required by analytical analysis for variables such as the Hertizian peak pressure, p_o, in Equation 2.6, the contact half-width, a, in Equation 2.8, and so forth Chan and Lee [29] wrote a program in FORTRAN named the "Ruiz Program." This program is used to generate values for the stress states anywhere along the contact length. It should be noted that the solutions generated by the Ruiz program are only valid for fretted test samples where the following condition is satisfied:

$$\frac{b}{a} \geq 10$$ (2.14)

If the ratio of specimen half thickness, b, to contact half width, a, is less than 10 the Ruiz program's values are no longer valid but may still be considered as approximations of the true values. In this study, this criterion is violated and thus can only be used for

15

approximations and other methods, such as Finite Element Analysis, could be used to make better approximations.

The Ruiz program uses two parameters, K_1 and K_2, to predict the crack nucleation location and propagation:

$$K_1 = (\sigma_T)_{\max} (\tau \delta)_{\max} \qquad (2.15)$$

$$K_2 = (\sigma_T \tau \delta)_{\max} \qquad (2.16)$$

K_1 uses the maximum surface tangential stress, $\sigma_{T \max}$, and the maximum value of shear stress and interface slip, $\tau \delta_{\max}$, to provide a parameter to predict the frictional work that nucleates the crack. K_2 combines the effects of surface tangential stress, σ_T, shear stress, τ, and the relative slip at the interface, δ, to predict how the crack opens and propagates. The combination of these two parameters yields one criterion that is used to describe both the crack's initiation and its growth characteristics.

2.3 Crack Nucleation and Growth

As previously noted, the initial stage in fretting fatigue is crack initiation in which the damage done to the material leads to the beginning of a crack which will later propagate until it causes the ultimate failure of the specimen of component. It has been determined that crack initiation is not merely an event in the fretting phenomenon but more of a process. It is this stage which consumes the majority of the fretting fatigue life in the specimen, yet it is poorly understood when compared to the other stages of fretting. It is therefore important to study crack initiation not only because it constitutes the majority of fretting fatigue life but also because it is so important in fretting and appears to be influenced by so many factors. Under normal, non-fretting fatigue conditions it is

inherent flaws (voids, inclusions, etc.) that naturally occur within the material or from external flaws which create stress concentrations which cause the initiation of cracks that eventually lead to hastened failure of the material. The existence of these inherent cracks is known but it is also known that they are too small to detect and therefore must be accepted. It is only when these cracks begin to grow within the material that they become detectable. This is only not the case under fretting conditions however. Under fretting conditions, cracks do not only originate from those originally located within the material but from cracks which are created near the edge of the contact region by increased local stresses.

An accepted theory that is used to explain the crack initiation stage is the Persistent Slip Band theory developed by Venkataraman et al [30]. In this study, it was shown that single crystals of materials such as copper oriented for single crystal slip and fatigued to saturation at low strain amplitudes exhibit highly localized cyclic strain accumulation in narrow bands. These bands are named persistent slip bands. Persistent slip bands consist of dense primary edge dipoles and it has been determined that these are mainly of the vacancy type because the non-linear elasticity effects preclude the extensive formation of interstitial dipoles [31]. These slip bands are subjected to the repetition of loading and unloading, characteristic of cyclic loading, which causes them to accumulate around obstacles such as inclusions and grain boundaries within the material. Over time these slip bands lead to the creation of extrusions and intrusions of material. Extrusions are surface features which appear in the material as narrow ribbons of "squeezed out" material. They are thought to be the consequence of reverse glide on the two closely spaced parallel planes which are oriented for slipping. Inclusions, as previously noted, are also observed but are thought to be valleys between adjacent

17

extrusions. Eventually, after enough cycles it becomes energetically favorable to form embryonic cracks, about the size of one grain but potentially up to two or three grain sizes long. The model has even been shown to be able to predict, in a very general sense, how long crack initiation should take based on three main parameters: slip amplitude, slip band length and the contact width of the fretting surface. The persistent slip band theory and the subsequent model can be used to predict crack initiation and can be used, once embryonic cracks are established, to model crack propagation until cracks are large enough to be modeled by other, further developed techniques.

The period of time and conditions required to transition from the crack initiation stage to the crack propagation stage are very difficult to clearly define. Often, small cracks are able to develop within a material and can later be arrested before they reach a point where they propagate completely throughout the material. This has been observed in very large power-generating turbines. There are many other factors which can aid in crack nucleation and these have been studied at great lengths. Szolwinski and Farris [32] showed that an increase in the coefficient of friction between the fretting members is caused by wear and an accumulation of debris on the surface during the first few hundred cycles. As the number of cycles applied increases, near-surface plastic deformation is observed, which can result in the nucleation of a series of grain-sized microcracks. These microcracks have the potential to join with other microcracks and can either be worn away in future cycles or form larger wear particles. When wear rates are high, usually when large slip amplitudes are present, these microcracks are more likely to form larger cracks and propagate throughout the bulk material. Fellows et al. [33] conducted several experiments involving the frequency of the bulk stress and the frequency of the fretting stress were devised to isolate the effect that different loading conditions had on

the initiation of fretting fatigue cracks. Their goal was to compare and contrast the macroscopic and microscopic approaches to the prediction of crack initiation in fretting fatigue. They highlighted the difficulties experienced in measuring initiation lives under fretting conditions. For two reasons, they concluded, their results were not conclusive. First, they found that it is virtually impossible to devise a loading scheme which influences fretting fatigue alone that does not affect propagation. Secondly, they concluded that controlling the ratio of fretting to bulk loading frequencies showed that the stick-slip regime arising is extremely sensitive to the exact loading pattern and this will modify the internal state of stress. This study was able to conclude that there is a critical shear stress amplitude, consistent with that occurring in plain fatigue, which exists for fretting fatigue. The authors ultimately make the conclusion that shear stress amplitude appears to be a good parameter for predicting the initiation of the previously discussed cracks which are caused by fretting and lead to the failure of materials.

As these cracks grow, they become large enough to enter the domain of regular fracture mechanics and can be modeled by several more macroscopic methodologies. These methodologies could include linear elastic fracture mechanics, elastic-plastic fracture mechanics, crack tip opening displacement, and J contour integrals, to name a few.   Hattori and Watanabe [34] have also studied the initiation of cracks in fretting fatigue. They found that during the early stages of fretting, fatigue cracks tend to close and propagate very slowly because of the high contact pressure acting near the contact edge. Wear on the contact surface then reduces the contact pressure near the contact edge and the cracks eventually start to propagate. It is in this stage, where small cracks initiate at the contact edge, in where fretting fatigue life is dominated. Hattori and Nakamura [35] have made estimations of fretting fatigue strength based on the stress intensity factor

at these crack tips. They state that the multiaxial stress states from the bulk stress and the contact stresses cause these small cracks to grow. In fact, once cracks are established they will grow at ever increasing rates until the critical stress intensity factor is reached and total fracture of the material occurs.

2.4 Gross and Partial Slip

As previously discussed, as fretting occurs stick and slip zones develop on the contact surfaces of the material. These zones do not form at the same time and the slip zone can form as either gross slip or partial slip. The first type of slippage, gross slip, forms when the contact surfaces are undergoing relatively large displacements with respect to one another during each cycle. This gross slippage leads to the two surfaces wearing upon each other causing damage by an abrasive interaction. This damage process is known as fretting wear.

The second type of slippage is partial slip and it is the opposite of gross slip. Under partial slip conditions there is no gross displacement between the contact surfaces. In this slip condition, the two surfaces will begin to stick to one another and are only under going slip near the edges of the contact zone. In this zone, the stick zone, there is no relative displacement between the contact surfaces and the surfaces are essentially welded together. Under fretting fatigue, to include this investigation, the contact surfaces are initially able to slip against each other as the axial load is applied. As the contact load, applied by the fretting pads against the specimen, is increased and the axial load continues to cycle, the specimen and fretting pads begin to stick to one another and any gross slip will cease. At this point, any large displacement will be inhibited. A clear stick zone can now be seen (Figure 2.4). This stick zone extends from –c to c. The other

zone, found immediately outside of the stick zone but still located in the contact zone and which extends from –a to a, is called the slip zone. The dimensions of these zones can be determined using the following equation [12]:

$$a^2 = \frac{4(1 - A^*)}{k\pi}$$

(2.17)

where P is the contact load distributed over the width of the specimen and A', for the contact bodies is given as:

$$A^* = \frac{4(1 - v^2)}{E}$$

(2.18)

where v is Poisson's Ratio, E is the Modulus of Elasticity, and k is the radius of curvature as defined by Equation 2.9. Under ideal fretting conditions the stick zone will form exactly in the center of the contact zone and the slip zone on each side will be symmetrical.

2.5 Predictive Fretting Fatigue Parameters

It has been of benefit to engineers to be able to use reliable predictive parameters in plain fatigue. These predictive parameters are of the utmost importance to engineers as they can be used in order to aid in the prediction of crack location, crack initiation angle, and fatigue life. Using these parameters will aid in the reduction of costly, unexpected, and catastrophic failures by providing estimates that can be used to better detect, repair, or replace affected components.

The wealth of knowledge that has been used in order to develop the predictive parameters for plain fatigue has enabled better ways to analyze fretting fatigue data and develop better models for fretting fatigue cracks. Over time several methods and

parameters have been developed and evaluated for their applicability in predicting plain fatigue life and now they are being extended to fretting fatigue.

The predictive parameters that have shown to be of most use in fretting fatigue are the Modified Shear Stress Range (MSSR) parameter, the Shear Stress Range (SSR) parameter, and the Critical Plane parameter. These parameters have been shown to be extremely useful, but have mostly only been investigated in titanium alloys. The suitability of these parameters for use with nickel-based alloys such as IN-100 has yet to be shown as very little investigation has been done. The following sections will detail three predictive parameters: Modified Shear Stress Range, Shear Stress Range, and Critical Plane.

2.5.1 Shear Stress Range

The stress range is influenced by local interfacial mechanistic parameters such as peak contact pressure, local shear stresses, slip amplitude, and local bulk stresses. The shear stress range can be defined, as by Iyer et al. [36], as follows:

$$\Delta\tau = \tau_{max} - \tau_{min} \tag{2.19}$$

where τ_{max} and τ_{min} are the shear values from the maximum and minimum axial loadings respectively. The following equation can be used to determine the maximum and minimum shear stress values, and therefore the shear stress range:

$$\tau|_{\theta} = -\frac{(\sigma_{xx} - \sigma_{yy})}{2}\sin(2\theta) + \tau\cos(2\theta) \tag{2.20}$$

for θ ranging from $-\frac{\pi}{2}$ to $+\frac{\pi}{2}$. However, this takes neither the effect of mean stress nor the effect of stress ratio into account, both which have been clearly shown to be

relevant to fatigue life. To aid in correcting these concerns, Walker [37] suggests an alternate method, seen below, which does take these factors into consideration.

$$SSR = \Delta \tau_{crit} = \tau_{max}(1 - R_T)^m \qquad (2.21)$$

In this equation m is a fitting parameter that is chosen to collapse plain fatigue initiation data at different strain ratios, which Lykins [38] has determined to be 0.45. R_T is the stress ratio on the critical plane and is evaluated as:

$$R_T = \frac{\tau_{min}}{\tau_{max}} \qquad (2.22)$$

Madhi [12] calculated the SSR parameter for IN-100 in his study and found that although it could predict crack location and orientation, it did not predict the fatigue life without dependence on pad geometry. It was determined that the crack location, crack initiation angle, and fatigue life could not be calculated using this method with a high degree of accuracy.

2.5.2 Critical Plane

In fretting fatigue, cracks initiate under a multi-axial state of stress within the contact region of the material. The state of stress is multi-axial in nature due to the combination of the bulk stress and the applied contact load within the region of interest. One of the predictive parameters focuses on the notion of a critical plane. This parameter focuses on the premise that cracks will initiate on a particular plane, called the critical plane. This critical plane is the plane where the maximum shear stress is located and this occurs at some angle between the contact line of the fretting pad and the specimen's surface. It has been theorized that, on this plane, normal stresses opens cracks and, in doing so, reduces the friction between the crack surfaces and the shear stress induces

dislocation along slip lines, causing nucleation and propagation of cracks. It is the goal of this approach to find the maximum shear strain amplitude and the plain on which it acts and then, using the maximum normal stress on this same plane, to determine the effect of a mean stress. The shear and normal stress can be determined for any plane if the state of stress, $\sigma_{xx}, \sigma_{yy}, \tau_{xy}$, is known for that point. Shear stress can be found from:

$$\tau = -\frac{\sigma_{xx} + \sigma_{yy}}{2}\sin(2\theta) + \tau_{xy}\cos(2\theta) \tag{2.23}$$

and the normal stress can be found using:

$$\sigma = \frac{\sigma_{xx} + \sigma_{yy}}{2} + \frac{\sigma_{xx} - \sigma_{yy}}{2}\cos(2\theta) + \tau_{xy}\cos(2\theta) \tag{2.24}$$

These equations depend on θ, which is evaluated from $-\frac{\pi}{2}$ to $+\frac{\pi}{2}$, in small intervals. It is very difficult to experimentally measure the state of stress in the fretting fatigue zone. Therefore analytical and finite element simulations are used to determine these values.

The critical plane model is popular among fretting fatigue researchers because of the multi-axial stress state in the contact region. Namjoshi et al. [7] studied several critical plane based fatigue models in order to investigate fretting fatigue crack initiation behavior in the titanium alloy Ti-6Al-4V. They were able to demonstrate that fretting fatigue crack initiation is a function of the shear stress on the critical plane and that fretting fatigue life is influenced by the normal stress acting on the critical plane. Though the use of this parameter is effective in predicting cycles to fatigue crack initiation, crack initiation location, and crack orientation, the exact role that the normal stress plays on the critical plane in fretting fatigue crack initiation is unclear.

2.5.3 Modified Shear Stress Range

The Modified Shear Stress Range (MSSR) parameter is considered by many fretting fatigue researchers and experts to be the premier predictive parameter of fretting behavior. As its name suggests it is a modification of the Shear Stress Range parameter that takes into account the effects of maximum normal stress and how it acts to open the crack surface. It has been shown that this parameter can also help to eliminate the effect of fretting pad geometry that Namjoshi et al. [7] felt hampered the Shear Stress Range parameter due to the inclusion of both the shear stress and normal stress in the calculation of the parameter. The MSSR is calculated by the following equation:

$$MSSR = A\Delta\tau_{crit}^{B} + C\sigma_{max}^{D} \qquad (2.25)$$

where A, B, C and D are constants that vary according to material. These constants were determined by Sabelkin et al [39] to be 0.75, 0.5, 0.75 and 0.5 respectively for Ti-6Al-4V. As with the SSR, the MSSR is calculated for all planes ranging from $-\dfrac{\pi}{2}$ to $+\dfrac{\pi}{2}$ at every point along the contact length between the specimen and the fretting pad. The MSSR parameter value is at a maximum at the critical plane orientation. Madhi [12] further analyzed the constants of the MSSR in his study of IN-100 and found that the best agreement came when he used values of 0.5, 0.25, 0.75 and 0.5 respectively for A, B, C and D. In his analysis, Mahdi found that the MSSR parameter was the best overall predictive parameter to predict fretting fatigue life, crack location, and crack initiation orientation in IN-100.

2.6 Previous Fretting Fatigue Studies

The following section will briefly summarize a portion of the studies into fretting fatigue that have already been completed. While there is not a great wealth of information available on fretting fatigue in nickel-based alloys, there are many resources available which instead utilized titanium alloys. By using these studies, one can learn a great deal about fretting fatigue in general and make conjectures as to how they relate to fretting fatigue in nickel-based alloys, namely IN-100. To begin, studies of fretting fatigue in titanium alloys at room temperature will be presented followed by similar studies in nickel alloys. These will serve as the knowledge base of fretting fatigue as studies at higher temperatures are presented. To serve as a comparison, high-temperature fretting studies of both titanium and nickel-based alloys will be presented. Finally, studies which investigate fretting fatigue under high contact stresses will be presented to specifically benefit this study.

2.6.1 Room Temperature Studies on Titanium alloys

As noted previously, Namjoshi et al. [7] studied the fretting fatigue behavior of Ti-6Al-4V under various fretting pad configurations. This study used five different pad geometries: cylindrical pads of radii 50.8 mm, 101.6 mm, and 304.8 mm as well as flat pads with edge radii 5.08 mm and 2.54 mm. As seen in previous sections of this report, the authors combined the fretting pad geometries into an investigation into several critical plane based multi-axial fatigue parameters. These pad geometries were used in order to run numerous experiments and compare their results (crack initiation location, crack orientation angle, number of cycles to fretting fatigue crack initiation) to the predicted values from the various parameters to find which one is best suited for use in fretting

fatigue. This study used the experimental results to conclude that fretting fatigue life decreased as the radii of the cylindrical fretting pads increased and the edge length of the flat pads were decreased. Based on the pad geometry, whether the radii of the cylindrical pads are increased or the edge length of the flat pads are decreased, the area of the fretting pad increases causing a larger contact area with the experimental specimen and a decrease in fretting fatigue life.

Sabelkin et al [39] also investigated fretting fatigue behavior of Ti-6Al-4V and focused on shot-peening, specifically the effect of the intensity of shot-peening, as a factor in the fatigue life. This study also used a cylinder-on-flat contact method and shot-peening intensities of 4A, 7A, and 10A were utilized. Shot-peening was shown to have a beneficial effect on fretting fatigue life with the greater shot-peening intensities having a greater effect, due to the fact that higher intensity shot-peening was shown to relieve residual stresses within the material. This moved the boundaries between positive and negative stresses to a greater depth in the material. After the fretting experiments were carried out to failure, the authors compared their results to the various predictive parameter presented earlier in this report. They found that, in their study, the MSSR parameter, computed for all cases from the finite element analysis, was very representative of the crack initiation locations and fretting fatigue life.

Yuksel [8], in his AFIT thesis, also evaluated the effects of shot-peening on the fretting fatigue behavior of Ti-6Al-4V. This study investigated and compared the results of the effect of shot-peening on specimens of two different thicknesses: 3.81 mm and 6.35 mm. It was determined, as was shown in the Sabelkin study, that shot-peening proved beneficial in lengthening the fretting fatigue life of the titanium alloy. There were differences, however, in the observed crack initiation locations between the 3.81 mm

27

specimen and the 6.35 mm specimen.   The cracks initiated on the contact surface for the thicker specimens while the cracks initiated in the thinner specimens at depths ranging from 200 micrometers to 300 micrometers from the contact surface.   The crack orientations also differed between the two thicknesses. The thinner specimen's cracks initiated close to the +/- 45 degree angle while the thicker specimen's cracks were oriented at -37 and -28 degrees, respectively, for primary and secondary cracks.

2.6.2 Room Temperature Studies on Nickel alloys

In their study into the role of internal stress and thermal ageing, Sondhi et al. [40] discovered the presence of an internal stress field within an as-received IN-100 alloy which was determined to be responsible for an unusual response of low and even negative creep rates in tension. The authors note that the IN-100 material can be used in the cast form to produce turbine blades and can also be used to make turbine discs through a powder metallurgical route.   It is recognized that these components will experience very different operating conditions during their service lives and that different microstructures for each component will be required in order to optimize their engineering performance. This study compared the as-received alloy to a pre-aged alloy in order to validate the internal stress field hypothesis regarding the internal stresses and pre-aging of the material. The absolute values of initial creep rates were significantly higher in compression than in tension, resulting in the asymmetric creep response thus proving the presence of the internal stress field. This asymmetry was easily removed by thermal ageing prior to testing.

Madhi [12] also studied the fretting fatigue behavior of IN-100 in room temperature conditions. He used two different cylindrical fretting pad radii, 50.8 mm and

304.8 mm, as well as low and high cycle loading under a constant contact load. The microstructure of the IN-100 used in his study was a coarse grained alloy with oblong grain dimensions of 10 microns by 50 microns. He investigated the validity of extending predictive parameters such as the Smith-Watson-Topper (SWT), Findley, Shear Stress Range (SSR) and Modified Shear Stress Range (MSSR) parameters that have proved useful in alloys of titanium to alloys of nickel such as IN-100. His results suggested that the MSSR parameter was the best parameter to accurately model the crack initiation location, orientation, and fretting fatigue life in IN-100. Due to the similar nature of study, a review and comparison of Mahdi's results to the results of this study will be presented in Chapter IV of this work.

Saladin [13] built on Mahdi's work and evaluated the effect of microstructure on the fretting fatigue behavior of IN-100 at room temperature. His study examined the differences in fretting fatigue crack initiation, location and propagation of fine grained (7 micrometer grain size) and coarse grained (10 by 50 micrometer oblong grain size) specimens of IN-100. His results suggested that the coarse grained microstructure had a greater resistance to crack initiation and therefore performed better under fretting fatigue conditions than the finer grained microstructure. Saladin made this conjecture because he found that the coarse grained microstructure contained a higher crack initiation threshold in the material when compared to that of the fine grain microstructure. Further, it was also found that this difference was greater in the high cycle fatigue region than in the low cycle fatigue region. Saladin concluded that microstructure had an effect on both crack initiation and crack propagation in IN-100. The coarser grain sized material had slower and non-linear crack propagation and the fine grained material was found to have a linear propagation rate. A review and comparison of Saladin's results will be presented in

29

Chapter IV due to the similar nature of study. Also, the microstructure of the specimens used by Saladin is identical to the annealed specimens used in this study as they were taken from the same plate.

2.6.3 High Temperature Studies on Titanium alloys

Hamdy and Waterhouse [41] studied the fretting fatigue behavior of Ti-6Al-4V and generated fatigue curves at temperatures of 20˚C, 200 ˚C, 400 ˚C, and 600 ˚C in fluctuating tension under a constant fretting contact load. They were able to determine that the fatigue life did, in fact, decrease with fretting and decreased slightly more with an increase in temperatures up to 600˚C. They attributed this decrease in fatigue endurance to changes in the fatigue properties of Ti-6Al-4V rather than an aggravation of the fretting damage process. The authors also noted that there was no formation of a beneficial glaze oxide, which has been found to counter fretting damage in nickel-based alloys and will be discussed later. This study further indicated that at higher temperatures the observed surface damage from fretting differed greatly from what is observed at room temperature.

Jin et al. [42] investigated the effect of an elevated temperature, 260 ˚C, on the fretting fatigue behavior of Ti-6Al-4V. It was found that the coefficient of friction increased in Ti-6Al-4V slightly at the onset of damage caused by fretting, as seen by Szolwinski and Farris [32]. Though this was the case, the increase of the coefficient of friction at 20˚C mirrored the increase at 260 ˚C. This was attributed to the fact that, similarly to Hamdy and Waterhouse's study, unlike nickel-based alloys, there was no glaze oxide formation to prolong the fatigue life. Likewise, it was found that there was no significant difference in the fretting fatigue life between the room temperature tests

and the high temperature tests. Both showed a reduction from the value associated with plain fatigue.   This study successfully showed that temperatures up to 260 ˚C do not benefit or detract from the fatigue endurance of Ti-6Al-4V.

Albinali [25] was able to evaluate the effects of both temperature and shot-peening intensity on the fretting fatigue behavior of Ti-6Al-4V. This study tested specimens that had received 4A, 7A and 10A shot-peening intensities, much like Sabelkin et al. [39], at both room temperature and at 260 ˚C. His results concluded that while the shot-peening did increase the fretting fatigue endurance of Ti-6Al-4V at room temperature it did not increase at 260 ˚C. The elevated temperature of 260 ˚C was shown to negate the effect of shot-peening, which on its own has been shown to increase fretting fatigue life at room temperature. The author concluded that the MSSR parameter was effective in predicting crack initiation location, crack initiation orientation for both room temperature and 260 ˚C .   The overall conclusion of this study is that the elevated temperature environment generally negated the effects of the shot-peening due to increased stress relaxation.

Gean and Farris [43] experimentally examined the fretting fatigue behavior of another titanium alloy, Ti-17, at temperatures of 260 ˚C with various surface coatings, lubricants, and shot-peening treatments. This material, as stated by the authors, is representative of the blade and disk attachments in the upper stages of a compressor in a gas turbine engine. Their purpose was to determine the influence, if any, these coatings and treatments had on the total fretting fatigue life of Ti-17. The study concluded that there is no significant change in the fretting fatigue life between the different coating and lubricant combinations. Contrary to the conclusion of Albinali, Gean and Farris concluded that the use of shot-peening at elevated temperatures provided a significant

improvement in the fretting fatigue life. It was not made explicitly clear by the authors by what method the shot-peening was thought to improve the fretting fatigue endurance only that it was the only aspect of testing to exhibit any difference.

2.6.4 High Temperature Studies on Nickel alloys

A study by Wan and Yue [21] investigated both smooth and notched specimens of a single-crystal nickel-based superalloy, DD3, at 620 ˚C in air and under load/stress control at a frequency of 0.17 Hz. As noted by the authors, nickel-based single-crystal superalloys are widely used as materials for gas turbine blades due to their superior creep, fracture, and fatigue properties compared with conventional cast alloys. Based on the experimental results, a low-cycle fretting fatigue life model was proposed for this single-crystal nickel-based superalloy under multi-axial stress. A relationship between shear stress and cycles to failure in the low-cycle fatigue region was developed using resolved shear stress and resolved shear strain of slip systems activated during the fatigue cycles. The resolved shear stress, τ^{α}, corresponding to a particular slip system, α, can be obtained from the following equation.

$$\tau^{\alpha} = \sigma : P(\alpha) \tag{2.26}$$

where $P(\alpha)$ is can be obtained from:

$$P(\alpha) = 0.5(\hat{m}^{\alpha}\hat{n}^{a^{T}} + \hat{n}^{\alpha}\hat{m}^{\alpha^{T}}) \tag{2.27}$$

The variables $\hat{n}^{\alpha}$ and $\hat{m}^{\alpha}$ in the previous equation are the unit vectors that are normal to the slip plane and along the slip direction of the system (α) respectively. A power-law relationship was assumed based on the crystallographic theory:

$$\frac{\Delta\tau_{\text{max}}}{2} = AN_f^b \tag{2.28}$$

where, $\frac{\Delta\tau_{\text{max}}}{2}$ is the maximum resolved shear stress amplitude of all the activated slip systems, A and b are parameters, and N_f is the fatigue life. Equation 2.28 is only valid for a mean stress of zero. If the mean stress is not zero then Equation 2.28 can be modified as follows:

$$\frac{\Delta\tau_{\text{max}}}{2} = AN_f^b \left\{ 1 - \left(\frac{\tau_m}{\tau_b} \right)^2 \right\} \tag{2.29}$$

where τ_m is the mean resolved shear stress on the slip system corresponding to maximum shear stress and τ_b is the resolved shear stress corresponding to the ultimate tensile strength. Using this model and the experimentally obtained parameters, the authors were able to obtain good agreement. Their results were further supported by scanning electron microscopy on the fracture surfaces, where the low-cycle fatigue deformation mechanisms in the DD3 nickel-based single-crystal superalloy at 620 ˚C under a multi-axial stress state were revealed.

In studies by Brien and Decamps [44, 45] the effect of microstructure of another single crystal nickel based super alloy, AM1, was examined under high temperature fatigue at 950 ˚C. For repeated fatigue ($R_e = 0$) throughout a range of cycles, two types of behavior were found depending on N, the number of cycles, and $\Delta\varepsilon^t$, total strain amplitude. This allowed the authors to construct a map of the microstructures versus N and $\Delta\varepsilon^t$ to be developed. A domain, called A, represents the anisotropic microstructures due either to a partition of the plasticity throughout the γ channels, or to an oriented

33

coarsening of the γ' precipitates of the so called type N (rafts perpendicular to the loading axis). The domain called H represents homogenous deformation microstructures. The presence of precipitates significantly affects the usual behavior of monocrystalline alloys under fatigue and localizes the plastic deformation in the channels. It should also be noted that very few $R_e = 0$ tests exhibited microstructures showing deformation bands.

In addition, Brien and Decamps claimed that there is a geometrical differentiation of plasticity due to heterogeneity on the local stress resulting from the presence of internal stresses. The authors also investigated alternate fatigue ($R_e = -1$) and showed that it also leads to the same type of coarsening, even for cycle numbers as low as N=113. It was shown that alternate fatigue has the ability to cause a three dimension distribution of the plastic deformation in the γ channels, since tension was seen to activate plastic flow in the channels perpendicular to [001] and compression in the others.

Piard et al [46] proposed a one-dimensional simulation of creep-fatigue crack growth in a nickel-based superalloy, Astroloy, at 750 °C under a high vacuum. The study focused particularly on the ΔK range where crack propagation occurs during the reloading phase only, although creep effects were found to play a very important role. Two simulations were used, one with a hold time of up to 1000 seconds and one without a hold time. The first simulation, without a hold time, was used to construct a Paris-type ΔK-da/dN crack growth curve. The second simulation incorporates a new creep-damage field, defined in another interval on the crack path. The fatigue and creep damage fields were then related to the creep crack opening displacements of the specimens. The predictive crack curves were found to accurately reflect the influence of hold time duration during the reloading phase.

Shyam and Milligan [20] developed a theoretical model for slip irreversibility in a polycrystalline nickel-base super alloy. This alloy, KM4, deforms in a planer manner. One of the more noteworthy characteristics of cyclic loading is the fact that a fraction of plasticity resulting from the loading is irreversible. This phenomenon is called slip irreversibility and is a result of the fact that the displacements imparted by the motion of the dislocations in the forward portion of the fatigue loading cycle are not completely recovered when the loading proceeds in the opposite direction. The slip irreversibility parameter that is used in this study was based on the fraction of dislocations which were found exiting the free surface as a direct result of the applied loading. As defined, the slip irreversibility parameter can take values between zero and one. The value approaches zero when the slip is fully reversible and one when the slip is not reversible at all. The experiments were conducted at temperatures of 20 ˚C, 550 ˚C and 650 ˚C. When the theoretical calculations in the study were compared to the experimental results, it followed that the observed slip irreversibility increased with increasing temperature. A clear relationship was noted between the observed irreversibility and fatigue-crack propagation thresholds at high load ratios. Overall, it was concluded that the activation and movement of slip systems are the basic mechanism of both the notched and rounded specimens used in this investigation.

Golden [47] conducted a study using René 88DT at elevated temperatures. As stated before, it is very hard to accurately model the dovetail joint which is critical in fretting fatigue in a turbine engine. This study focused on creating a fretting fatigue fixture that more closely resembles the dovetail geometry of the turbine engine environment, especially at an elevated temperature of 650 ˚C. Six tests were conducted and the results showed very little correlation and were not conclusive. This result, though

not conclusive, shows that a very wide range of scatter can occur when testing the behavior of nickel based alloys at elevated temperatures. No reasoning was given for the scatter of the data, but it might be attributable to inconsistencies in the experimental setup which did not accurately model the turbine engine environment.

Kawagoishi et al. [23] studied the nickel-based alloy Inconel 718 under rotary fatigue conditions at temperatures of 300 ˚C, 500˚C, and 600 ˚C in air. They then compared this fatigue performance at elevated temperatures to that at room temperature. Their results led to the conclusion that the fatigue strength of a plain specimen was much higher at elevated temperatures when compared to that at room temperature, though the static strength was shown to decrease with increasing temperature. The effect of temperature on the fatigue strength was examined in terms of the initiation and early growth behavior of small cracks. The authors were able to make a few conclusions based on their data and results. They found that the initiation and propagation of are promoted at elevated temperatures due to the softening of the nickel matrix of the material. It was also shown that the initiation and propagation of small cracks in the range of 20-30 micrometers was suppressed by the formation of an oxide as well as plasticity induced crack closure. Because most of fatigue life is spent in the growth of small cracks, this is this reason why higher temperatures result in longer life. Overall, fatigue life increases with increase in temperature, except in short life region and it especially increases over room temperature. This indicates that the crack initiation and propagation suppression characteristics of the high temperature environment have a great impact on fatigue life.

Hamdy and Waterhouse discussed in the previous section the effect of an oxide glaze on fretting fatigue. In their previous study [41], the authors noted that there was

very little evidence of a glaze oxide formation on the titanium alloy Ti-6Al-4V, which was proven to be seen as beneficial to the fretting fatigue life in nickel-based alloys. In their study with Inconel 718 [48, 49], it was found that the beneficial glaze oxide had formed and did affect the fretting fatigue life. Their experimental results showed that as the temperature increased from 28℃ to 540 ℃, the fretting fatigue strength was increased by a factor of 130%. They attributed this increase to the formation of the previously mentioned glaze oxide which was formed under the conjoint action of oxidation and sliding. These findings confirm that the formation of a glaze oxide on the surfaces of nickel-based alloys at high temperatures, unlike those alloys of titanium, is beneficial to the fretting fatigue life.

Murthy, Gao and Farris [18, 22, 50, 51] further studied the fretting fatigue behavior of single-crystal nickel contacting with IN-100 at an elevated temperature of 610 ℃. These four studies investigated specimens subject to a range of loading conditions. As with other studies, different fatigue parameters were investigated for the degree of which they are able to predict the initiation life of the specimens. Estimations of crack propagation life were made using conventional fracture mechanics approaches. The predicted lives were compared with the experimentally observed failure lives. The similarity of the fatigue lives from the experimental and theoretical data provides more confidence in the notion that conventional life prediction tools can be used to assess fretting fatigue at elevated temperatures.

Waterhouse [52] investigated the fretting fatigue behaviors of austenitic steel type 321 and nickel-based alloy Inconel 718 at elevated temperatures. He concluded that it is the chromium content within these materials that forms Cr_2O_3 at high temperatures, the protective glaze oxide referenced in previous studies. The alloying elements which are

mostly added in order to improve the mechanical properties of the metal were shown to make important contributions to the oxidation behavior, providing a lengthened fretting fatigue life. In the austenitic steel, Waterhouse found that at 400 ˚C there was some development of smooth areas on the fretting surface, suggesting that the glaze oxide was beginning to form. As the temperature increased to 500 ˚C, larger areas of the fretting surface developed glaze oxide and at 600 ˚C this oxide was even more developed. Similarly in the IN-718 specimens at 540 ˚C, a smooth glaze oxide was observed at the two amplitudes studies. The oxide was found, however, only to form at the higher tested amplitude at the lower experimental temperature of 280 ˚C. This suggests a temperature dependence as well as a dependence on load in the formation of a glaze oxide layer in fretting fatigue in both the steel and nickel-based alloys.

2.6.5 Elevated Contact Load Studies

The influence of the contact load on the fretting fatigue behavior has not been ignored.   A study into the influence of contact pressure on fretting fatigue life was conducted by Sadeler [53]. Using a rotating bending fatigue, he first investigated the fretting fatigue life of an aluminum alloy without the presence of any fretting. He then repeated the same experiment multiple times, increasing the fretting contact load with each successive test. The first test, at zero contact load, ran for 10^7 cycles before fracture. As contact loads, beginning at 20 MPa, were applied the number of cycles to failure quickly fell to around the order of 10^3 cycles. At this point, a slight decrease in the fretting fatigue life was observed as the contact load approached 100 MPa. At this point, the fretting fatigue life was seen to slowly, and slightly, increase as contact load was increased to a level of 150 MPa. The author attributed this change to the possibility that,

at higher levels of contact load, the increased loads might act in a way to close any cracks responsible for fracture due to high compressive forces.

Adibnazari and Hoeppner [54] chose to study a supposed threshold at which any increase in contact load will not cause any further decrease in fatigue life. To do so, they used the aluminum alloy 7075-T6 under two different axial loads. They then ran multiple experiments in order to determine the effect of an incrementally increased contact load. The authors hypothesize that below the contact load threshold fretting fatigue failure is a function of the normal pressure and the change in normal pressure and therefore, ultimately, is a function of frictional stress and the change in frictional stress. Through this study, the authors were able to conclude that there is, indeed, a contact load threshold and that the relationship between the axial load and the contact load threshold one of inverse proportionality. Below the threshold, the authors found that the failure of the specimen was a function of normal pressure, frictional stress, applied axial load, and any variations in these variables. Above the threshold, it was found that failure was a function of axial load and its variation, normal pressure, and frictional stress.

Nakazawa et al [55] conducted a similar investigation using solution-treated austenitic steel. They were further able to make conjectures about the method of crack initiation both above and below the contact load threshold. As in previous studies, the authors found that at low incremental increases in the contact load (15 Mpa-45 MPa), the fretting fatigue life was relatively unchanged. The fatigue life was observed to be drastically reduced as the contact load was increased (above 60 MPa). The frictional stress amplitude was observed to increase in a linear fashion with the increase in contact load. At the lower contact loads, the stress concentrations due to fretting damage were found to occur at the middle portion of the fretted area and the main crack responsible for

failure also initiated there. At the higher contact loads, a deep concavity was observed to have formed. It was here that the main crack initiated, on the outer edge corner. This was thought to act as a notch for crack initiation purposes. The authors concluded that this suggested that the stress concentrations play a critical role in the fatigue life.

Ramakrishna and Raman [56] also investigated the effect of increased contact load on fretting fatigue, using the Al-Mg-Si alloy AA 6061. These authors, as has been mentioned previously, recognize how many variables affect the fretting fatigue life. They report that over 50 variables could influence the magnitude and rate of the fretting process. Of all of these variables, the authors felt that the coefficient of friction is the main influence into the fretting fatigue process. As with Sadeler, these authors observed a variable behavior with an increase in the fretting contact load. A marked decrease of the fretting fatigue life was observed as the contact load was increased. At a contact load of 100 Mpa, the fretting fatigue life was at a minimum. A maximum fretting fatigue life was then observed at an intermediate contact load of 150 Mpa. It then decreased again with an increase in the contact load. This behavior was attributed to changes in frictional stress, critical relative slip, crack growth retardation, due to crack closure at high contact loads, and the affects of stress concentrations.

Overall, there seems to be a consensus as to the effect of an increase in contact load in reference to the fretting fatigue life. Some authors observed a decrease followed by an increase and others observed a constant threshold value. Those that saw an increase attributed it to crack closure due to the high contact load. A variety of materials have been used ranging from austenitic steel to alloys of aluminum. The present study will now investigate this effect with a nickel-based superalloy.
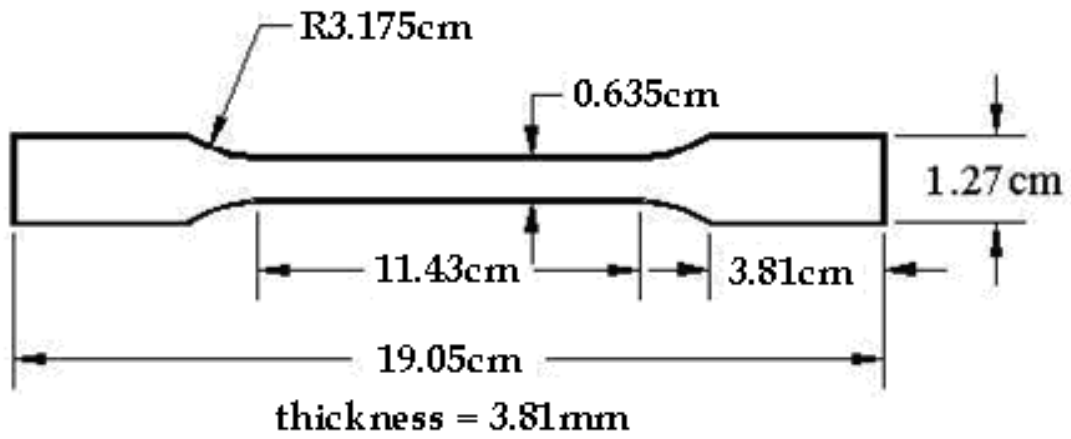
Figure 2.1 – Specimen Dimensions
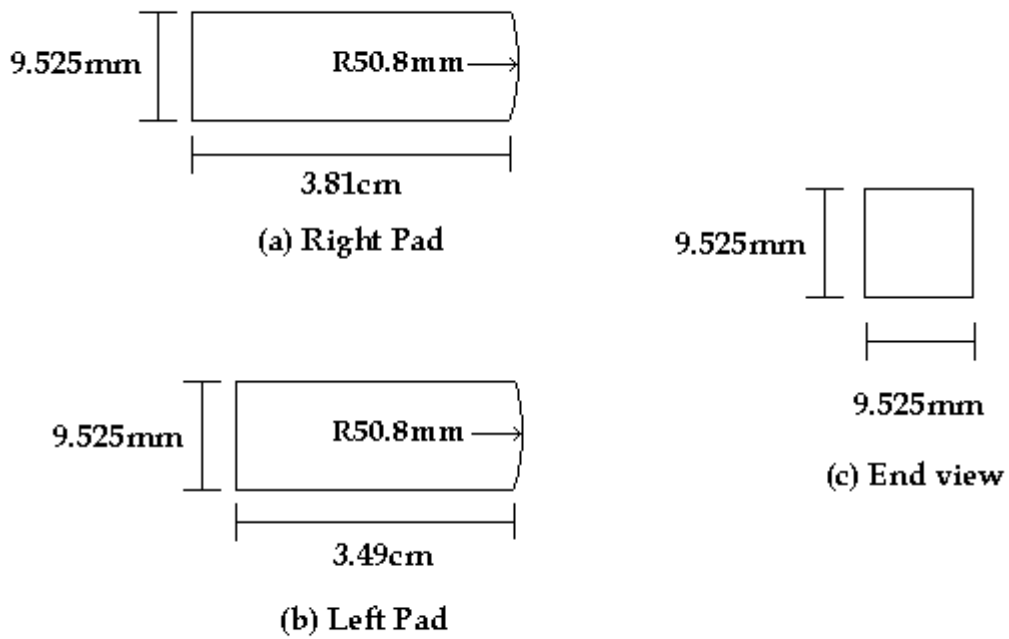
Figure 2.2 – Fretting Pad Dimensions; (a) Right, (b) Left, and (c) End View
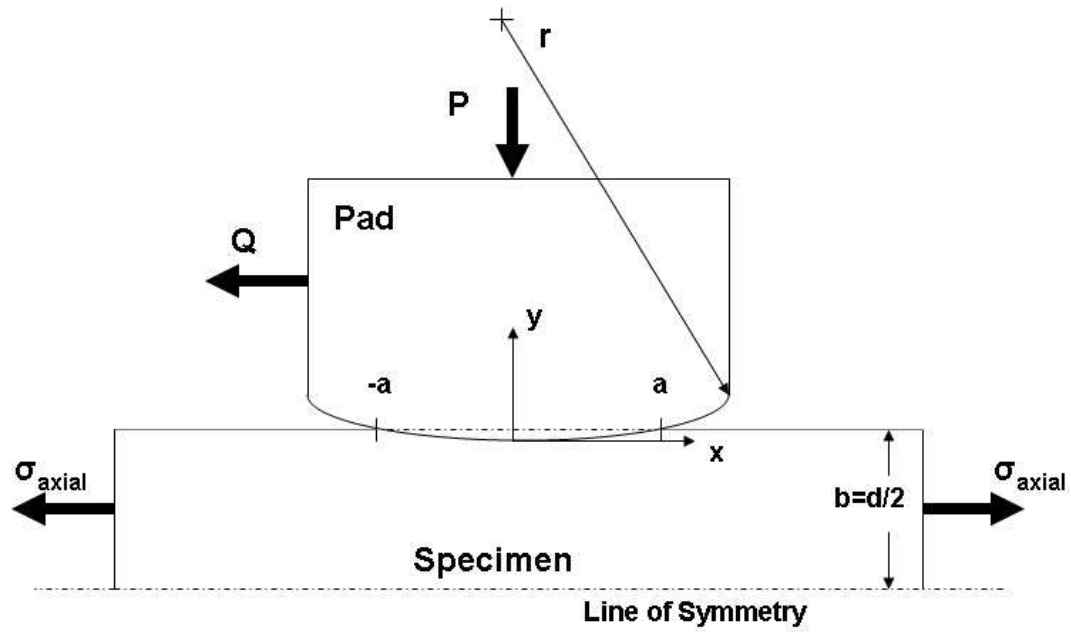
Figure 2.3 Diagram of cylinder on flat fretting fatigue configuration [12]
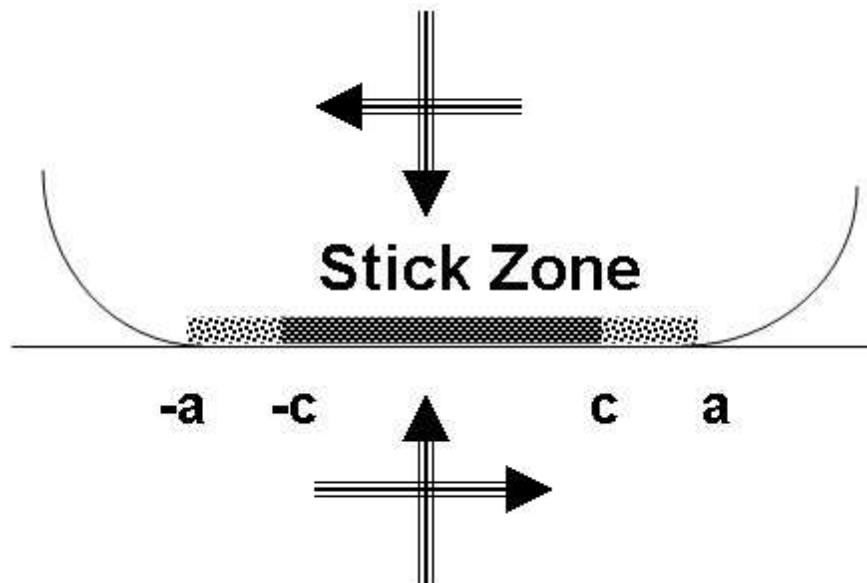
Figure 2.4 Diagram of stick zone [12]

III. Experimental Method

This chapter documents and discusses the experimental design in further detail as well as present the data collected during each test of this study. The experimental method used in this study is substantially similar to the methods used by Madhi [12] and Saladin [13] but has been modified significantly in order to facilitate the testing conditions of elevated temperature and therefore is the same experimental setup of Ownby [11]. The following chapter contains a brief description of the testing apparatus, the specimens and fretting pads, load determination, and the experimental procedures. Particular attention is paid to those areas which were developed or modified to accommodate the high temperature and contact load aspects of testing.

3.1 Test Set-up

The test set-up in this study was intended to closely mirror that used by Mahdi and Saladin in their studies as this is a continuation of their work on fretting fatigue of IN-100 at room temperature. Ownby, through his study, modified the experimental setup using the more advanced equipment available. He also added the elevated temperature set-up, which required some modifications to the experimental setup. As this study is directly related to the study of Ownby, but with an increased contact load, the experimental setup was kept exactly the same for the sake of continuity. Ownby mentions that the modification of the experimental setup required a great deal of effort. This was the case due to space constraints as well as many obstacles that had to be overcome in order to create a working experimental setup. As in Ownby's study, the testing machine used for all of the experiments is an MTS 22 kip servo-hydraulic axial and a 1 kip servo-hydraulic horizontal test machine (Figure 3.1). For each experimental

trial, the IN-100 specimen is loaded into the hydraulic grips that are attached to the upper and lower actuators (Figure 3.2). The upper grip, unlike the previous test apparatus used by Madhi [12] and Saladin [13], is not a stationary cross head but a fully movable actuator. For this study, the upper grips were programmed to remain in displacement control in order to provide an approximately rigid boundary condition. Both upper and lower grips contain load cells which were used to monitor the axial loading conditions of the specimen.

The actuators and test equipment are controlled by Multi-Purpose Test (MPT) software from a connected desktop computer (Figure 3.3). This software allows the user to set the magnitude, frequency, and waveform of the applied load. It also allows the user to monitor these and other parameters during each experiment. The MPT software also has included functions such as a ramp function, which allows loads or temperatures to be changed over a specified period of time. This software proved extremely valuable in monitoring the progress of each test in order to ensure that the proper test conditions were met throughout the entire run.

The fretting actuator provides the contact load between the fretting pads and the specimen during each test. This is accomplished through a simple hydraulic actuator that is horizontally mounted on a movable sled with a load cell in the fixed receiving end. This load cell monitors and controls the contact load throughout each experiment (Figure 3.4). Ownby's study, as mentioned previously, attempted to mirror the studies of Mahdi and Saladin, but with more capable apparatus. It is at this point where a great improvement has been made in the experimental setup. Both Mahdi and Saladin's fretting force was provided by fretting pads attached to a spring loaded frame. The current setup allows for much greater control and oversight over the fretting contact load.

Thought this setup was a definite improvement, it was not perfect and the issues will be discussed later in this chapter. Each actuator was actively cooled through a chilled water system which was provided from a separate stand-alone apparatus. This was required because the load cells will only function in the temperature range of -40 ˚C to 177 ˚C. As this study investigated fretting fatigue at an elevated temperature of 600 ˚C, the cooling of the grips became a necessity.

During each experimental trial, the temperature is closely monitored and controlled by an MTS temperature controller with two platinum rhodesium R type thermocouples and two heater boxes mounted in the front and rear sides of the machine. Each thermocouple controls two electric resistance heating elements which protrude from each heater box. Each thermocouple is mounted in such a way that it protrudes from the heater box and remains in the high temperature zone between each set of heating elements. The heating element and thermocouple apparatus can be seen, in use, in Figure 3.5. In order to measure and maintain the appropriate temperature on the specimen, Ownby investigated welding the thermocouples to the specimen but found that this caused stress concentrations in the specimen at the weld areas. As this would affect the experimental results, it was decided that the thermocouples would be separated from the specimen in the manner used in his study. This study used this same method of temperature measurement and control. As such, the thermocouple heads are aligned in the same horizontal plane as the center line of the fretting pads but are removed from the actual fretting pad and specimen interface area by approximately 1.5 centimeters. This necessitated making a correlation between the desired specimen temperature and the temperature read by each thermocouple. This calibration will be discussed further later in this chapter.

Each of the four heating elements is attached to one of the two heater boxes. One heater box is mounted to the sled which contains the fretting actuator. The heating elements extend from the side of the heater box closest to the specimen. One heating element is oriented at an angle of approximately 30 degrees above the horizontal and the other is located approximately 30 degrees below the horizontal. The heating elements from one heater box are oriented such that one is located on the left side of the specimen and the other is located on the right side of the specimen. One the opposite heater box, the same is true such that the heating elements are located above, below, left, and right of the fretting contact area with the thermocouples located within this zone oriented at the front and back of the specimen. Each heater box is secured to the sled by two screws located on each side of the box through a narrow channel running along the entire side of the heater box. This channel allows the boxes to slide from the outer edge of the sled towards the specimen and pads once they are installed and aligned. This also allows a confidence that, for each test, the heater boxes are aligned in the same position because of the constraints placed on them by the channels and screws.

The thermocouples, which play a crucial role in maintaining the appropriate temperature throughout each experiment, are attached to the heater boxes at an approximate 45 degree angle and protrude into the elevated temperature zone. As these are rigidly attached to the heater boxes and the heater boxes are in the same position for each test, it is assumed that these thermocouples are located at the same position relative to the specimen for each experimental trial. In order to maintain a reliable and repeatable experiment this fact is crucial. This experimental setup is open to the ambient air of the laboratory environment, which is in no means a stable thermal environment. As such the actual temperature of the specimen and pads in the elevated temperature zone is likely

to fluctuate over the course of the test. Measures such as acrylic baffles and a close monitoring and controlling of the ambient environment lessened the severity of these effects, though they could not be completely negated.

As mentioned earlier, the thermocouple apparatus required calibration due to the fact that there was a 1.5 centimeter separation of each thermocouple from the specimen. Calibration was accomplished through the use of a specially prepared specimen. This specimen, identical to those used in the study, had one thermocouple welded to each of the front and rear. It was then mounted in place and configured in accordance to the experimental procedure. The commanded temperature to be delivered by the heating elements was then raised incrementally. The temperature of the specimen, as shown by the welded thermocouples, was then recorded manually. Once the temperature was observed to stabilize, the commanded temperature of the heating elements was raised. This was done until the temperature of the specimen stabilized at 600 ˚C. The results of this calibration can be seen in detail in Appendix A.

Through this calibration procedure, it was determined that a commanded temperature of 369 ˚C led to a specimen temperature of around 600 ˚C. The ambient environment did not permit an exact temperature to be achieved but a range of 596 ˚C to 610 ˚C, ± 1 ˚C, was obtained through a commanded temperature of 369 ˚C. It should be noted, though, that the position of the fretting pads plays a large role in the temperature of the specimen. Ownby, in his study, observed that if the specimen is brought to the temperature of 600 ˚C and the fretting pads are applied to the specimen, the specimen temperature drops quickly and dramatically because the fretting sled acts as a heat sink. The thermal energy imparted to the specimen equilibrates with the relatively cold fretting

pads and the sled to which the apparatus is attached. How this was mitigated will be discussed later in this chapter.

3.2 Experimental Configuration

The overarching purpose of this study is to load the specimens under fretting fatigue conditions until complete fracture in order to develop S-N curves for IN-100 at 600 °C and at an increased contact load of 8006 N. In order to successfully complete this larger goal, there are numerous steps that must be taken in order to ensure the successfully completion of the individual tests.

The first step in these tests is to measure the physical dimensions of the test specimen and the fretting pads. An indelible marker is used to mark the center line of each fretting pad as well as the specimen. These lines will later be used to ensure that the pads are properly aligned, a very important step to ensure proper testing configuration. Each section's gauge section is then measured in order to determine the cross-sectional area for use in load determination. The specimen and the fretting pads are now properly prepared for use.

The next and, as mentioned, one of the most important steps in executing a quality test is properly aligning the specimen and the fretting pads in the grips and the fretting actuators. Each specimen must be loaded in the center of the upper and lower grips such that the middle of the gauge section aligns with the centerline of the fretting pads. It is also very important to ensure that the specimen is aligned completely vertically in order to prevent any torsion or bending loads during testing. The fretting pads are loaded in the fretting actuator by way of a collar system (Figure 3.6), allowing no motion except that of a rotational manner along their longitudinal axis. The fretting pads can be aligned using a

simple leveling technique devised by Ownby. It has been shown that this method results in an estimated error of no more than 0.4 degrees from horizontal and the curved faces of the fretting pads are aligned such that the front, back, top and bottom surfaces are flush. The center line drawn on each fretting pad should line up exactly with the center line drawn on the other pad and the line drawn on the center of the gage section of the specimen. The proof of good alignment is taken by using pressure sensitive paper inserted between the fretting pads faces and the specimen (Figure 3.7). The fretting pads are closed by applying a force using the fretting actuator. If the alignment of the pads is appropriate, then the Hertzian shape embossed on the pressure sensitive paper should be a symmetric rectangle on both sides of the specimen. If this is not the case the pads are adjusted until the alignment is as close to ideal as possible. This is a trial and error process and has the potential to be extremely sensitive to adjustments. Once the fretting pads are properly aligned, the setup is almost completely prepared.

In order to ensure that the proper loads are applied to the test specimen, the next step tunes the servo-hydraulic controller. This is accomplished using the internal auto-tuning process that is built into the MPT software. By tuning the controllers before each test, any unnecessary error can be avoided because different specimens require different loads and will respond differently to these differing loads. The fretting load used for all tests in this study was a constant load of 8006 N, twice the fretting load used by Ownby, while the axial load was a sinusoidal waveform with a frequency of 10 Hz with a constant stress ratio of 0.03. This stress ratio and the specimen cross-sectional area were used to calculate the desired maximum and minimum load required for each specific test. These values are then used as input for the MPT software. Using these values, a specific sequence of events is loaded into a procedure which will be used by the software to

automatically control the equipment. This allows the tests to be run without constant input and observation. Each test has its own automated procedure using values specific to the desired loading conditions.

As mentioned, the test procedure that is put into the MPT software controls each step of the experiment from start to finish. Each procedure consists of several carefully ordered steps that are executed to control the temperature and loading conditions. The procedures are also formatted to collect data and cease loading as soon as the specimen fractures. The first step every procedure is to increase the commanded temperature to a value of 369˚C over a period of fifteen minutes.   After the commanded temperature reaches the value of 369˚C, and the specimen reaches the desired value of 600 ˚C, the temperature is held, within a range of ± 15 ˚C, for a period of fifteen minutes. This ensures that the temperature of the specimen reaches a full equilibrium with the sled that holds the fretting actuator and the heater boxes. The procedure is designed such that the next step will not commence until the temperature has remained at 369˚C for this period of time. Should the temperature exceed this range, the dwell period commences again.

After the temperature is successfully held at 369˚C for the full dwell period, the procedure commences applying the fretting pads. As noted by Ownby, this was done in a manner to avoid introducing a large heat sink while the specimen was at its operating temperature. Ownby accomplished this by applying the fretting pads with a small load of about 132 N to allow the specimen to slip easily in between the fretting pads. This is necessary because as the fretting pads were applied and the heat sink was introduced, the specimen would contract quickly. If this were to happen under the full testing load it would pinch the specimen and keep the top portion from moving freely as it underwent normal thermal changes. This then led to the top portion of the specimen being initially

50

held in a compressive load of approximately 300 to 400 N which ultimately biased the shear force data.

The next step saw the maximum axial load, as previously calculated, applied through a ramp function followed by the application of the full fretting load of 8006 N. Once the initial loading conditions were achieved the fatigue loading portion of the test would begin. The fatigue loading step is programmed to apply sinusoidal waveform of frequency 10 Hz using a peak-valley compensator to ensure that the target maximum and minimum axial loads to the specimen are met. This ensured a constant stress ratio of 0.03 while simultaneously applying a constant fretting load of 8006 N.

Concurrent with the commencement of the fatigue loading, the procedure would automatically begin collecting data. The data collected included the load cell values of the upper and lower grips, the applied fretting force, the upper and lower displacements, the running time and cycle count of the experiment and the temperature reading of each thermocouple. Data was collected at a linear interval of every 200 cycles as well as logarithmically up to 10,000,000 cycles. The fatigue loading and data collection steps continue until the machine detects that the specimen has fractured. At this time, the procedure automatically shuts down hydraulic power to both sets of grips and the fretting actuator.

3.3 Specimen and Fretting Pad Geometry

The complete dimensions of the dog bone specimens were previously presented in Figure 2.1. The gauge section of these specimens were 3.81 mm thick by 6.35 mm wide, yielding a cross sectional area of 24.1935 mm^2. The edges of the specimens were rounded slightly by grinding wheel and then were hand polished along with a very fine

grain sand paper to remove as many potential surface flaws as possible. The complete dimensions for the fretting pads, as presented in Figure 2.2, were 34.925 mm and 38.1 mm long for the left and right side pads respectively. The height and width of each pad was 9.525 mm and the curved circular surface had a radius of 50.8 mm. One half of the specimens and all of the fretting pads were cut from the same plate of stress relieved IN-100 by wire electrical discharge method and then ground to the final dimensions and a smooth surface. The other half of the specimens were cut from a plate of virgin IN-100 with no stress relief.

3.4 Load Determination

The loading conditions placed on each specimen during the test are determined for later analysis. It can easily be seen that the axial stress is the force measured by the lower load cell applied across the cross sectional area of the gage section, which was calculated previously. The shear force is not as obviously inferred and can be calculated from the data collected by the following equation:

$$Q = \frac{V - W}{2} \qquad (3.1)$$

where V is the force measured by the lower load cell and W the force measured by the upper load cell and Q is the resulting shear force on each side of the specimen that is obtained from the logarithmically spaced data file prepared by the MPT software. These values of the shear forces will prove to be very useful in order to demonstrate how well the fretting conditions were met during each study. By plotting the number of cycles against the observed Q values for each test, a hysteresis plot will develop. These hysteresis loops should be of an oval shape at low numbers of cycles, but should form a

52

straight line at higher numbers of cycles. This will indicate good fretting conditions because no mechanical energy is being lost to slip. This is the point where the fretting pads no longer undergo gross slip with respect to the specimen.

As this is a continuation of Ownby's [11] study, this study continued to exhibit a key problem with reference to the fretting actuators. It was observed that the applied contact load was slightly out of phase with the applied axial load, varying slightly from the specified constant value of 8006N. A screen capture from the MPT software can be seen in Figure 3.8. From this figure, it can be seen that the transverse contact load is roughly 8 microseconds behind the axial load as measured by the lower load cell. Ownby determined that this issue was due to the design of the fretting actuator in that it was behaving like a cantilever beam and exhibiting a relatively large oscillatory motion due to the axial loading. Ownby made attempts to try and arrest this vibration to no effect. It was determined that this problem could be corrected by applying a small phase shift to the measured transverse contact load. Once this was done, the hysteresis plots better resembled their expected behavior. This analysis will be discussed in more detail in Chapter IV.

3.5 Crack Development

Observing the crack initiation location, orientation, and the various stages of its growth within each specimen are all crucial to understanding fretting fatigue. After fracture, a fretting fatigue specimen should be carefully analyzed under microscopes in order to determine the above as well as the manner in which it failed. This will give great insight into what each specimen experienced during a test. Each set of fretting pads will leave very clear markings on the contact area of the specimen that can be observed and

measured to determine the actual contact half width and contact shape of the test. These markings are also referred to as fretting scars due to the fact that the fretting pads leave this damage during the fretting process. An example of fretting scars on a set of fretting pads can be observed in Figure 3.9. In this figure, with the left side of the specimen on the upper left and the right side of the specimen on the upper right, the scars can be clearly seen. The damage done to the pads can also be seen, with the left pad on the left and the right pad on the right. By analyzing these fretting scars from each of the tests, one can easily determine where the crack ultimately responsible for the failure of the specimen initiated. It is expected that the cracks will initiate near the edge of the contact region. A Scanning Electron Microscope (SEM) can also be used to observe in great detail the fracture surfaces of the specimens. The image of the fracture surface can then be analyzed for the point at which the crack initiates, its orientation, and the stages of propagation. An example of an SEM micrograph from this study can be seen in Figure 3.10. The full complement of micrographs from this study can be seen in Appendix B.

Figure 3.1 – MTS Machine
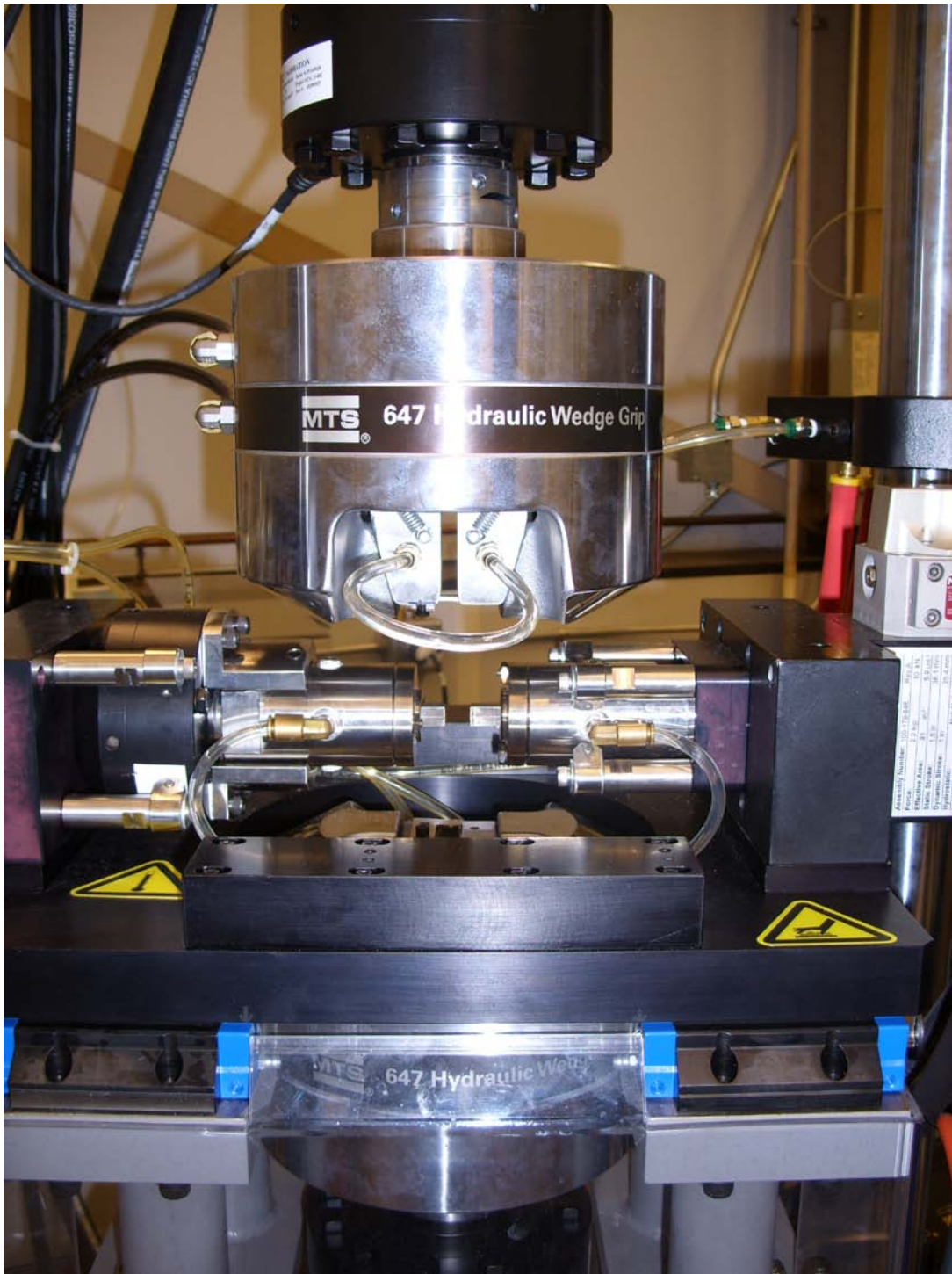
Figure 3.2 – Close-up of Upper and Lower Grips
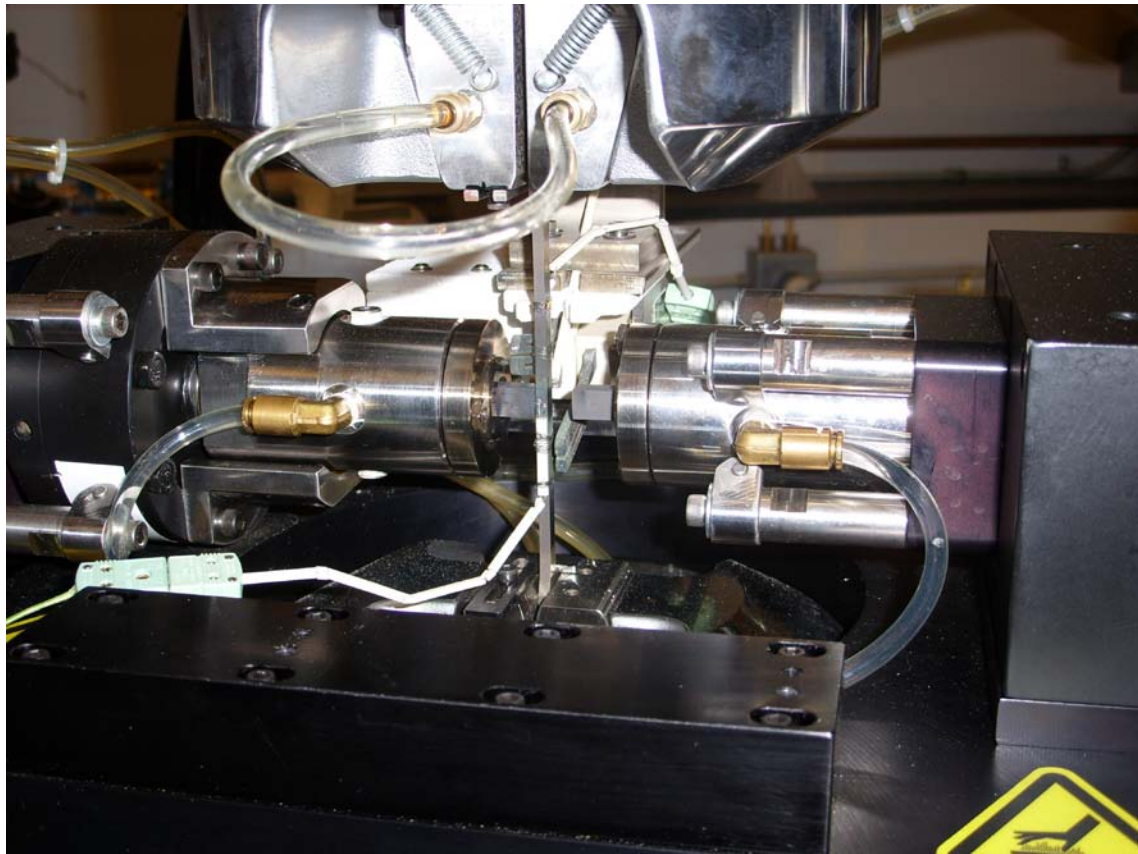
Figure 3.3 – Close-up of fretting actuator
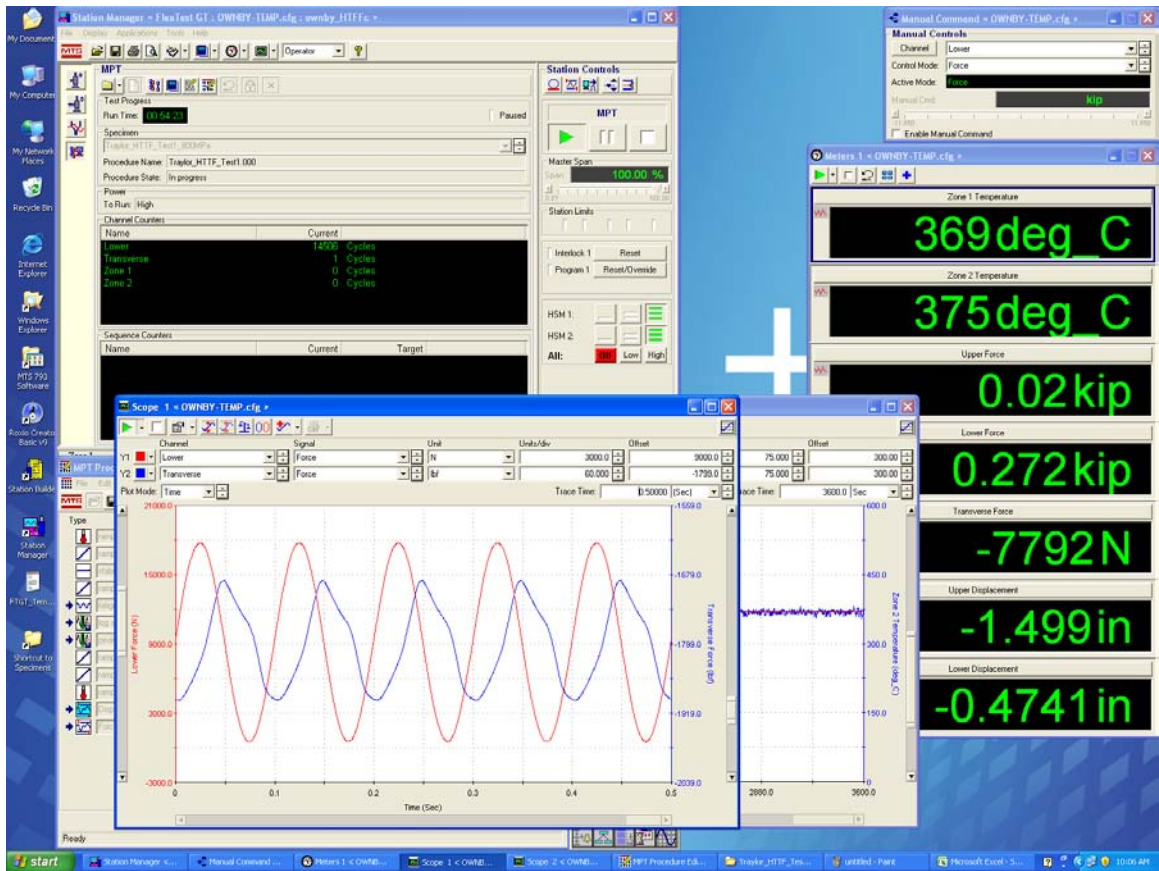
Figure 3.4 – MPT Software, Specimen #1

Figure 3.5 – Heating element/thermocouple apparatus

Figure 3.6 – Fretting pad collar assembly
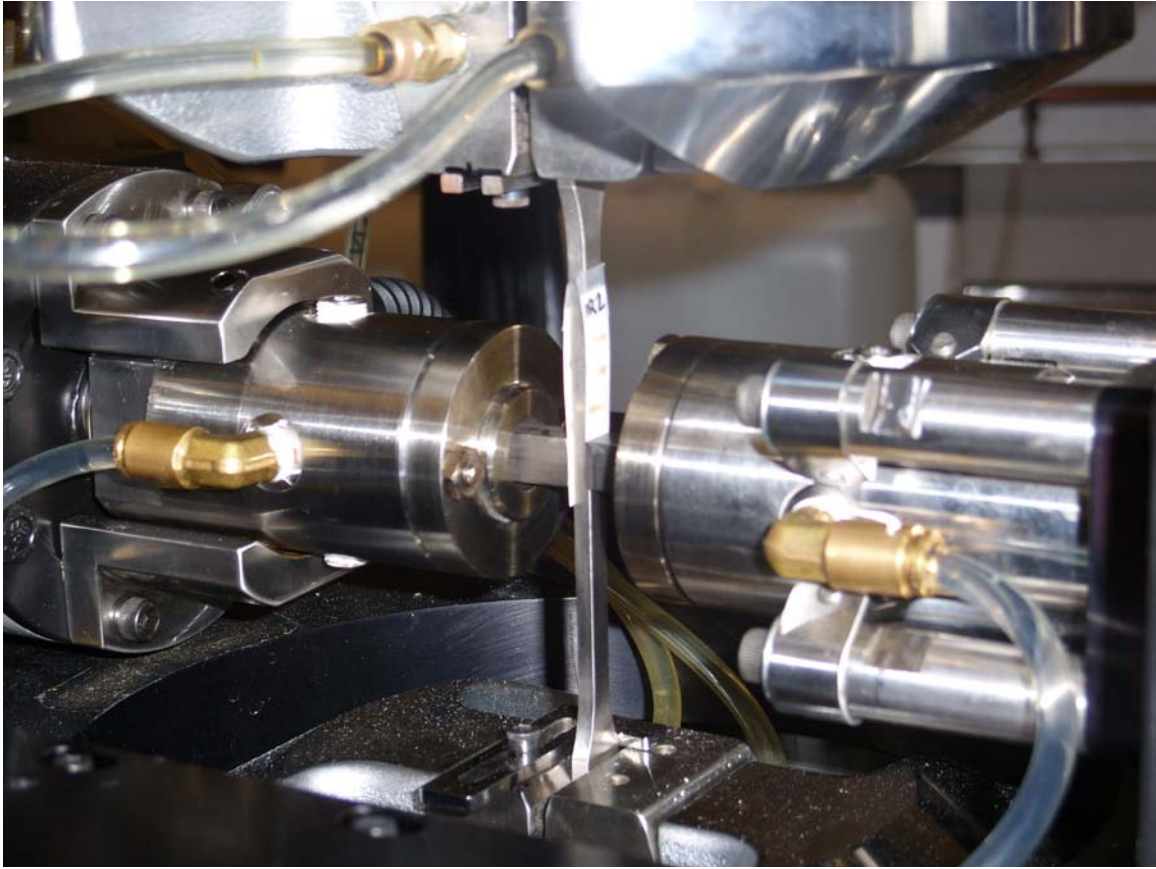
Figure 3.7 – Pad alignment using pressure sensitive paper
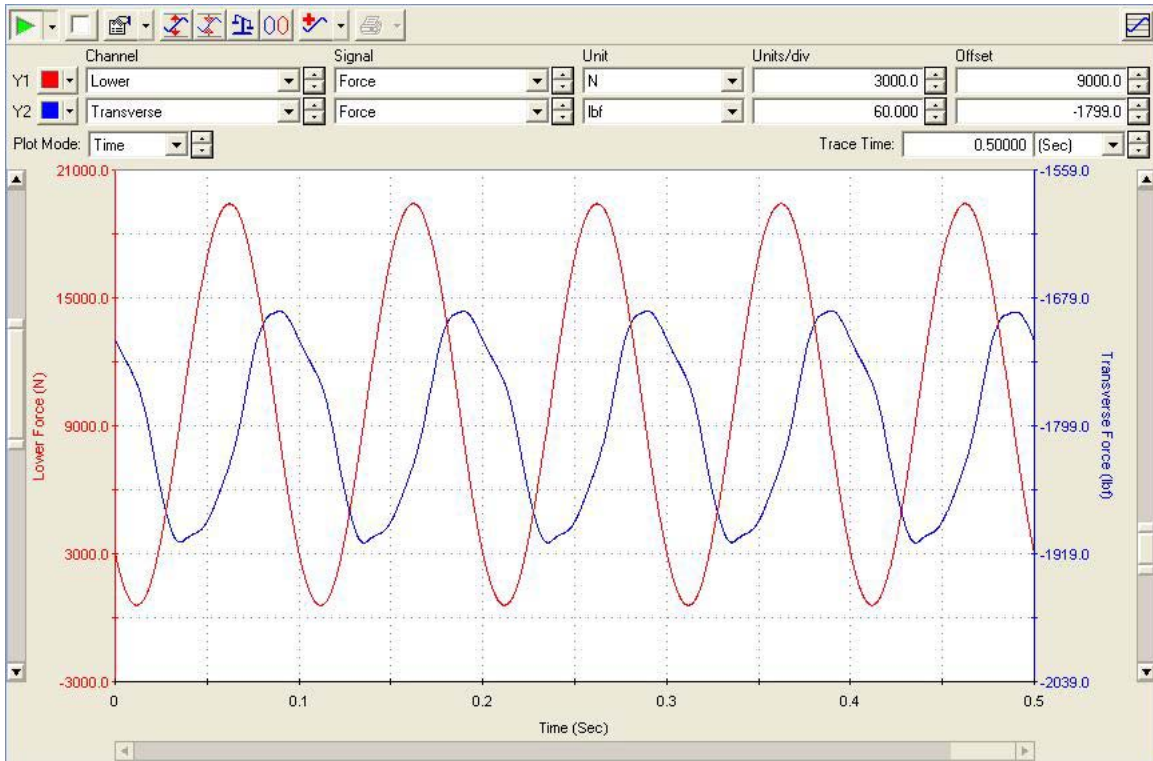
Figure 3.8 – Out of phase contact load

Figure 3.9 – Optical micrographs of Specimen #2
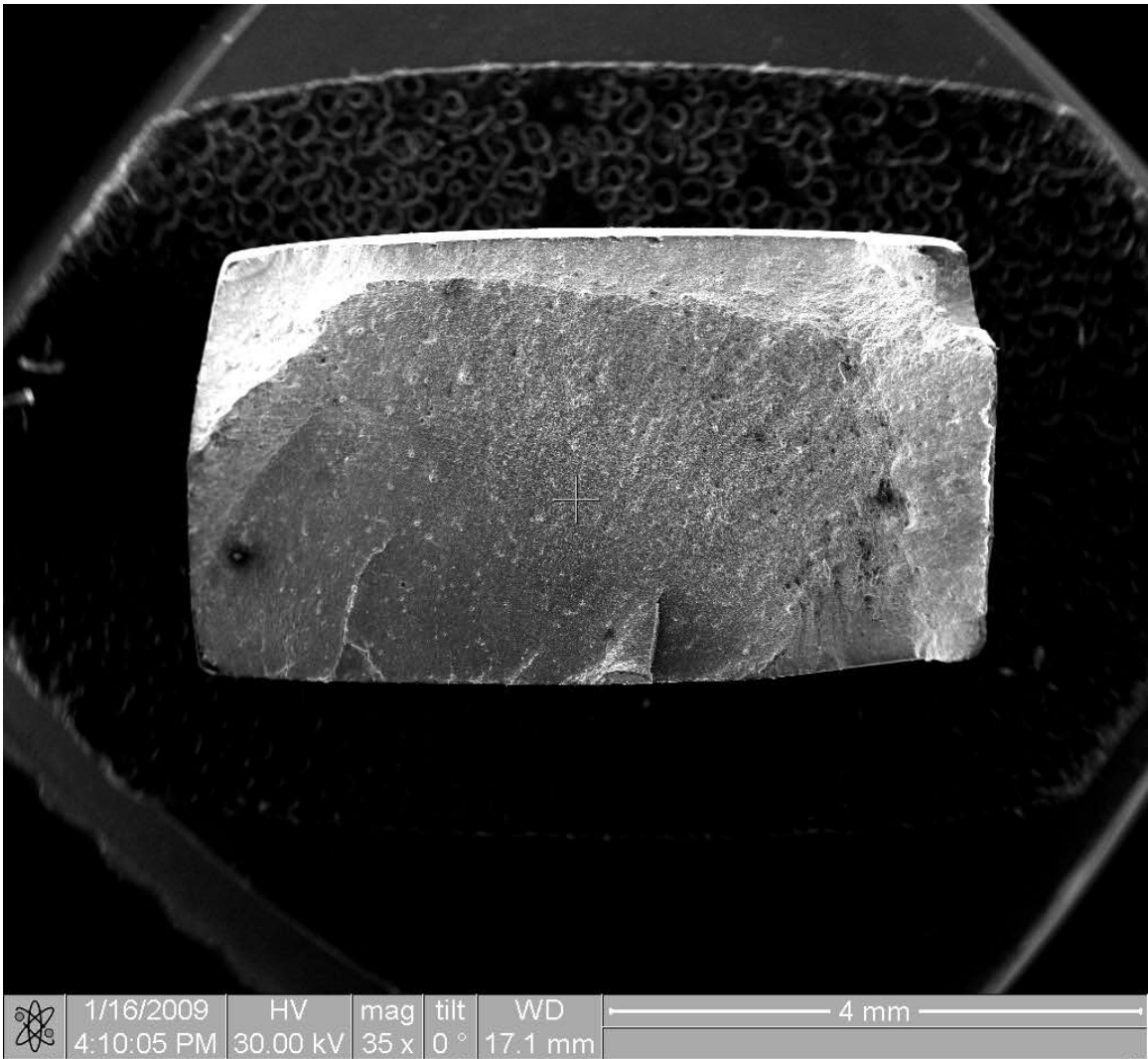
Figure 3.10 – SEM micrograph of Specimen #2

IV. Results and Discussion

This chapter will focus on the experimental data. It will begin with an evaluation of the various aspects of the fretting condition such as partial slip, contact width, the fracture surface and crack initiation locations and progression. This will be followed by a comparison of the data from previous tests by Ownby [11], Mahdi [12], and Saladin [13], with Ownby's study being the most similar to this study. Finally, comparisons are made between the results of this study and other published studies of both high temperature and high contact load using various materials. This will be used to evaluate the relevance and applicability of this study.

4.1 Experimental Results

Throughout this study, a total of ten independent tests were conducted. Five tests were conducted under high temperature and an elevated contact load with the annealed IN-100 used by Ownby [11]. The other five tests were conducted using samples of IN-100 from a virgin, un-annealed material. A summary of the results of this study can be seen in Table 4.1. As previously mentioned, the stress ratio for each test was kept at a constant value of R=0.03. All tests were conducted with fretting pads of the same geometry and under the same contact loading conditions with varying axial loads.

The accomplishment of this study was the generation of a plot of the applied stress range versus the number of cycles to failure, commonly called an S-N curve. This curve gives great insight into the performance of a material under fatigue loading conditions and can greatly aid in maintenance of critical components. The S-N curve for this study, IN-100 under increased contact load and elevated temperature, can be seen in Figure 4.1. Tests 1 through 5 were conducted using specimens from Ownby's previous

work, an annealed IN-100. This material was also the same materials tested by Saladin [13] at room temperature. Though Ownby [11], Mahdi [12], and Saladin [13] all conducted fretting fatigue studies with IN-100, this study will refer mostly to Ownby due to the similar nature of study, differing only in contact load. A comparison to Ownby's high temperature fretting fatigue data can be seen in Figure 4.2. Tests 6 through 10 were performed with a un-annealed plate of IN-100. It should be noted that all tests were conducted using different axial loading. The only exception to this is tests 8 and 9. During test 8, a power outage caused a mechanical shutdown of the test equipment. The last known value of the number of cycles is reported but is not the number of cycles to failure. Test 9 used the same axial loading value in order to obtain a value for number of cycles to failure at this level. It should be noted that tests 5, 8, 9, and 10 were not carried out until specimen failure. These tests, except 8, were all carried out over several million cycles before it was determined that this values would suffice in a normal loading situation for a typical turbine engine component. All specimens which were loaded until failure were observed to fail in the fretting contact region as expected. The exact method of failure for each specimen will be discussed later in this chapter. It was observed that the contact load of 8006 N led to a decreased fatigue life when compared to that at 4003 N studied by Ownby [11]. A difference was also seen in the fatigue life of the annealed specimens when compared to the un-annealed specimens in that the un-annealed specimens exhibited more scatter in comparison to the almost linear relationship for the annealed specimens. These results will be analyzed and discussed later in this chapter.

4.1.1 Evaluation of Fretting Fatigue Conditions

There are several various criteria which can be applied to ensure that the proper conditions were met for a successful fretting fatigue test. In order to validate that a test met requisite fretting fatigue conditions, one should confirm that a microslip condition was achieved. An indirect method to accomplish this can be used by using the data collected from the MPT software. By calculating the shear force, Q, using Equation 3.1 and plotting it against the applied axial stress one can develop hysteresis plots. These plots, as mentioned previously, a hysteresis plot can be used to indicate fretting conditions because they should show no mechanical energy being lost to slip. A straight line shows that no energy is being lost to slippage and, therefore, partial slip fretting is occurring. As the number of cycles increases, it is expected that this will happen. Typically the fretting condition should be reached within the first 1,000 cycles of the test.

Using the same experimental setup and MPT software as Ownby, experiencing the same anomaly in data collection that was noticed in his results was expected. He showed that the data from each of the fretting tests in this study did not initially indicate a fretting condition. He found, as did this author, that the peak axial stress and peak shear force were slightly out of phase with one another. Using the correction method derived by Ownby, applying a small phase differential to the shear force, the hysteresis plots collapse to form a line as originally expected. The following section describes this technique in more detail.

4.1.2 Establishment of Partial Slip Condition Using Ownby's Correction

The contact load, P, was commanded to be constant value of 8006 N for all fretting fatigue tests. During the entirety of the tests, this value should remain a constant.

It was observed, as mentioned in Section 3.4, that this was not the case and a slight sinusoidal loading was observed. It was also observed that this loading was slightly out of phase with the axial loading. While the contact load was observed to be sinusoidal, a relatively constant variation was observed over all tests. This was not seen as a factor affecting the results. It does, however, pose a problem for the generation of hysteresis plots.

As Ownby observed, in order to correct for this phase difference first the axial loading must be compared with the calculated tangential loading. It can be seen in Figure 4.3 that the sinusoidal waveforms of both the applied axial loads and the calculated tangential load over time for test 5 at the 1,000,000[th] cycle are not in alignment as one would expect. From this it can be discerned that there is a slight phase difference equal to approximately 17.5 degrees.

After this correction was applied, by shifting the shear force by 17.5 degrees, a new hysteresis plot was created (Figure 4.4). This plot shows that once the phase correction was applied, the hysteresis loop approached the expected straight line. After this adjustment in the loading, it would be expected that as the specimen and pad would certainly be experiencing the fretting conditions without slip. Similar analyses were completed for the other tests conducted in this study and it was found that this phase difference was constant over the range of all specimens and did not vary with varying axial load. This correction can now be applied to all of the data collected by the MPT software.

4.1.3 Half Contact Width

Another characteristic of a proper fretting fatigue test is the fretting scar that is left on each side of each specimen as well on each fretting pad. This is one of the more obvious and visible suggestions that fretting has occurred. The half contact width, which was presented previously in Equation 2.8a, can be calculated theoretically. It can also be measured experimentally after a fretting experiment. In this study, each specimen and each set of fretting pads were analyzed under an optical microscope for the purpose of comparing the theoretical values of half contact width to the experimental values. A summary of these values can be seen in Table 4.3. Though these tests do not exactly match the theoretical value calculated for this loading condition, $2a_{exp}=1632$ micrometers, they all closely approximate the expected value. In an experimental setup with as many variables as this, it would be very difficult to achieve a test that exactly matched the theoretical value. One of the main concerns, with reference to why the experimental values for the half contact width do not exactly match the theoretical value, could more than likely be the variable sinusoidal load seen in the contact load. This should be a constant value but it was shown that it was not. This made it harder to distinguish the exact width that was the half contact width. Optical micrographs from the specimens and fretting pads can be seen in Appendix B.

4.1.4 Crack Initiation Location and Angle

According to theory, cracks should initiate at the location within the material where the contact stress conditions, namely the shear stress, is at a maximum. It has been shown previously that the point of maximum shear stress can be found on a critical plane which is located between the contact surface and the contact load. Fortunately, it

is possible to analyze each specimen after failure in order to determine the crack initiation location and angle of initiation. Using a scanning electron microscope, in combination with the previously captured optical microscope images of each specimen, the exact nature, location, and angle of the initiated crack can be determined. For these images, please see Appendix B.

It can be seen in the images in Appendix B that the fatigue cracks caused by the fretting conditions originate at or near the edge of the contact region, as expected after a review of the analytical predictions in the previous sections. These images, both from the optical as well as from the scanning electron microscope, clearly show that fretting fatigue crack initiation occurs near the edge of the contact region. The optical micrographs show that the fracture of each specimen began at the edge of the fretting scar left on the specimen by each fretting pad. This is expected as these scars coincide with the contact regions. In each of the SEM images of the fracture surfaces, the crack initiation location is easily determined. These locations are examined in greater detail using higher magnification and can be seen in Figures 4.7 through 4.14. The complete set of SEM images for all specimens can be seen in Appendix B. Once the crack initiation locations are determined, it is then possible to determine the crack initiation angles by sectioning the specimen and examining each with the SEM. The sectioned specimen, from test 2, was used to determine the crack initiation angle of 45˚ (Figure 4.15). Buy using these microscopy images, a validation of proper fretting fatigue testing conditions can be achieved. The specimens in this study all failed in the expected method and show the characteristic traits of fretting fatigue.

4.1.5 Fracture Surface

The fracture surface is exactly as it sounds; it is the face on each portion of the fractured specimen where the material separated at failure. The careful analysis of this surface gives great insight into the mechanisms which caused the failure. It should be evident that each fracture surface is a mirror of the other as each separated from the other during failure. Due to the experimental setup in this study, only the lower fracture surfaces are analyzed. After each specimen fractures, the lower grip of the MTS machine lowered out of the elevated temperature zone because it was kept in force control while the upper grip remained in displacement control. The upper fracture surface remained in this zone until the operator turned off the heater boxes and therefore was extremely oxidized and unusable for the purposes of further microscopy analysis.

As noted in previous sections, there are four stages of fatigue crack growth: I. crack initiation, II. crack propagation due to bulk and contact stresses, III. propagation due to bulk stresses, and IV. fracture. These zones can be clearly seen in the SEM micrographs presented in Figures 4.16 and 4.17. Dashed lines have been added as well as text labels to highlight the different regions each labeled with a roman numeral, I - IV, associating it with the particular stage of crack development of that region. Also labeled is the location determined to be the origin of the fretting induced crack.

Of particular interest are the relative sizes of each zone. The crack initiation zone is usually the smallest. Each successive zone is usually larger the previous zone. This is due to the fact that as the crack propagates, its rate of propagation increases. It should not be thought that the relative size of each zone is representative of the time spent in that zone of crack growth. As an example, zone IV appears to be the largest in most specimens. This zone is where fracture of the specimen occurs. This zone is actually the

71

zone where the least time is spent in crack propagation. This is because as the cracks grow large enough such that the combination of crack geometry and loading is found to be equal to the critical stress intensity factor, K_{IC}, fracture occurs instantly. On the other hand, zone I is usually observed to be the smallest stage in most specimens. It should be noted that it was presented in Chapter II that most time in crack propagation is spent in this zone. Hence, it can be seen that the length of each crack initiation stage is inversely proportional the area of the respective zone on the fracture surface. This shows that cracks initiate very slowly and continue to propagate with ever increasing speed.

Much like above, another general relationship can be inferred through the comparison of the relative sizes of the zones associated with same stages from different specimens and the relationship of the applied loads from those stages. This will help to visualize how the axial loading contributes to both the crack initiation as well as the speed at which cracks propagate under fretting conditions. The best specimens where this can be observed are from tests 1 through 4. Coincidently, these tests all were conducted with annealed IN-100 specimens. These specimens showed a clearer delineation between the zones of crack propagation. These same zones of the un-annealed specimens were not as distinct because of the variability in the composition of the material with respect to the individual grains and internal stresses which were not relieved as in the annealed specimens. In order of increasing axial load, these specimens are arranged: Test 4 ($\Delta\sigma$=630.5 MPa), test 2 ($\Delta\sigma$=703.25 MPa), test 1 ($\Delta\sigma$=776 MPa), and test 3 ($\Delta\sigma$=848.75 MPa). It can be roughly shown that as the axial load increases the size of the respectively zones of propagation I through III decrease and zone IV increases. As noted previously, the size of these zones are inversely proportional to the time spent in each respective zone. This would show that, in general, as the axial load was increased

the cracks initiated and propagated quicker and fracture occurs in a much more catastrophic manner.

4.2 Contact Load Effect on Fretting Fatigue

The ultimate purpose of this study is to determine what effect an increased contact load has on the fretting fatigue properties of IN-100 at an elevated temperature of $600\,°C$. In order to effectively determine the effects of an increased contact load it is best to compare data from several different similar experimental scenarios in order to isolate the characteristics that are unique to a high contact load fretting environment. It would follow that that these isolated characteristics are what must be responsible for any change in behavior. Due to the similar nature of study, this study utilizes the data provided from Ownby's [11] study as a primary comparison but also uses Madhi's [12] and Saladin's [13] previous IN-100 fretting fatigue studies.

4.2.1 Contact Load versus High Temperature Fretting Fatigue

The conclusions reached by Ownby [11], Mahdi [12] and Saladin [13] all confirm that fretting fatigue life is less than plain fatigue life under identical stress ranges. Ownby showed that fretting fatigue life under elevated temperatures is increased when compared to identical experimental conditions at room temperature. These results are all summarized and presented in Table 4.4. They can be seen visually in a compilation of S-N curves in Figures 4.18 through 4.21. Now to take these results a step further, they will be compared to an experimental setup which also includes a much higher fretting contact load. The contact load used by Ownby was set at a constant value of 4003 N while the contact load used in this study was twice that, 8006 N. By comparing results, it can be

73

seen that the results of this study, namely the fretting fatigue life at an elevated temperature of 600˚C, show a marked decrease in fretting fatigue life at the increased contact load. It has been determined that the elevated contact load decreased the fretting fatigue life of each IN-100 specimen anywhere from 70% to 92% of the value observed by Ownby. This is a drastic decrease in fatigue life which one must consider before the use of this metal in an environment where it will be exposed to both fretting fatigue and increased contact loads. As turbine engines become more powerful, they are bound to experience these increase contact loads as more and better performance is demanded of them by engineers. Engineers should keep this relationship in mind at all times for the safety of those involved.

4.2.2 Elevated Temperature & Contact Load versus RoomTemperature Fretting Fatigue

Though not directly comparable, the relationship between a fretting fatigue study under an increased contact load and elevated temperature and a room temperature fretting fatigue study showed interesting results. Both Mahdi [12] and Saladin [13] preceded Ownby by conducting fretting fatigue tests with IN-100 at room temperature. By comparing the data from this study to these studies, it can be conjectured that an increased contact load might reduce the fretting fatigue life of a component experiencing fretting at room temperature by 26% to 80% based on the axial loading conditions. Unlike the reduction presented in the previous subsection, a direct correlation can be observed between the axial load and the subsequent reduction in fretting fatigue life with increased contact load. Again, it should be kept in mind that this data cannot be directly compared due to the dissimilarities in the experimental setup though the results of this comparison are interesting.

4.2.3 Annealed versus Un-Annealed Specimens

A new introduction into the present study is the inclusion of IN-100 specimens of both an annealed and an un-annealed nature. Both Ownby and Saladin used specimens that were cut from the same annealed IN-100 plate as specimens 1 through 5 in this study. Specimens 6 though 10 in this study were cut from an extruded, un-annealed plate of IN-100 from which Mahdi's specimens were cut. None of these previous studies included both types of specimens for comparison. Since these two types of specimens were tested under the exact same conditions, they can easily be compared.

Annealing is a process involving heating and cooling by which the microstructure is altered, causing changes in the material properties. This process can be used to change the ductility and strength and has been shown to relieve internal stresses, refine the internal structure of the metal, and negate the effects of cold working. Internal stresses can develop in metals due to plastic deformation processes such as machining and grinding, through non-uniform cooling during processing, or from a phase transformation that is induced upon cooling wherein parent and product phases have different densities [57]. A common annealing process to relieve internal stresses in a material is accomplished by heating the metal to a recommended temperature, holding it there long enough to attain a uniform temperature, and then allowing it to cool very slowly.

The results of this study show a generally clear decreasing trend in the fretting fatigue life of specimens as the axial stress is increased. The annealed specimens are almost aligned perfectly, except for test 3. The specimens of un-annealed IN-100, though, are not as clearly correlated. The first two tests conducted, 6 and 7, showed an encouraging trend similar to that of the annealed specimens. Tests 8 and 9 were the next un-annealed specimens to be tests. The problem with test 8 was previously discussed and

75

test 9 ran much longer than expected. It was anticipated that, after the first two tests with the un-annealed specimens, a trend similar to that of the annealed specimens would develop. This was not the case for these two specimens. Test 10 ran for almost 5 million cycles, more than the interpolated fatigue life of annealed specimens, but not excessively.

Overall, it was seen that a clear trend was observed for the annealed specimens. A less obvious trend was also observed for the un-annealed specimens. This can be attributed to the fact that the un-annealed specimens have not been relieved of their internal stresses as discussed above. This means that each specimen has the potential to fail based on these stresses, which could vary widely from specimen to specimen. In order to mitigate this, it is suggested that an annealing process be used with IN-100.

4.3 Relevance to Other Increased Contact Load Fretting Studies

This section will focus on the comparison of this study's results with other studies involving the effect of increased contact loads on fretting fatigue behavior. It was mentioned previously that few studies have been conducted on this topic and this author could find none that were conducted with any nickel-based alloy. While they are not ideal to the study of a nickel-based alloy, there were studies on the effects of contact load on other materials. Comparisons will be made between examinations of the effect of increased contact load on three aluminum alloys and austenitic stainless steel. The similarities and differences of each study's testing materials and conditions are discussed as well as the similarities and differences of their conclusions of the effect of increased contact loads. While these studies differ slightly in the experimental approach as well as in their material of study, many parallels and conclusions can be drawn that will be of great benefit in the study of this phenomenon in the nickel-based superalloy IN-100.

4.3.1 Comparison to Contact Load Effects on Al Alloy Fretting Studies

Several studies were introduced in Chapter II that examined the effect of an increased contact load on the fretting fatigue life of various aluminum alloys. Sadeler [53] investigated AA 2014 alloy, Adibnazari and Hoeppner [54] used the alloy 7075-T6, while Naidu and Raman [56] studied the Al-Mg-Si alloy AA 6061. Though each of these studies also focused on the effects of an increased contact load, a direct comparison to the results of this study is difficult to make. This study utilized a constant increased contact load with a varying axial load to predict the effects on the fretting fatigue life. The three aforementioned studies all utilized one or two axial loads and a varying increased contact load. Their goal was to determine if a contact load threshold existed where the effect of an increased contact load is negligible. While this study and these studies of aluminum alloys do not have the same objective, it is still possible to make conclusions from the results. These studies found that the fretting fatigue life did drastically decrease with an increase in contact load under a constant axial loading. A threshold was observed by the various authors at which no further effect is seen in the fretting fatigue life.

An example of these results that shows a decrease in fretting fatigue life with the increase of contact load, from the study by Naidu and Raman, can be seen in Figure 4.22. As mentioned previously, the authors concluded that a rapid increase in the coefficient of friction during the early stages of fretting is followed by a stabilization in which the coefficient remains approximately constant (Figure 4.23). It is this stabilization of the coefficient of friction between the fretting pads and the specimen which is responsible for the lack of an effect of any increase in contact load at higher values.

While these other studies were very similar in nature, this study showed that an increased contact load drastically decreased the fretting fatigue life of IN-100 over a

range of axial loadings. Even though these studies vary in the exact nature of their investigation, the results reveal a similar conclusion regarding the decrease in fretting fatigue life with an increase in contact load.

4.3.2 Comparison to Contact Load on Steel Fretting Study

Also in Chapter II, a study by Nakazawa et al [55] which examined the effect of an increased contact load on austenitic stainless steel was presented. Like the studies in the previous section, this study investigated how a variably increased contact load affected the fretting fatigue life. While this is not the exact method taken in this study, certain conclusions can still be made. These authors found that their stainless steel specimens acted much in the same manner as the aluminum specimens presented in the previous section. It was observed that as the contact load increased, the fretting fatigue life decreased drastically to a point. At this point, any increase in the contact load netted very little change in the fretting fatigue life (Figure 4.24). This study also drew a link between this apparent stabilization of the observed coefficient of friction and the lack of a response due to a further increase in contact load.

This can be applied to a nickel-based alloy due to the fact that the underlying mechanisms of fretting are common regardless of the material of interest. It is hard to say, however, how the coefficient of friction in IN-100, or any other nickel-based alloy, would behave during a study of a variably increasing contact load due to the effect of a glaze oxide formation. Overall, as with the studies of Aluminum alloys, the basic premise that as contact load increases the fretting fatigue life decreases can be extended. It is yet to be seen how IN-100 behaves under higher and higher contact loads.
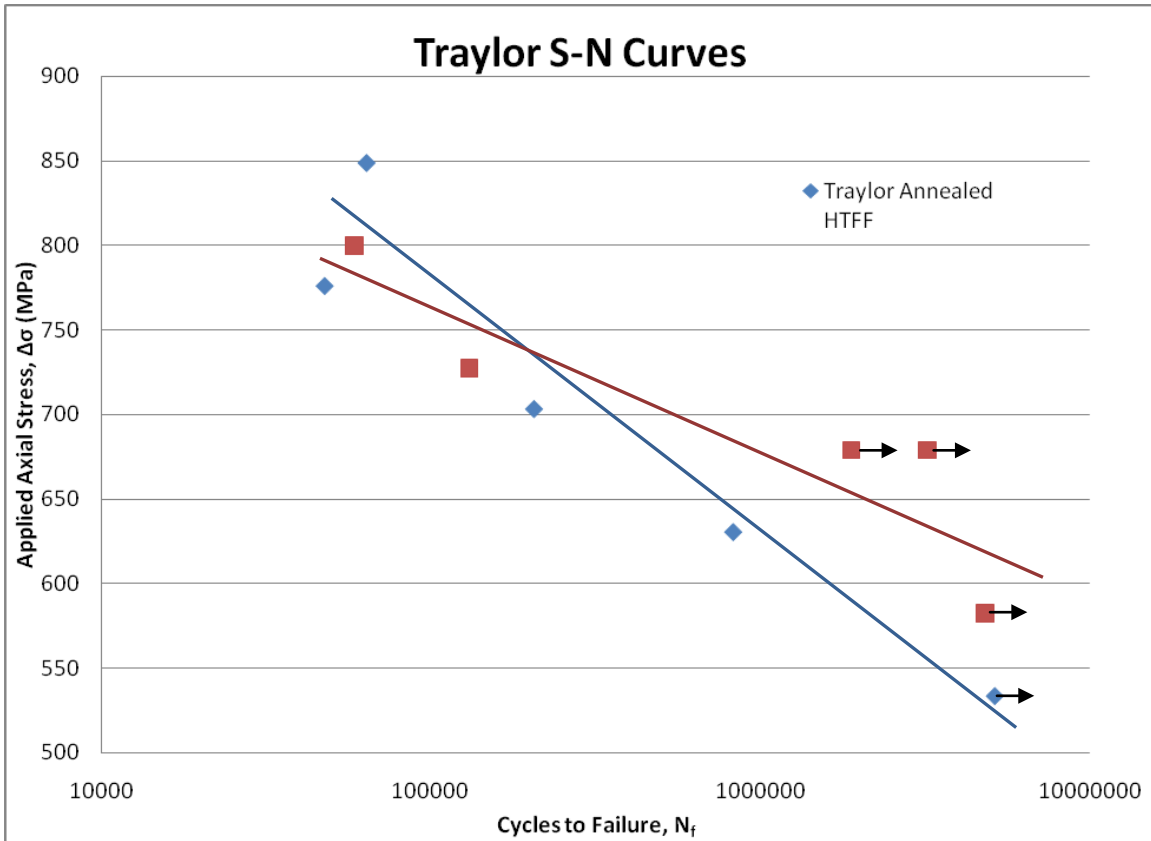
Figure 4.1 S-N curves for this study

(HTTF: High Temperature Fretting Fatigue)
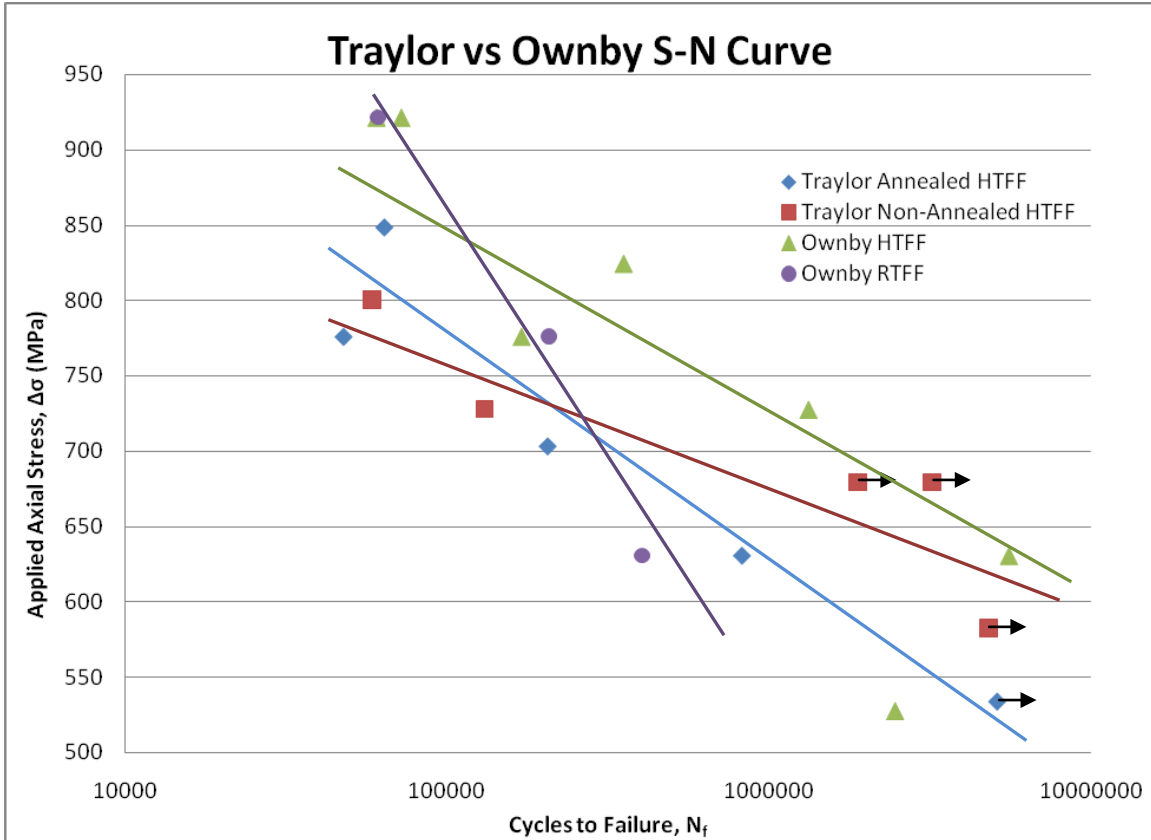
Figure 4.2 S-N curves for Traylor and Ownby

(RTTF: Room Temperature Fretting Fatigue)
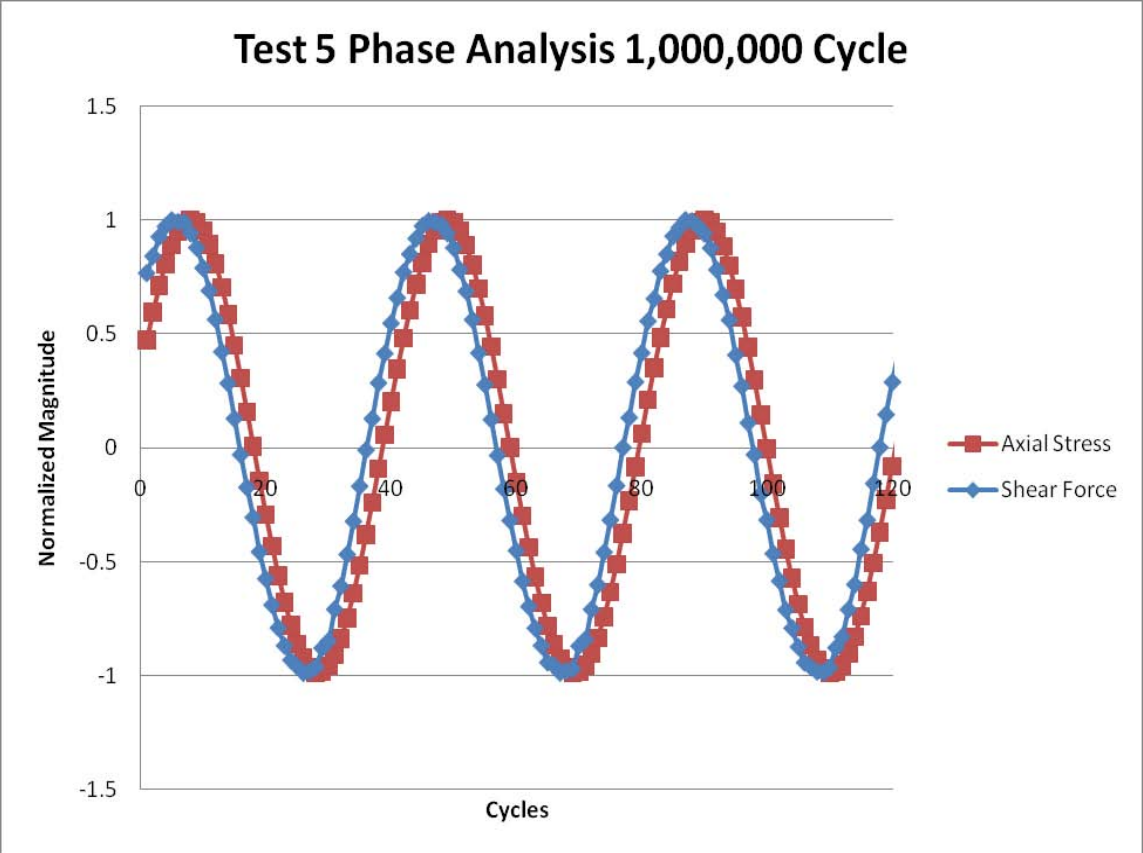
Figure 4.3 - Test 5 Phase analysis at 1,000,000[th] cycle
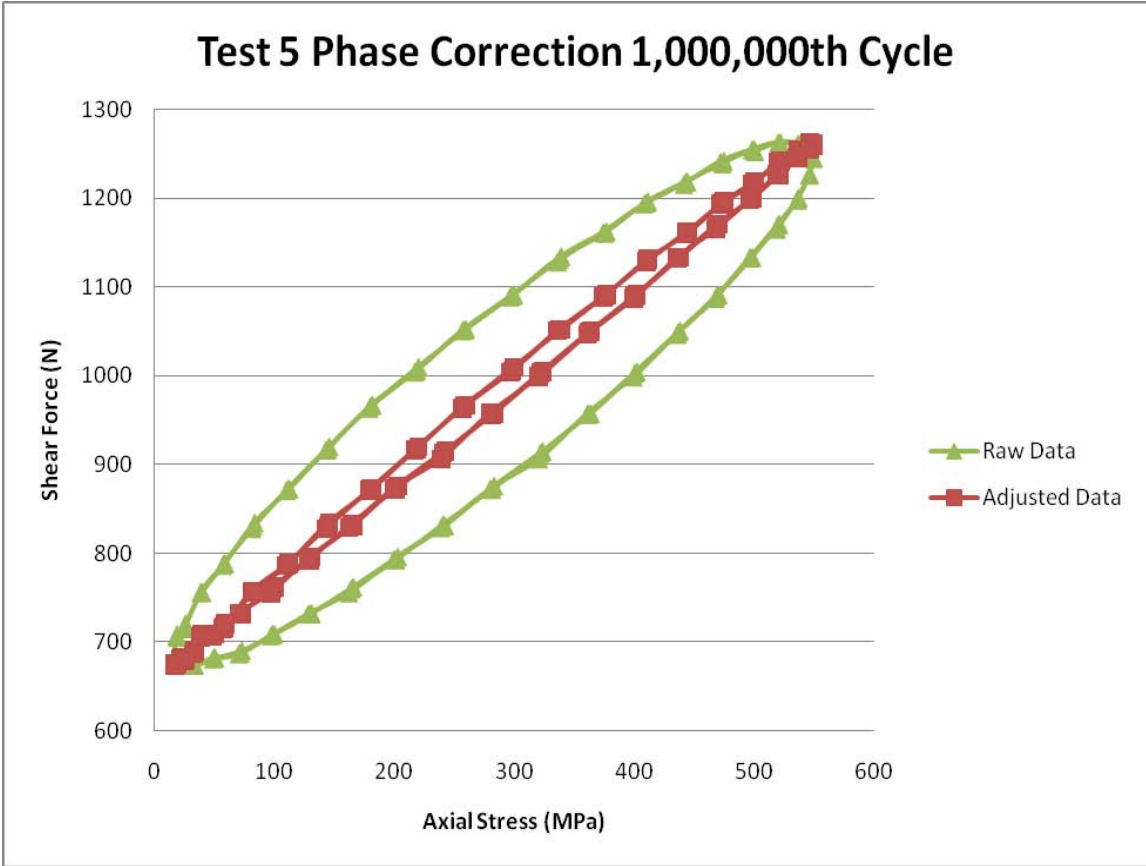
Figure 4.4 – Test 5 corrected and uncorrected hysteresis loop
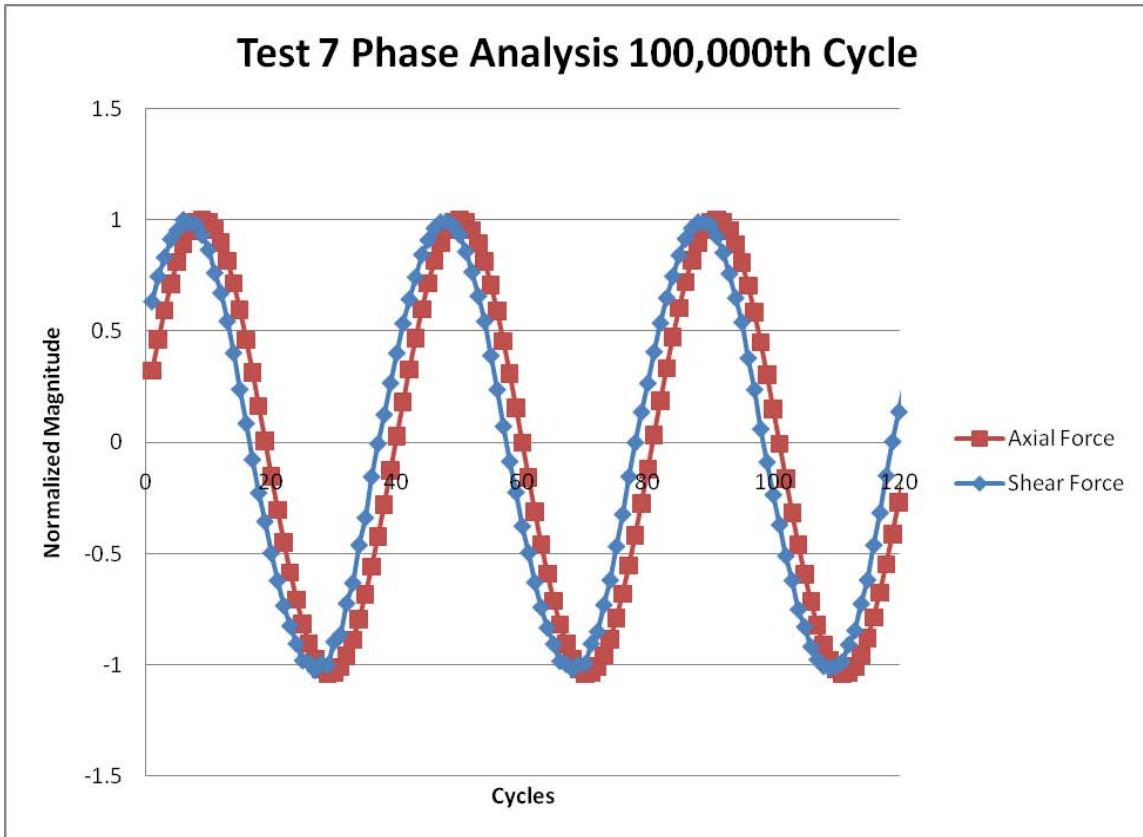
Figure 4.5 – Test 7 Phase analysis at 100,000th cycle
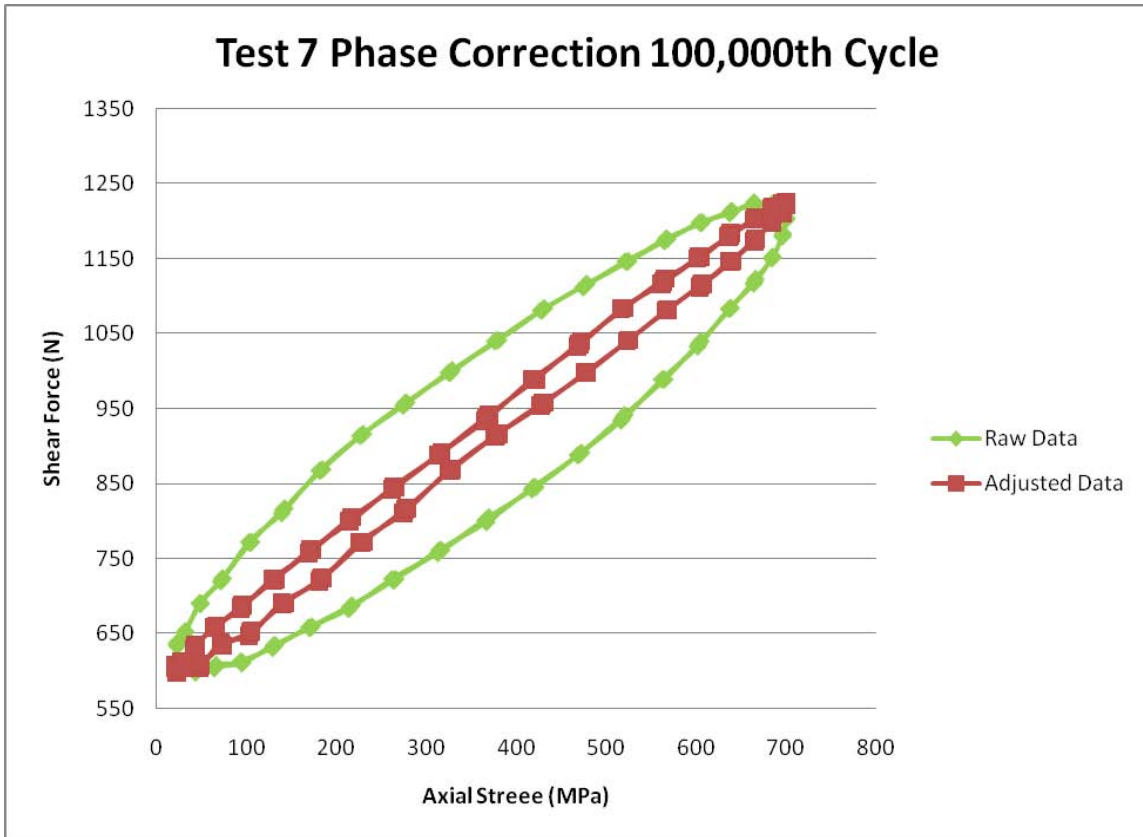
Figure 4.6 – Test 7 corrected and uncorrected hysteresis loop
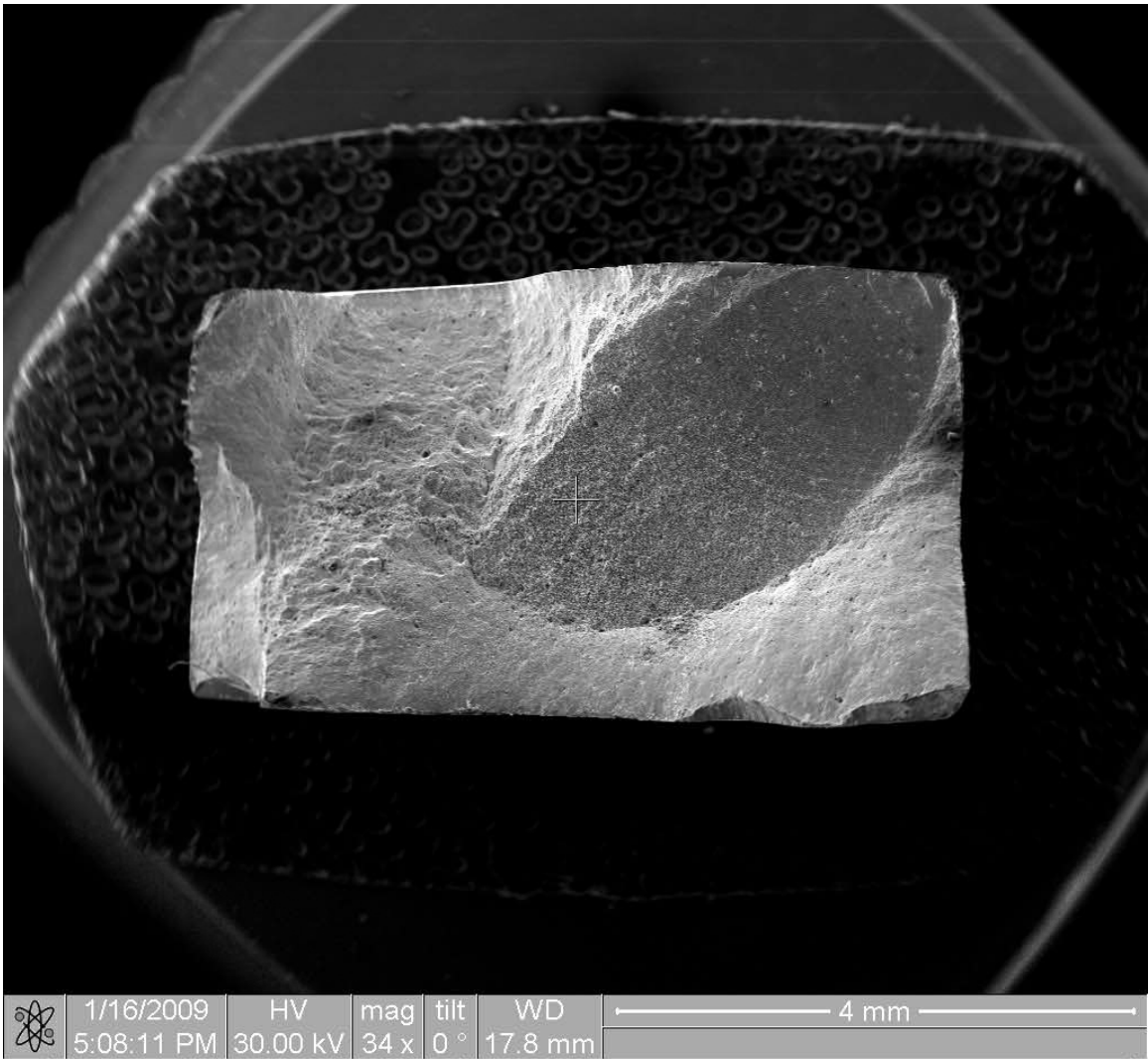
Figure 4.7 – Specimen 3, fracture surface
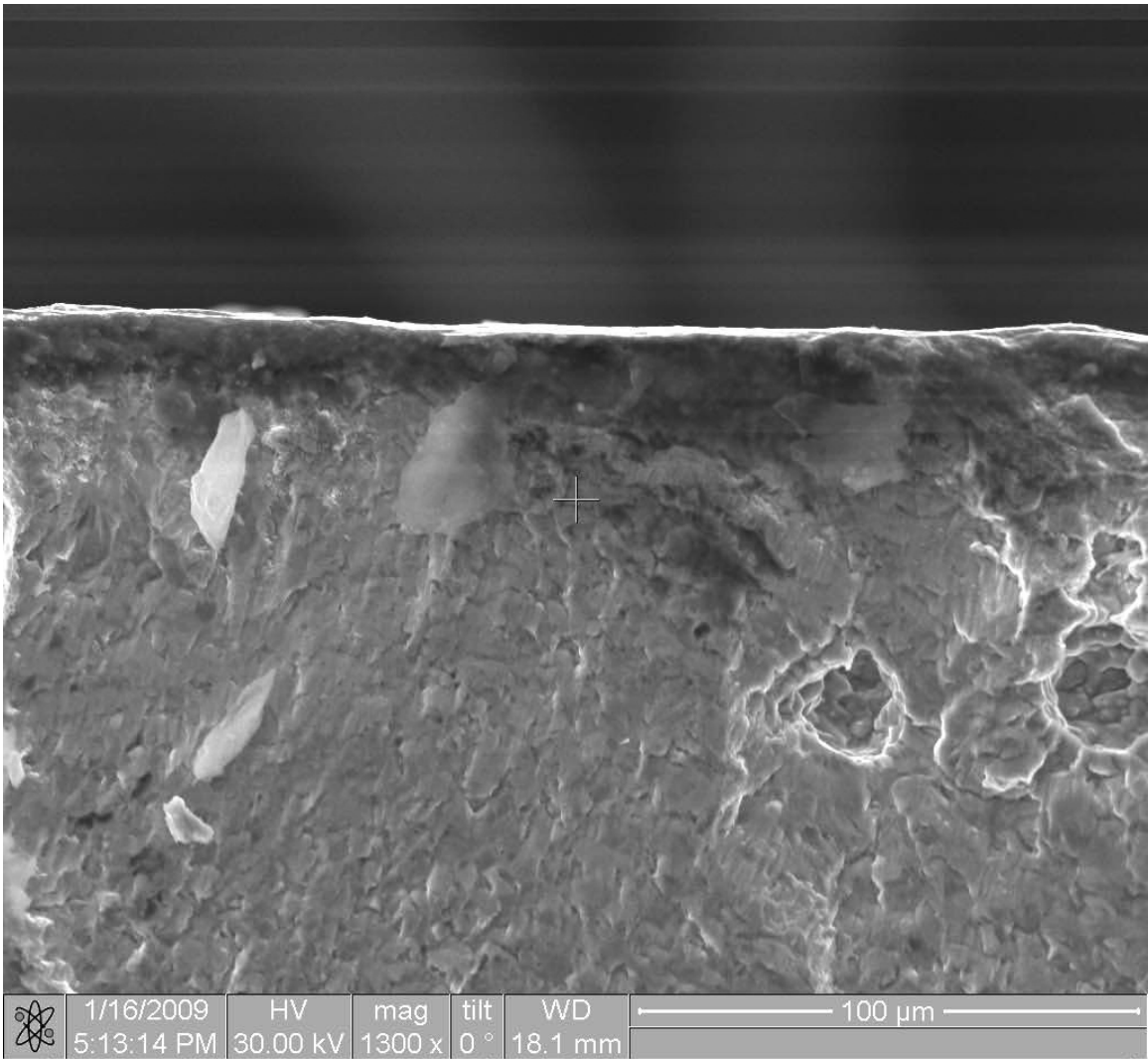
Figure 4.8 – Specimen 3, crack initiation
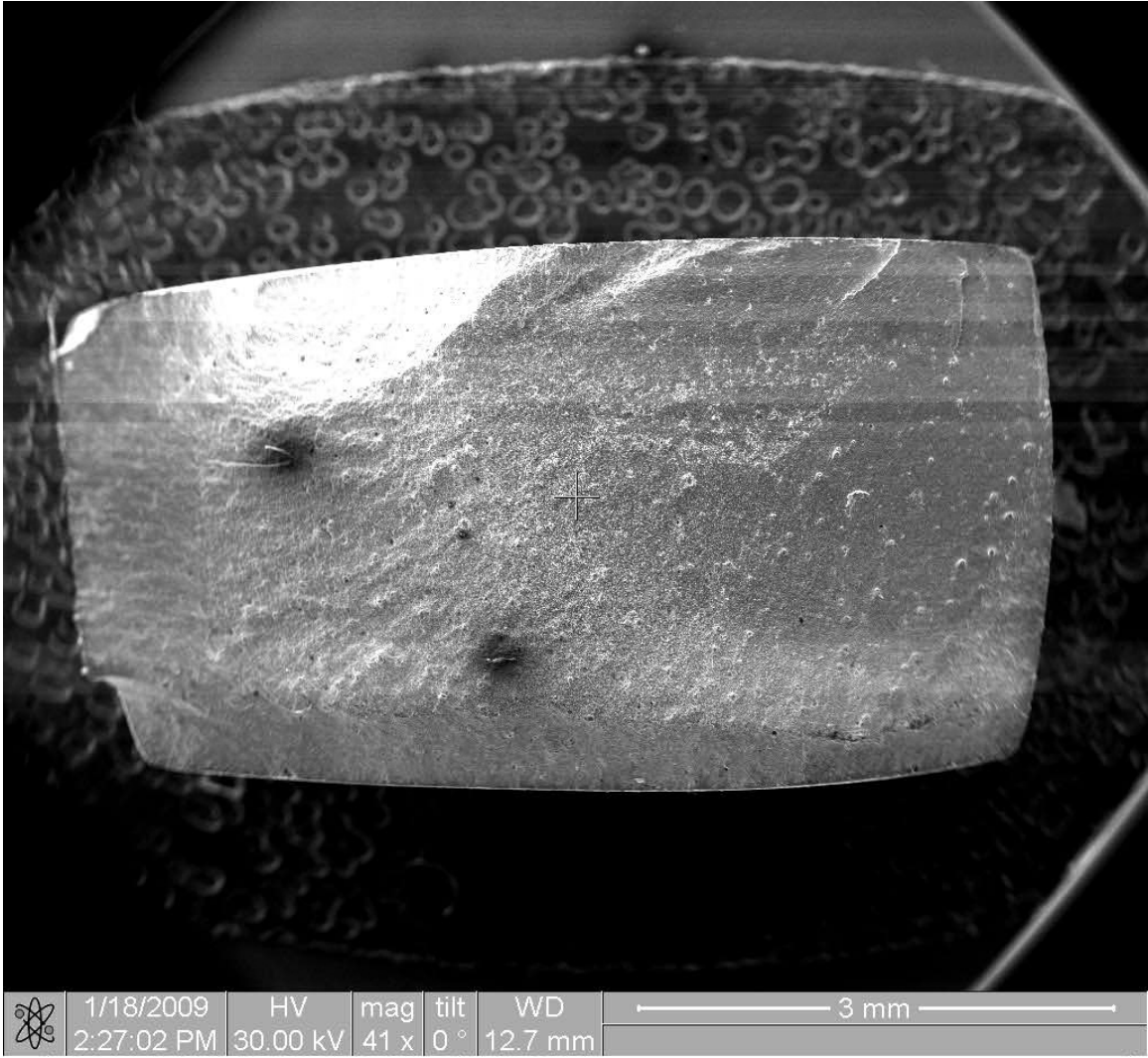
Figure 4.9 – Specimen 4, fracture surface
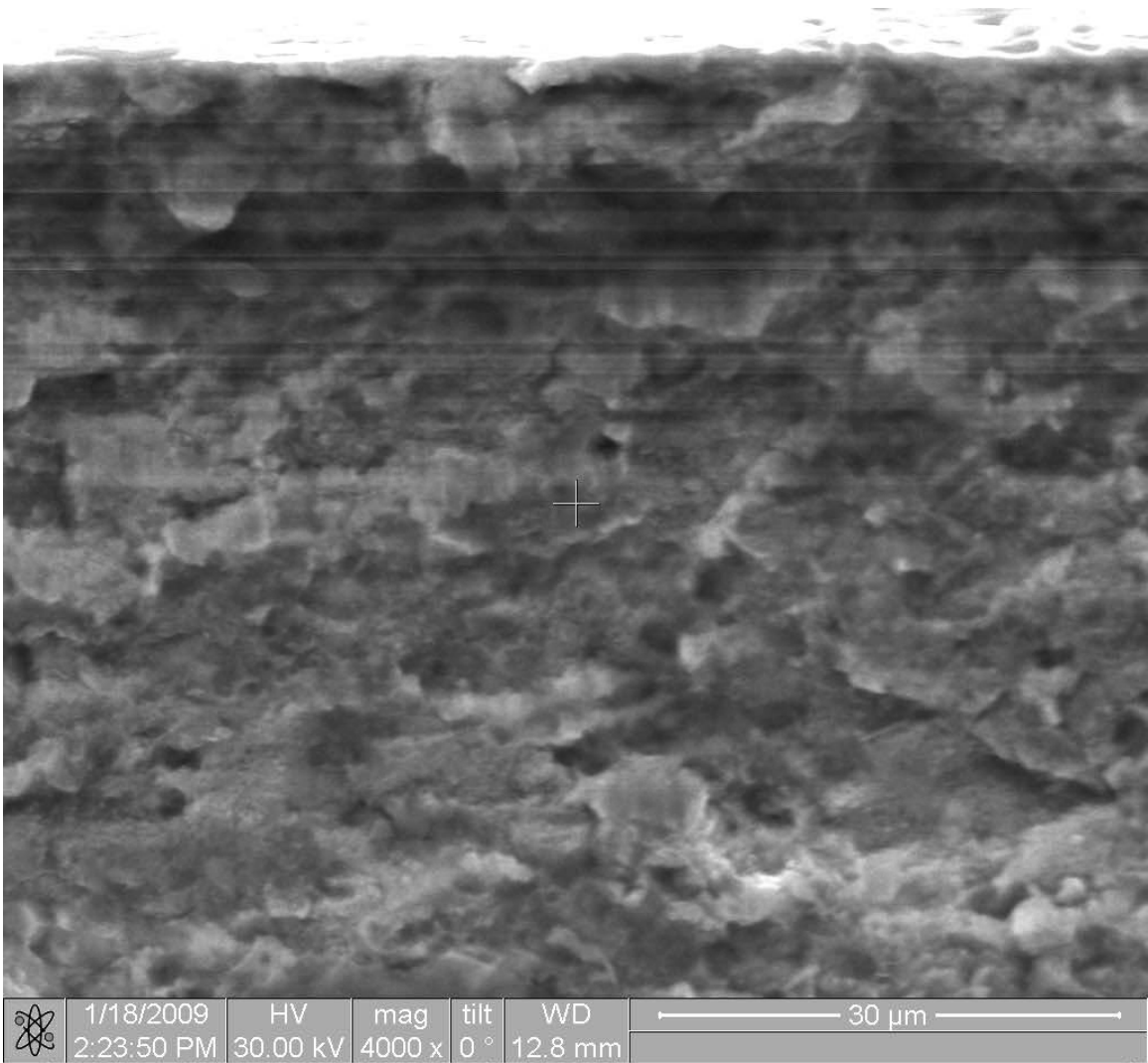
Figure 4.10 – Specimen 4, crack initiation
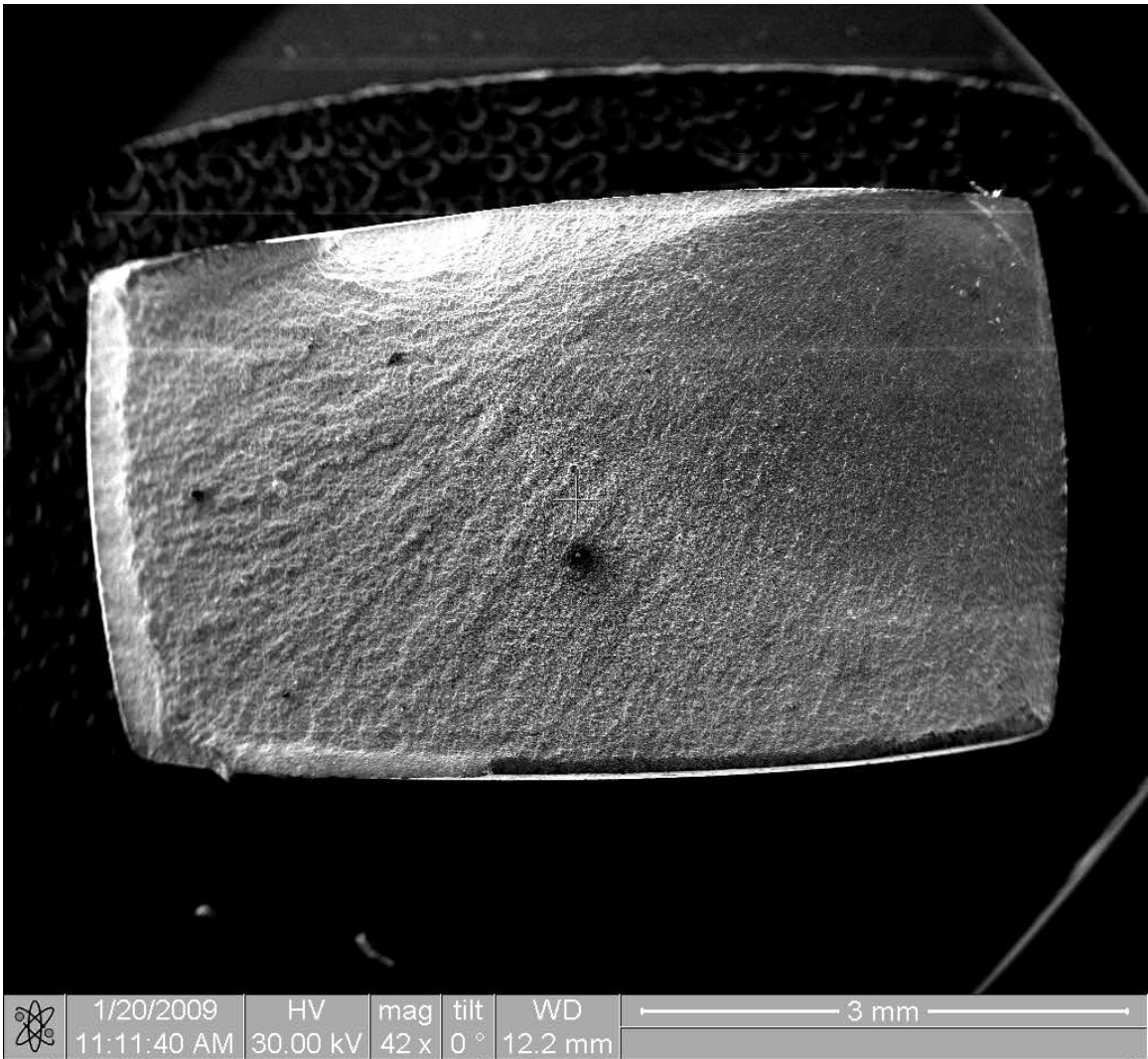
Figure 4.11 – Specimen 6, fracture surface
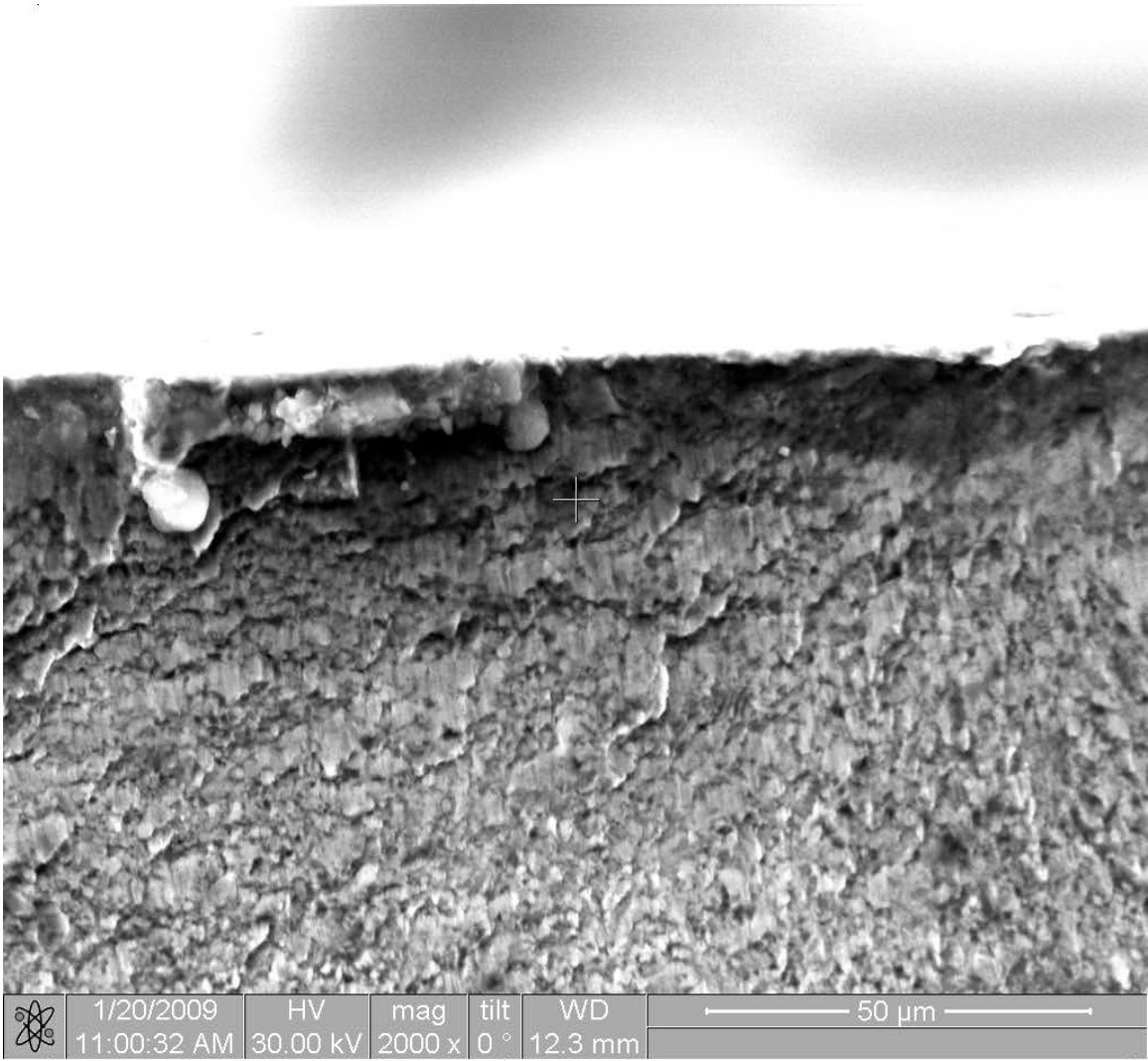
Figure 4.12 – Specimen 6, crack initiation
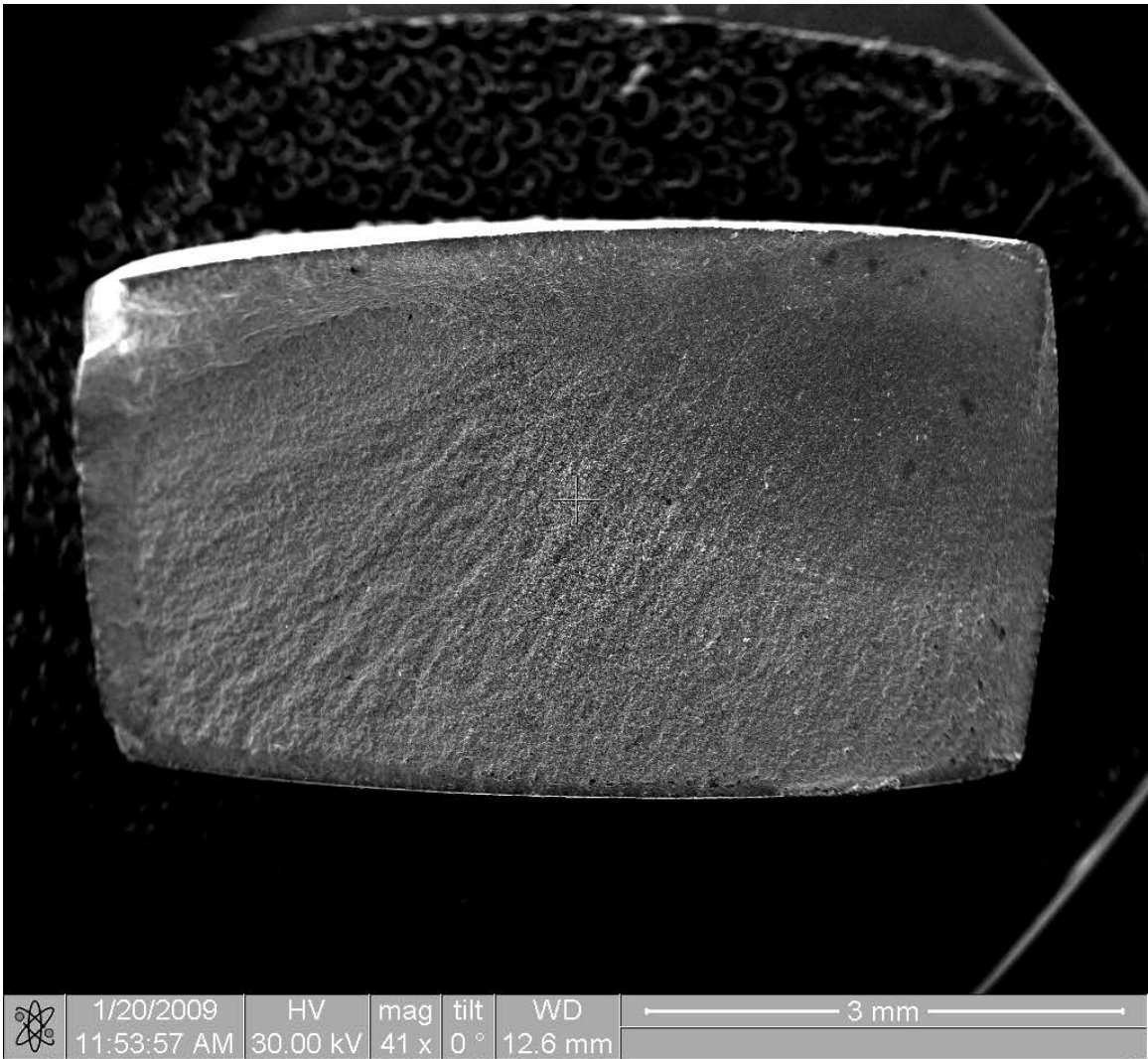
Figure 4.13 – Specimen 7, fracture area
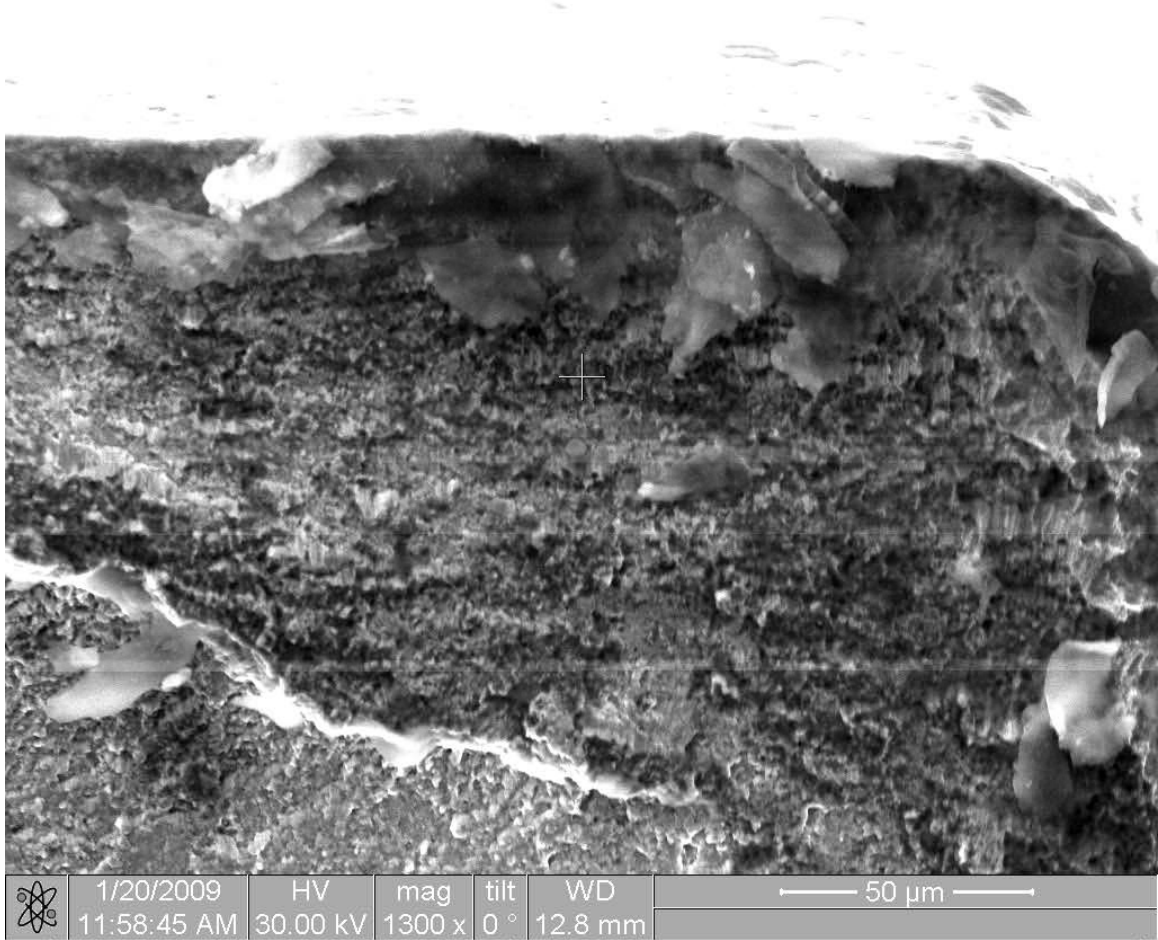
Figure 4.14 – Specimen 7, crack initiation
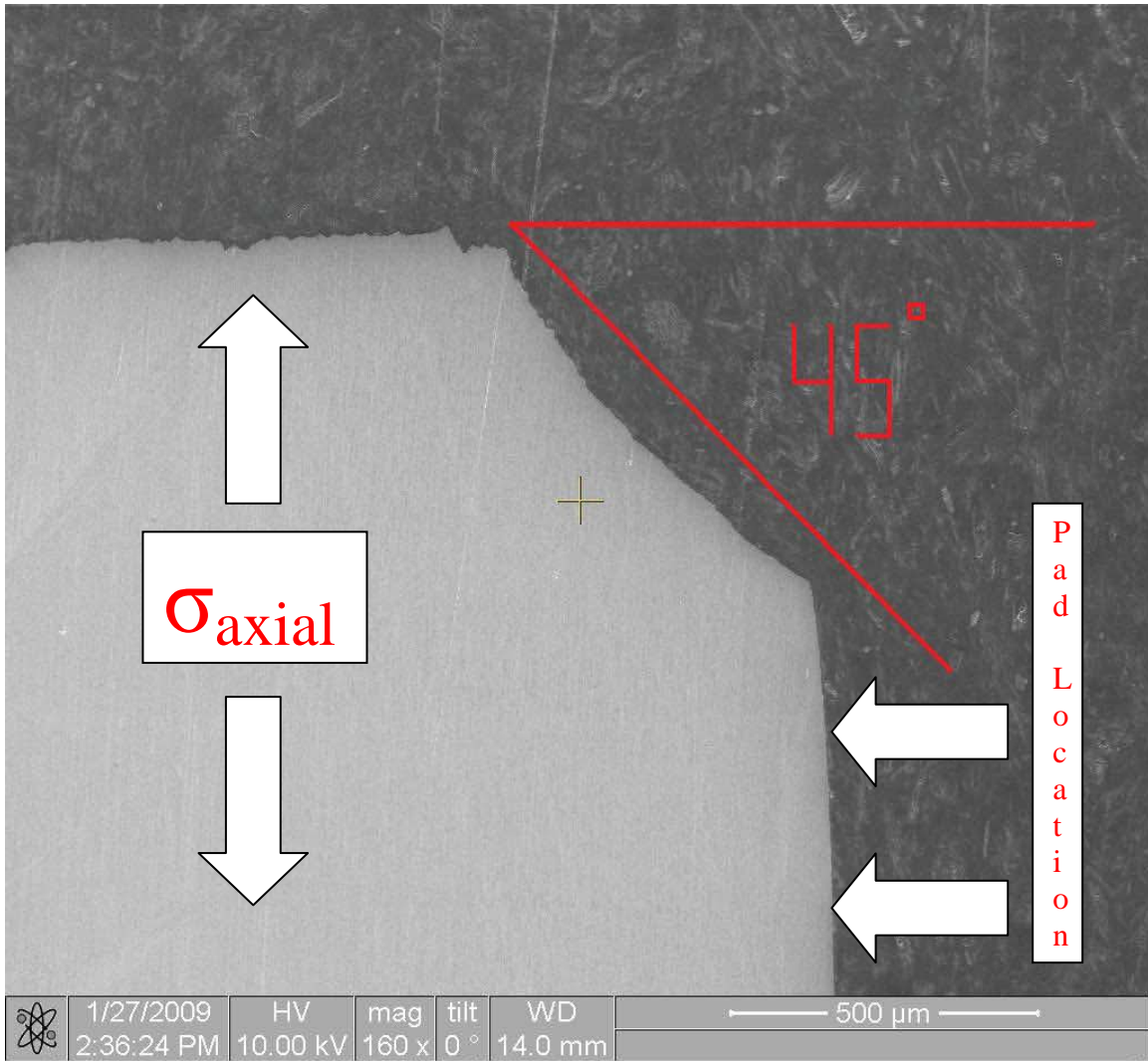
Figure 4.15 – Specimen 2, crack initiation angle
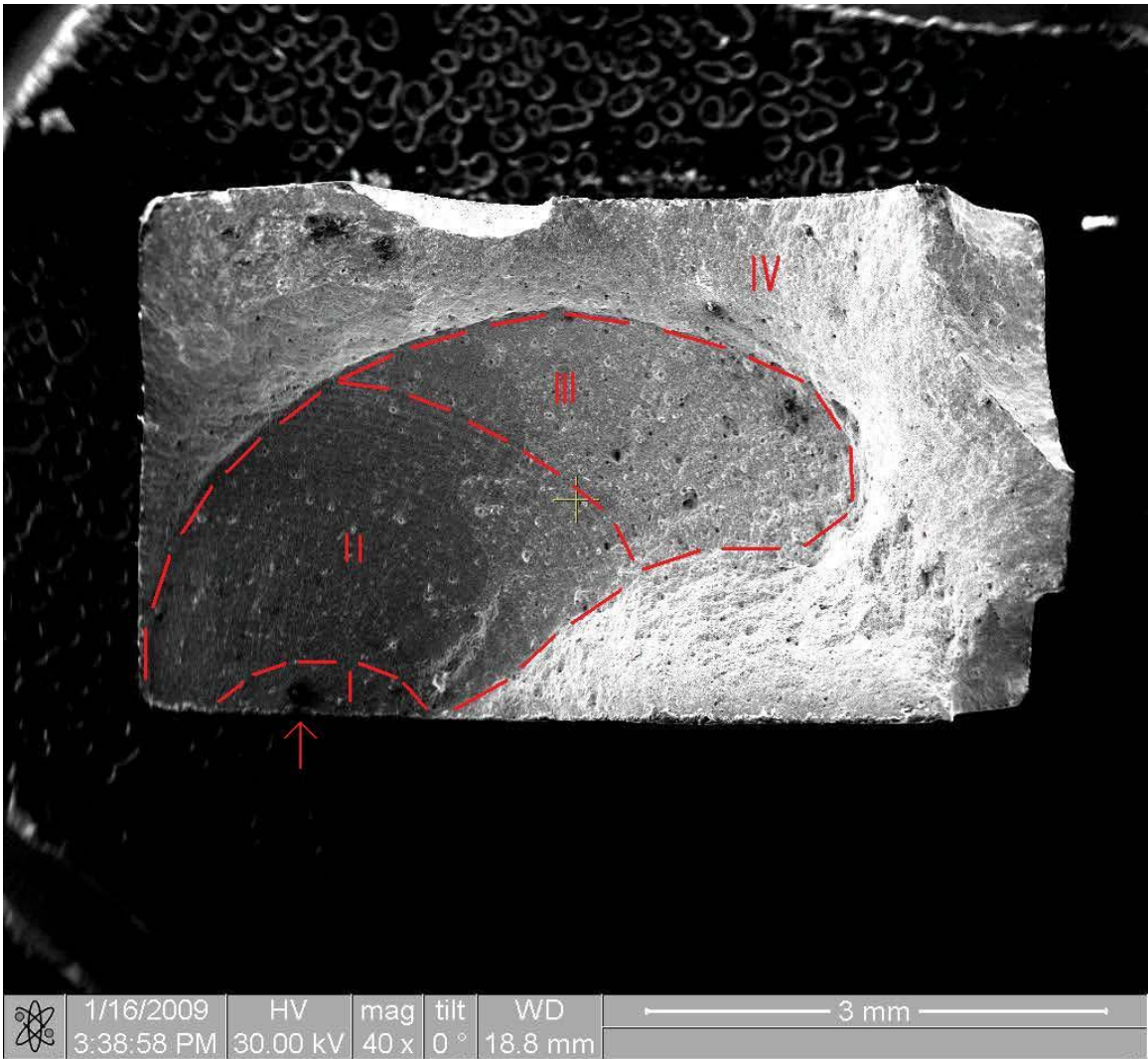
Figure 4.16 – Specimen 1 crack propagation zones
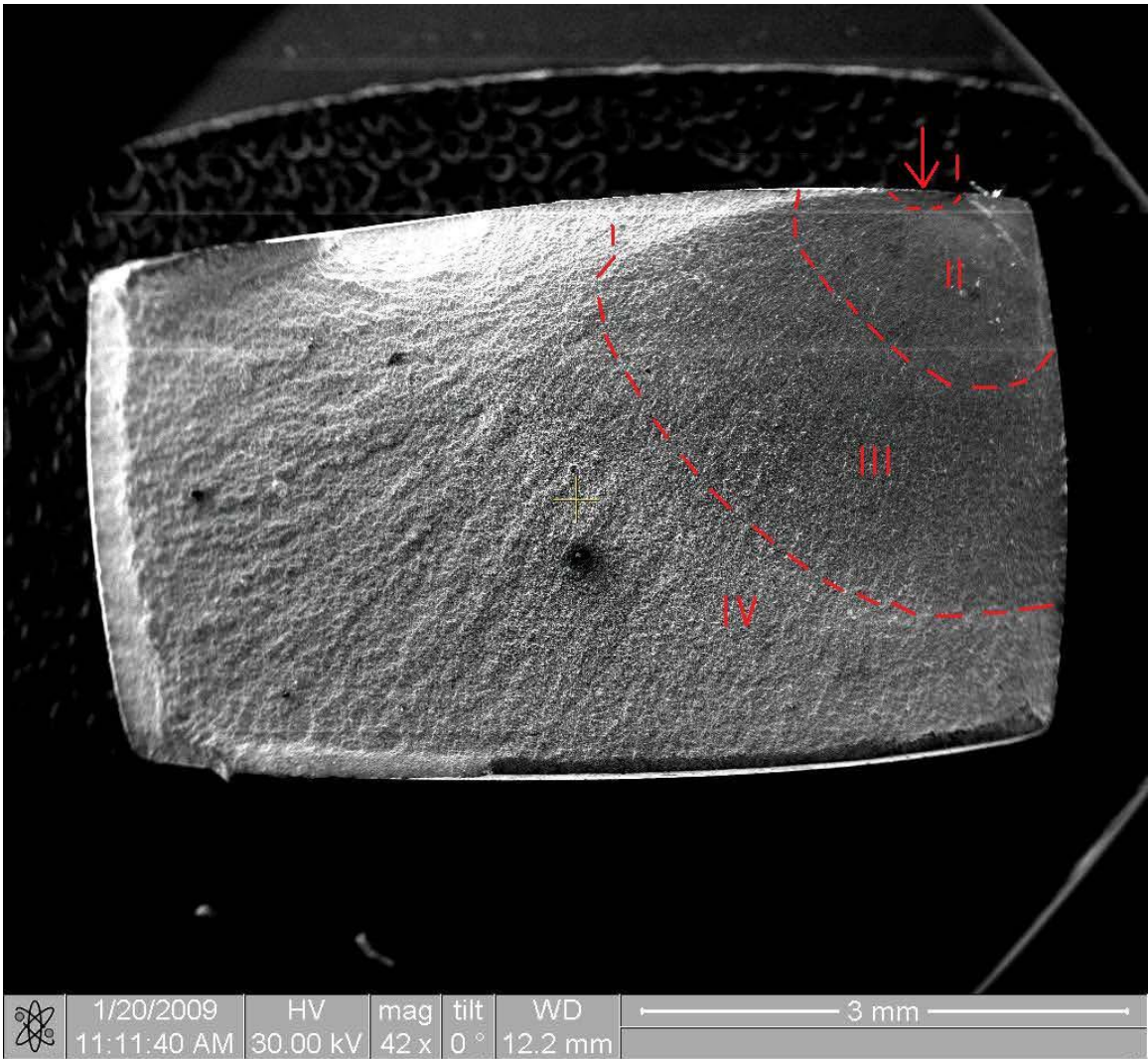
Figure 4.17 – Specimen 6 crack propagation zones
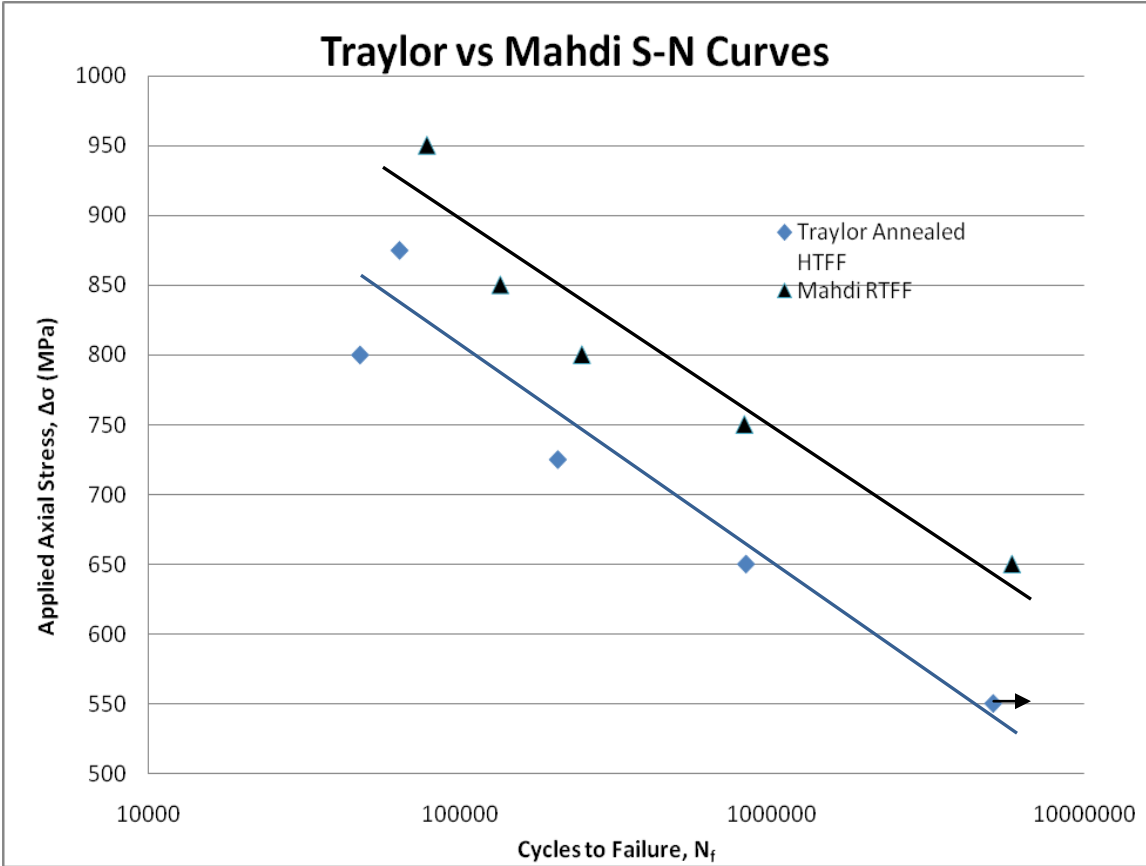
Figure 4.18 – Comparison of Traylor annealed and Mahdi data
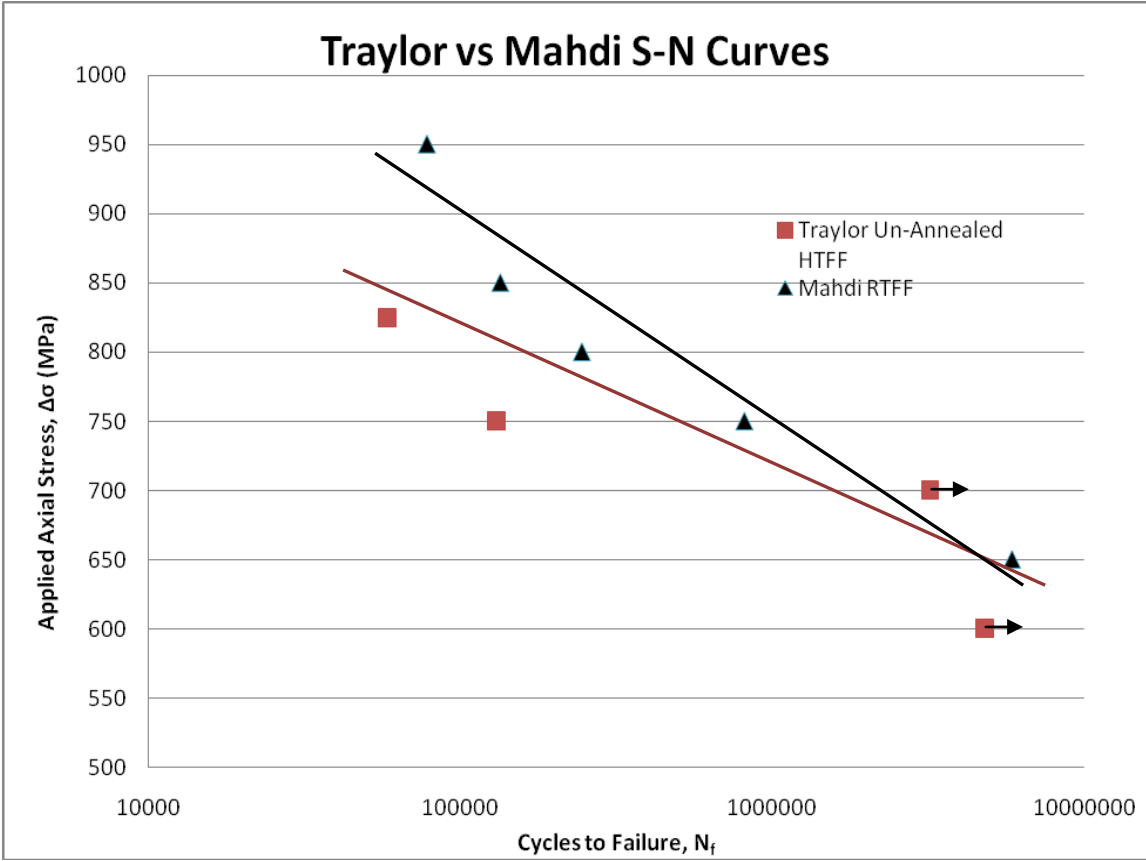
Figure 4.19 – Comparison of Traylor un-annealed and Mahdi data
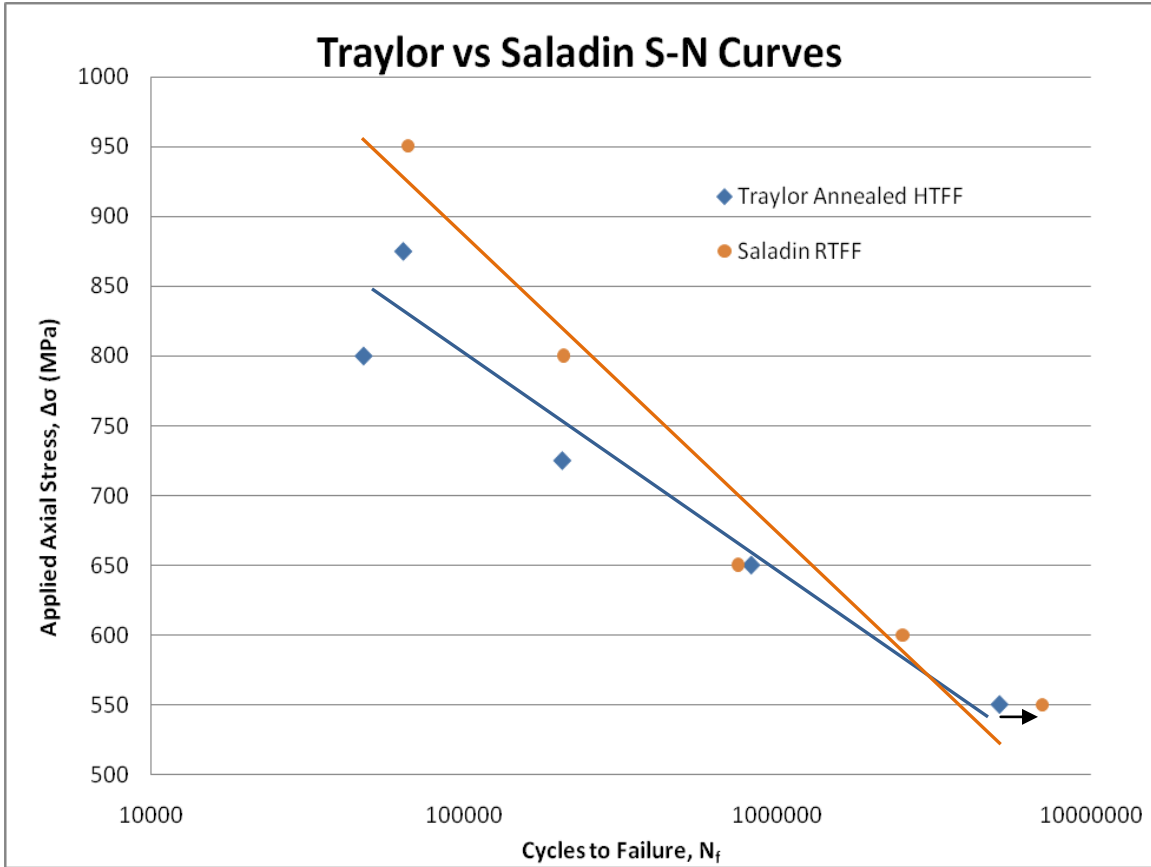
Figure 4.20 – Comparison of Traylor annealed and Saladin data
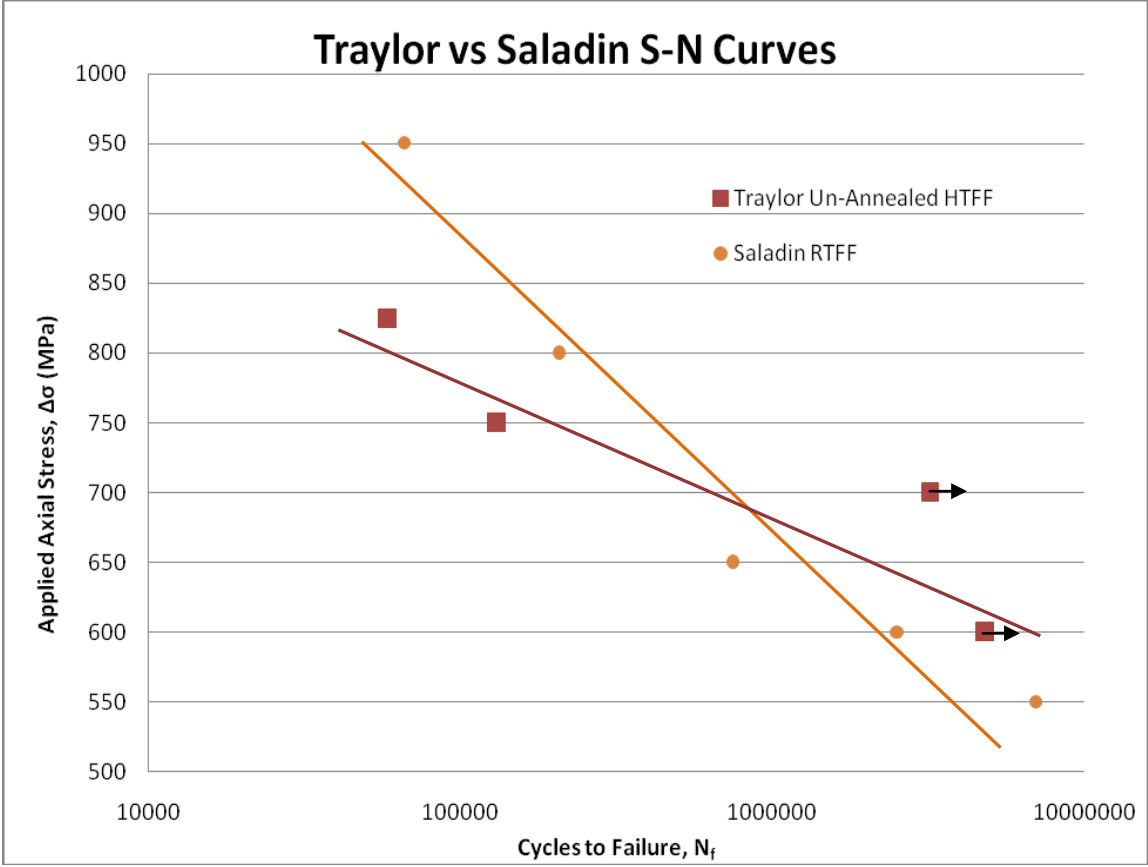
Figure 4.21 – Comparison of Traylor un-annealed and Saladin data
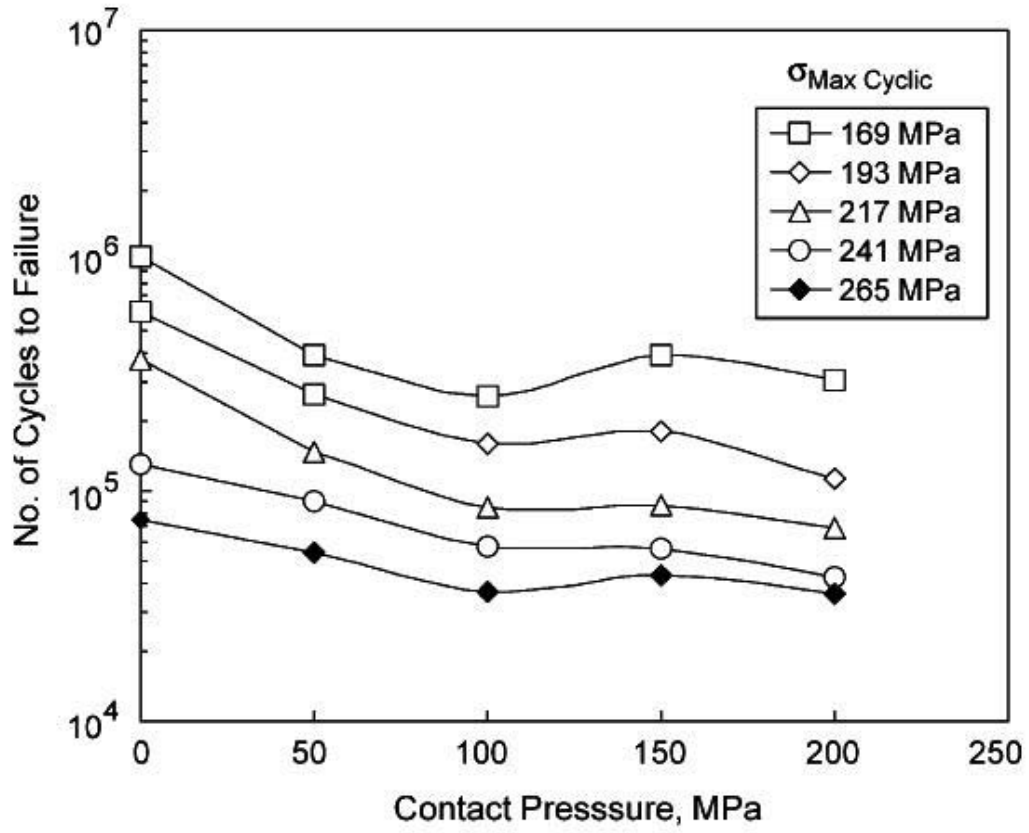
Figure 4.22 - Results of increased contact load study by Naidu, Raman [56]
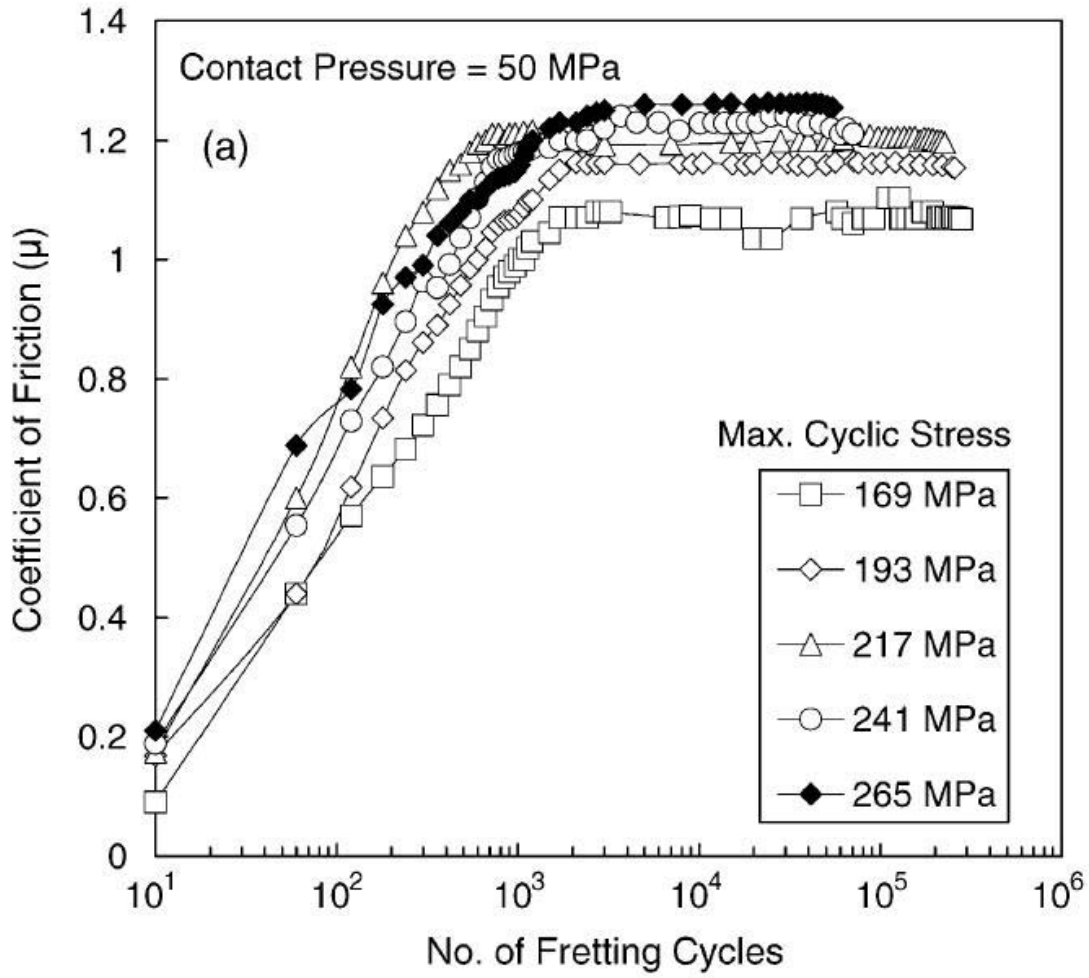
Figure 4.23 – Coefficient of friction as a function of number of cycles [56]
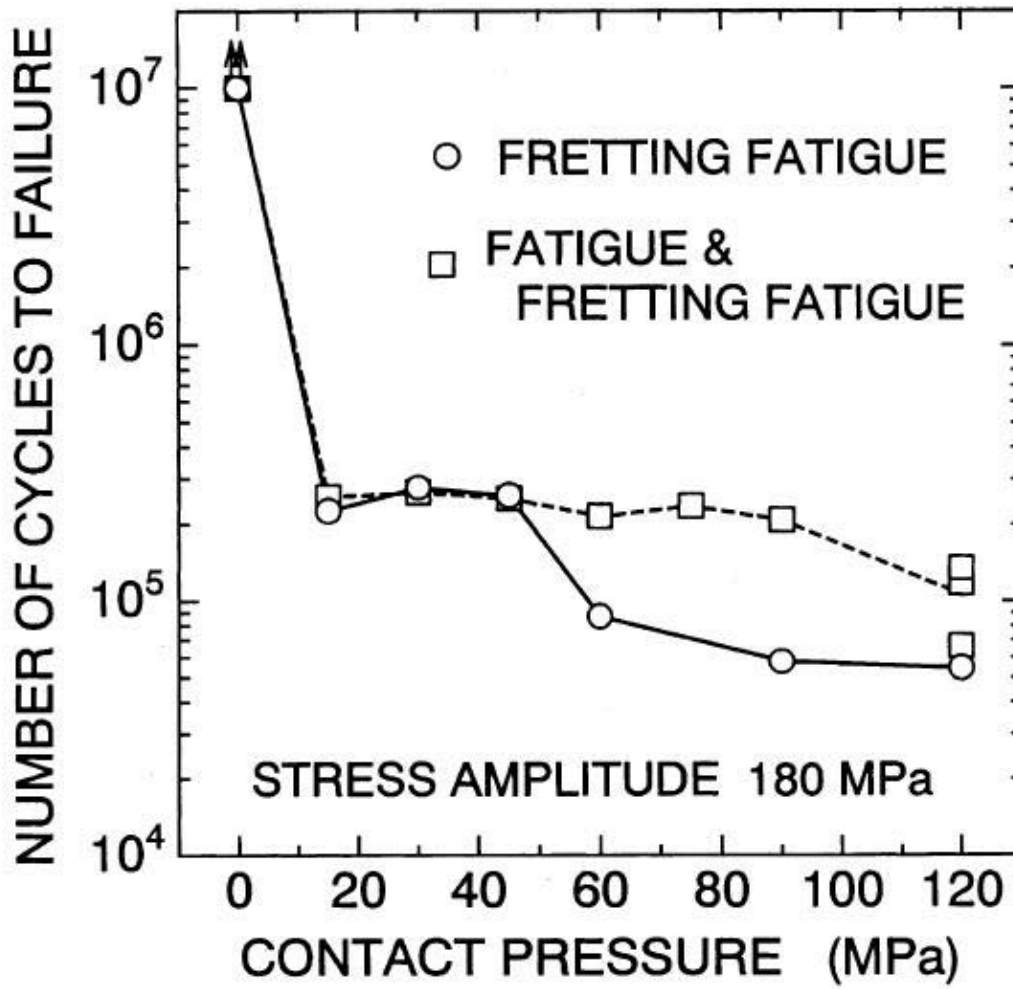
Figure 4.24 – Decrease in the effect of increased contact load [55]

Table 4.1 – Testing conditions and cycles to failure for this study

Test #	Specimen Material	σ_{max} (MPa)	σ_{min} (MPa)	$\Delta\sigma$ (MPa)	Q_{max} (N)	Q_{min} (N)	ΔQ (N)	Cycles to Failure
1	Annealed	800	24.00	776.00	1461.78	509.63	952.15	47729
2	Annealed	725	21.75	703.25	1321.21	394.45	926.76	205905
3	Annealed	875	26.25	848.75	1244.84	222.36	1022.48	63926
4	Annealed	650	19.50	630.50	1244.54	356.15	888.39	827588
5†	Annealed	550	16.50	533.50	1526.22	491.78	1034.44	5144800
6	Un-Annealed	750	22.50	727.50	1310.95	188.25	1122.7	130899
7	Un-Annealed	825	24.75	800.25	1199.46	261.42	938.04	58404
8*†	Un-Annealed	700	21.00	679.00	-	-	-	1891780
9†	Un-Annealed	700	21.00	679.00	1328.78	330.61	998.17	3214219
10†	Un-Annealed	600	18.00	582.00	1401.7	436.5	965.2	4825224

*Test 8 ended early due to mechanical failure of machinery, last known data provided
† Did not fail under given loading and number of cycles

Table 4.2 - Testing conditions and cycles to failure from Ownby [11]

Test #	Test Type	σ_{max} MPa	σ_{min} MPa	$\Delta\sigma$ MPa	σ_{eff} MPa	Q_{max} N	Q_{min} N	ΔQ N	Cycles to Failure
2	HT Fretting	650	122.5	527.5	641.15	1099.58	332.63	766.95	2,464,530
3	HT Fretting	800	24	776	789.11	698.14	1.06	697.08	170,160
4	HT Fretting	750	22.5	727.5	739.79	994.75	153.46	841.29	1,326,201
5	HT Fretting	850	25.5	824.5	838.43	1038.49	186.79	851.7	353,127
7	HT Fretting	950	28.5	921.5	937.07	876.64	-240.83	1117.47	60,232
8	HT Fretting	650	19.5	630.5	641.15	1021.88	141.39	880.49	5,565,917
9	HT Fretting	950	28.5	921.5	937.07	600.05	-409.44	1009.49	71,951
10	HT Plain	800	24	776	789.11				2,087,613
11	HT Plain	1050	31.5	1018.5	1035.71				14,370
12	HT Plain	950	28.5	921.5	937.07				165,509
13	HT Plain	900	27	873	887.75				1,052,188
14	HT Plain	1000	30	970	986.39				89,647
15	RT Fretting	650	19.5	630.5	641.15	472.49	-124.88	597.37	403,435
16	RT Fretting	950	28.5	921.5	937.07	614.18	-487.04	1101.22	60,765
17	RT Fretting	800	24	776	789.11			0	206,653

Note: HT indicates a high temperature test at 600 ˚C and RT indicates a room temperature test at ~20 ˚C

Table 4.3 - Observed contacts width from tests in this study

Fretting scar on specimen
Total contact width = $2a_{exp}$

Test #	Left side	Right side
	μm	μm
1	1728	1852
2	1700	1798
3	1700	1692
4	1701	1711
5	1726	1700
6	1656	1689
7	1644	1658
8	1674	1689
9	1635	1647
10	1640	1644

Note: Theoretical value of $2a = 1632$ μm

Table 4.4 – Summary of data across Traylor, Ownby, Mahdi, Saladin

Traylor				Ownby			
Annealed		Un-Annealed		HTFF		RTFF	
σ_{max} (MPa)	N_f (cycles)	σ_{max} (MPa)	N_f (cycles)	σ_{max} (MPa)	N_f (cycles)	σ_{max} (MPa)	N_f (cycles)
550	5144800	600	4825224	650	5565917	650	403435
650	827588	700	3214219	650	2464530	800	206653
725	205905	750	130899	750	1326201	950	60765
800	47729	825	58404	800	170160		
875	63926			850	353127		
				950	60232		

Mahdi		Saladin	
RTFF		RTFF	
σ_{max} (MPa)	N_f (cycles)	σ_{max} (MPa)	N_f (cycles)
650	5900000	550	7000000
750	815449	600	2511439
800	245000	650	750028
850	134103	800	207938
950	77937	950	66181

V. Conclusions and Recommendations

This chapter will summarize the results of this study and use previous results to make a set of conclusions about the nature of fretting fatigue behavior of IN-100 at an elevated temperature of 600°C subjected to an increased contact load of 8006 N. A summary of the tests will be provided followed by a summary of the analytical methods used to analyze the subsequent data. This will be followed by a set of conclusions which were drawn from these experiments. Lastly, recommendations for future work in this area of fretting fatigue will be suggested.

5.1 Summary

As stated in Chapter I, the ultimate purpose of this study was to determine the effect of increased contact load had on the fretting fatigue behavior of the nickel-based alloy IN-100 at an elevated temperature of 600°C. Five experiments were carried out using annealed specimens and five experiments were conducted using un-annealed specimens for a total of 10 specimens. Various axial loads were applied, ranging from a minimum of 550 MPa to a maximum of 875 MPa. The stress ratio was maintained at a constant value of R=0.03 in accordance with previous studies by Ownby [11], Mahdi [12], and Saladin [13]. Each test used pads of the same geometry, a cylinder-on-flat contact with fretting pad radii of 50.8 mm. The experimental equipment was controlled by sophisticated software which recorded many of the experimental values used in this study. The collected values were used in order to derive other experimental values which were of use in this study. Of the 10 experiments, only nine provided useful data due to a mechanical failure during one test which rendered the specimen useless.

The experimental data gathered from each experimental trial was then used to construct several S-N curves comparing the fretting fatigue life of IN-100 under an increased contact load of 8006 N and at an elevated temperature of 600 °C to previous studies of IN-100 at 600 °C under a contact load of 4003 N. This experimental data was also compared to previous studies of IN-100 at room temperature as well as to studies of other materials to include austenitic stainless steel and three alloys of Aluminum. The fretting conditions were verified in all cases for the partial slip condition. Contact width, crack initiation location, and fracture surfaces were measured and analyzed with the aid of optical and scanning electron microscopes.

5.2 Conclusions

1. The crack initiation location for all tests was at the trailing edge at a location of approximately x/a=±1 along the longitudinal direction.

2. The crack initiation angle for test 2 was 45°, as expected from the predictive parameters discussed previously as well as previous studies of IN-100 [12, 13].

3. The area of the fracture surfaces related to each of the four stages of crack propagation showed an inverse relationship to the time spent in that stage.

4. While elevated temperatures of 600 °C have been shown to have beneficial effect on fretting fatigue life due to the formation of a glaze oxide, an increase in contact load counteracted this increase by causing premature crack initiation.

5. No observed difference existed between the general effect of contact load on the annealed and un-annealed specimens. Of the previous studies of fretting fatigue of IN-100 [11-13], Ownby [11] and Saladin [13] used the same annealed specimen as this study. Mahdi [12] used the un-annealed material that was used in this study. It was shown that both the annealed and the un-annealed specimens exhibited a marked decrease in their fatigue lives under fretting conditions at an elevated temperature of 600 °C and a contact load of 8006 N when compared to the fatigue life at 4003 N. It should be noted that the greatest reduction was seen at higher stress levels.

6. A difference in the specific effect of an increase in contact load was observed between the annealed and un-annealed specimens. This can be attributed to the internal stresses found in the un-annealed specimens which are not found in the annealed specimens. This caused a variation in the number of cycles to failure for the un-annealed specimens and a wider scatter of data. It can be seen, as an example, in Figures B.27 through B.30 that the annealed specimens in Zone II exhibit a much coarser fracture surface while the surface of the un-annealed specimen appears to be much less so.

5.3 Recommendations for Future Work

1. This study focused on the effect of just one major experimental factor, contact load, to determine its impact on the fretting fatigue life of IN-100 at an elevated temperature of 600 °C. For a complete investigation into the effects of an increased contact load, the effects of a varying contact load over a constant axial load should be investigated. This will give great insight into whether a threshold exists for IN-100. A conclusion could also be made as to the effect of a glaze oxide characteristic of nickel-based alloys at high

temperature has on the coefficient of friction. Because the coefficient of friction plays such a large role in fretting, this would be very insightful.

2. Regardless of contact load, the effect of an environment other than air on fretting fatigue should be investigated. Though turbine engines are mostly used in an air environment, this is not the only component that may have an effect on the life of a component experiencing fretting. A priority should be placed on investigating the effect of a steam environment on the fretting fatigue behavior of IN-100 should be investigated. This would more closely recreate the environment in which most turbine engines operate, whether it is a jet engine turbine or a power producing turbine in a nuclear power plant

3. More work should be conducted to determine the effect of a wider range of temperatures of the fretting fatigue behavior of IN-100. It would be interesting to see how the glaze oxide formation is effected by an increase in temperature as well how this affects the coefficient of friction and fatigue life of the material. Temperatures should approach the melting temperature of IN-100 in order to determine if any effects are noticed as the material prepares to change phase.

4. An investigation into fretting fatigue of IN-100 with a dissimilar mating material would be applicable as well. This would cover the situations where an IN-100 component is experiencing fretting due to contacting with a different material. Suggested mating materials would include Aluminum and its alloys, Titanium and its alloys, and steels. These materials are very common in turbine environments and should be investigated for any effects.

5. Differing the pad geometry in fretting fatigue experiments would give insight into the mechanisms in which fretting takes place. By altering the contact geometry, different mechanics will be used and different results should be expected. While the cylinder-on-flat geometry is convenient and well-studied, it is not the only geometry which can be used to model fretting conditions. Other geometries could include the flat-on-flat geometry or the sphere-on-flat geometry.

6. An investigation into differing surface treatments, such as shot-peening, and their effects on fretting fatigue in IN-100 would be very interesting and would provide valuable knowledge about ways to mitigate or reduce fretting fatigue.

Appendix A. Temperature Calibration

It was previously mentioned that in order for this test to be have an accurate account of the elevated temperature, a calibration was needed. This arises from the fact that the thermocouples which measure the temperature of the specimen are not attached to the specimen, and therefore would be a poor indicator. To do this, a special specimen was fitted with spot-welded thermocouples and placed in the experimental equipment. These thermocouples were used to measure the temperature of the specimen as the commanded temperature was changed. The commanded temperature was incrementally increased and the temperature of the specimen was allowed to stabilize and then recorded.   A series of calibrations were conducted and can be seen below. The first calibration took place on 17 September 2008 (Figure A.1). The sharp decrease seen around 20 minutes is the application of the fretting pads, which introduced a large heat sink which instantly lowered the system temperature. This calibration was not found to be useful due to the large spread in the specimen's front and rear readings. The second calibration attempt, on 22 September 08, was much improved (Figure A.2).   The specimen front and rear thermocouple readings aligned much better, though nothing was done to the equipment to make this happen. This calibration led to a conclusion that a commanded temperature of $369°C$ led to a specimen temperature $600 °C$. On 25 September, a heating element for one of the heater boxes fractured and required replacement. This necessitated another calibration to ensure accuracy. This can be seen in Figure A.3. No change in the required commanded temperature was observed and the experimental value for the commanded temperature was determined to be $369°C$ for the entirety of the study.
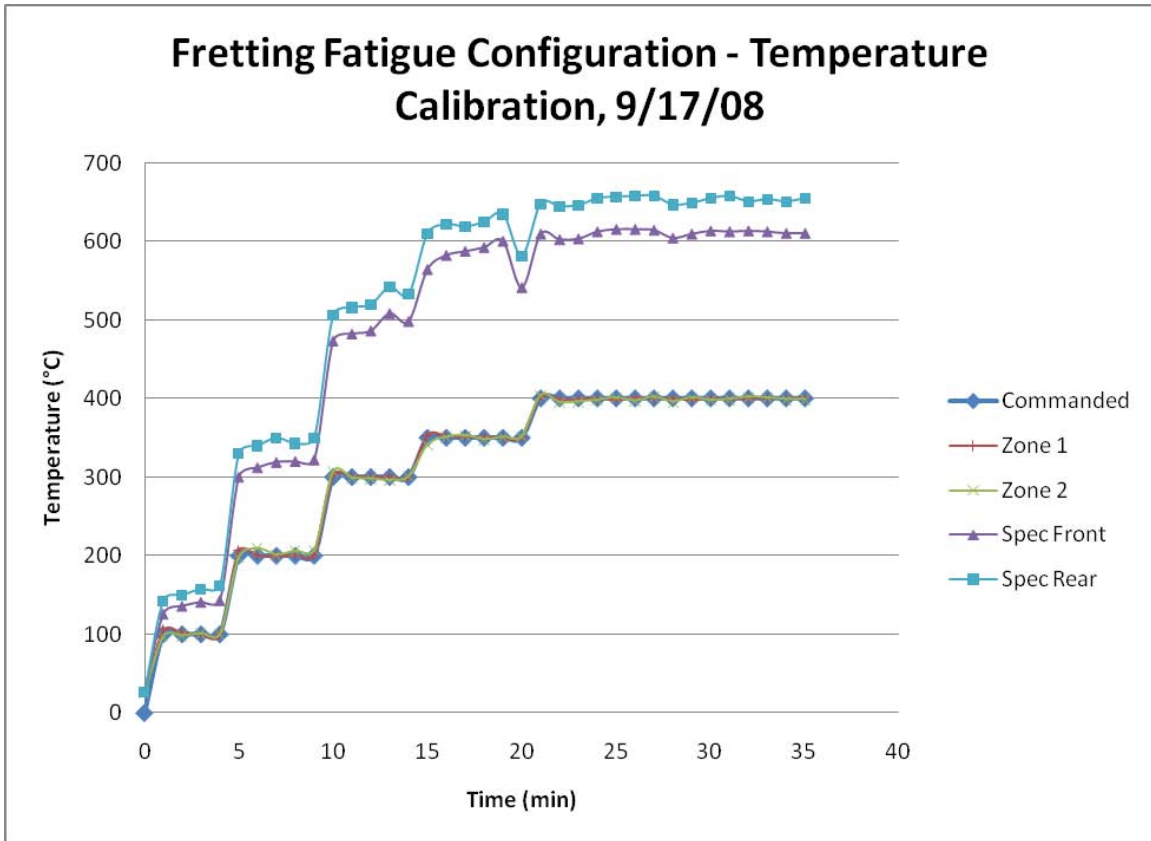
Figure A.1 Fretting fatigue condition calibration data from 17 Sep 08
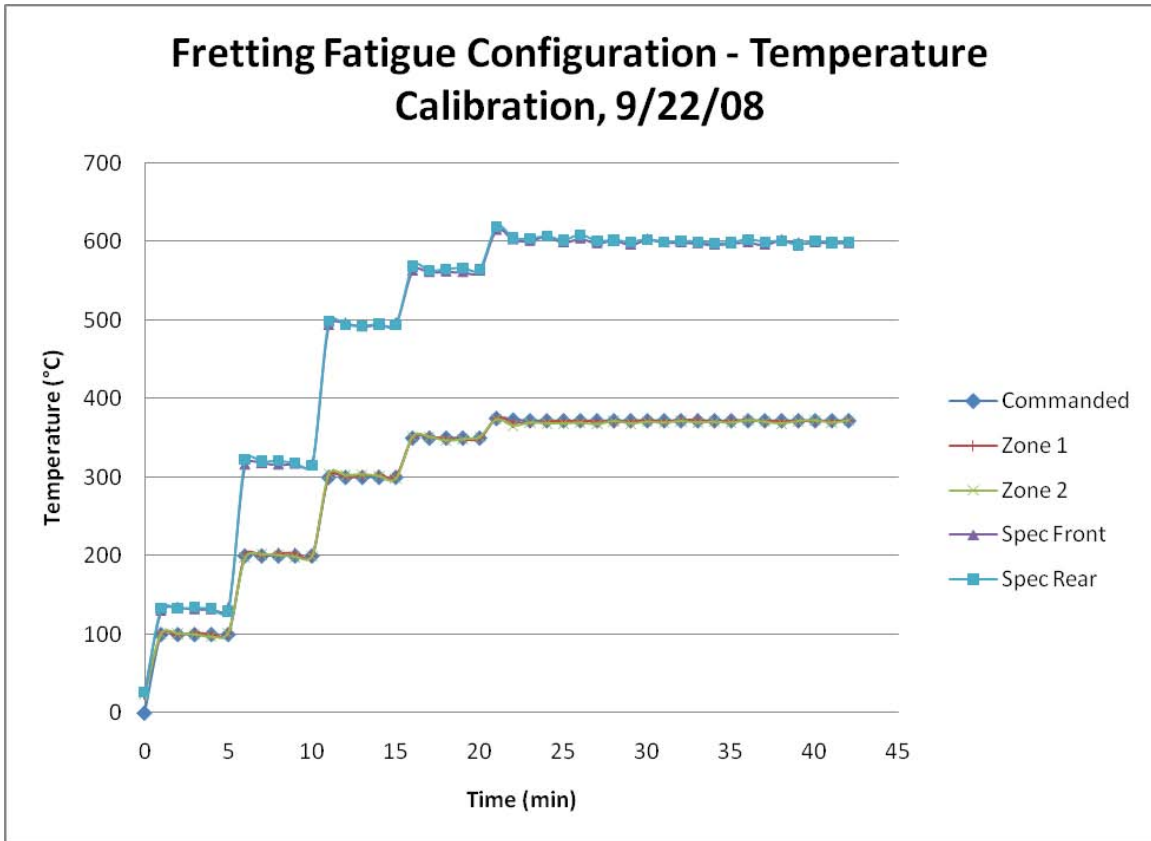
Figure A.2 Fretting fatigue condition calibration data from 22 Sep 08
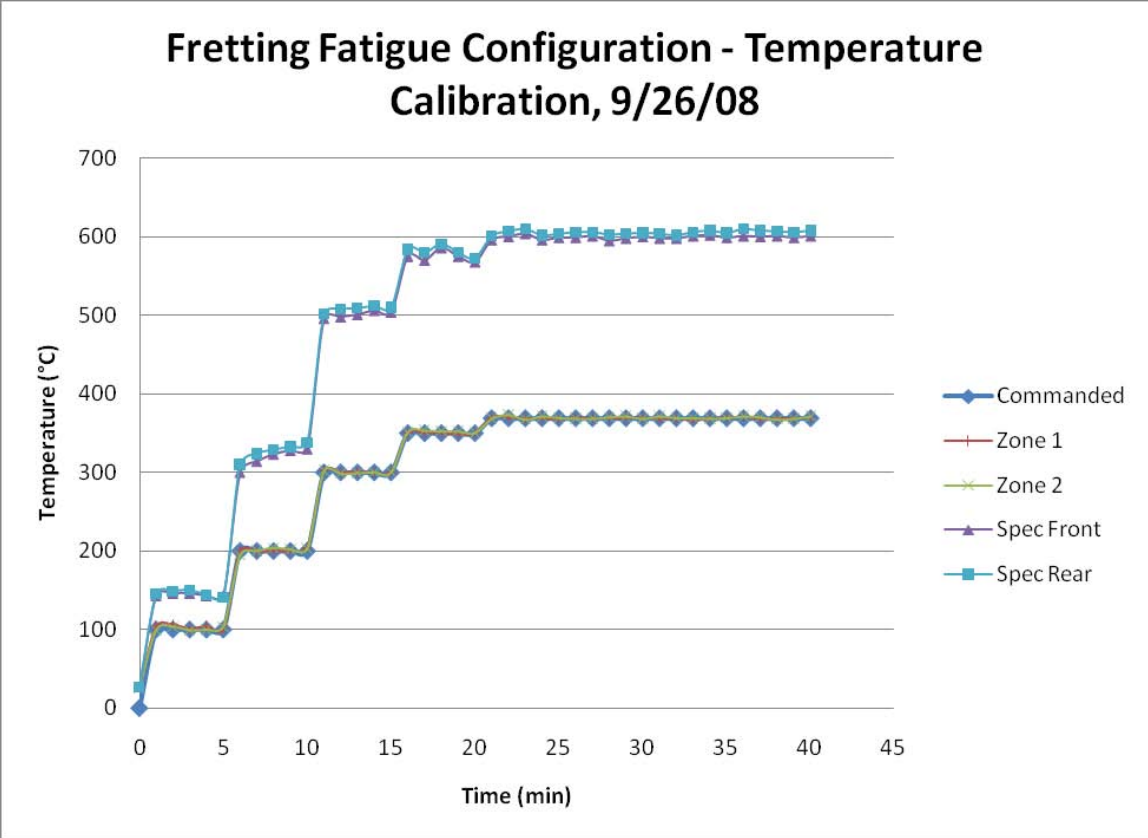
Figure A.3 Fretting fatigue condition calibration data from 26 Sep 08
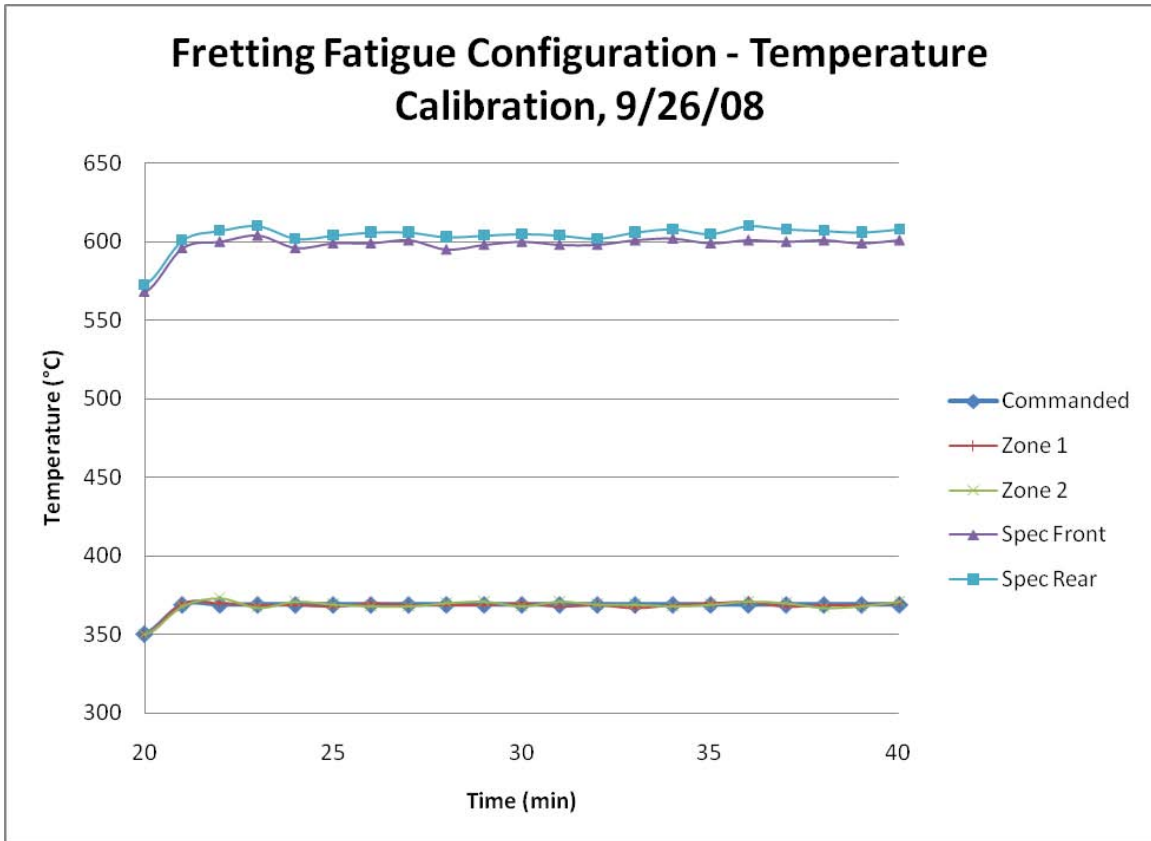
Figure A.4 - Detail of 26 Sep 08 calibration

Appendix B. Microscopy Images

This section will detail the images from both the optical microscope as well as the scanning electron microscope for all sets of fretting pads and all fractured specimens. These are the images which were used to determine the half-contact widths, crack propagation zone sizes, crack initiation locations, and crack initiation angles. For half-contact width values, see Table 4.3.
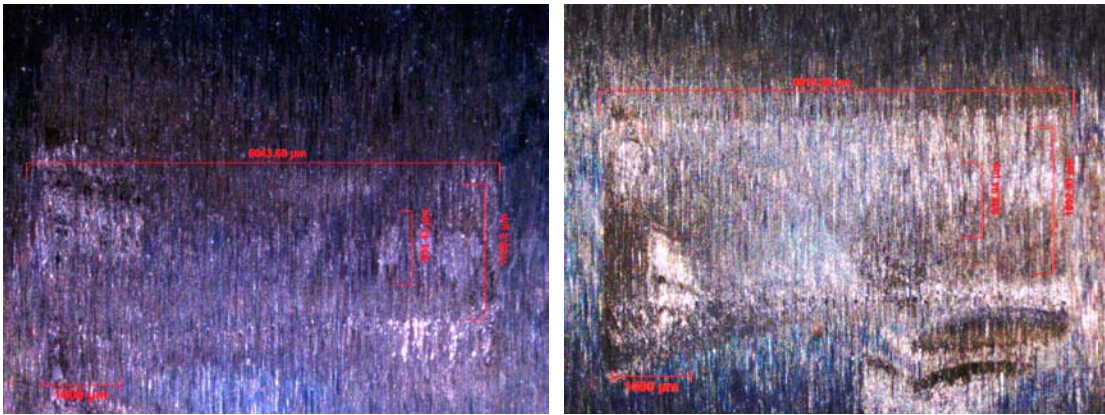
Figure B.1 – Left and right fretting pads, test 1
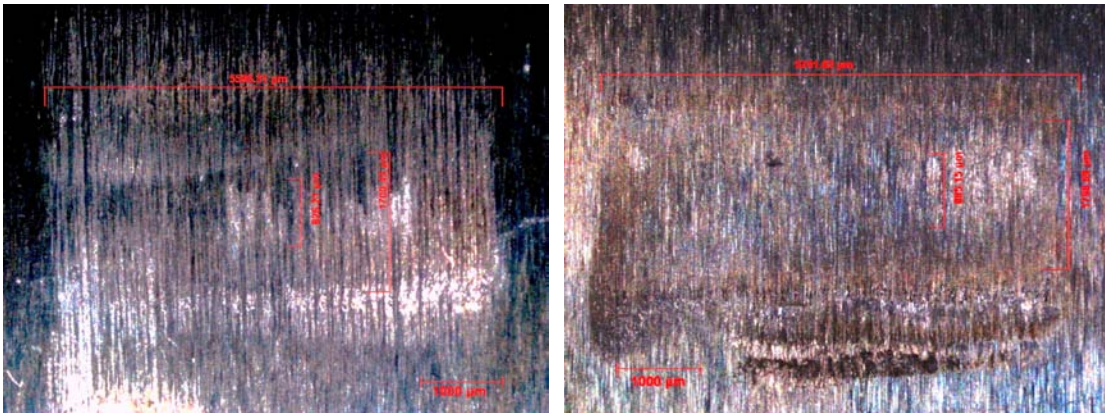
Figure B.2 – Left and right fretting pads, test 2
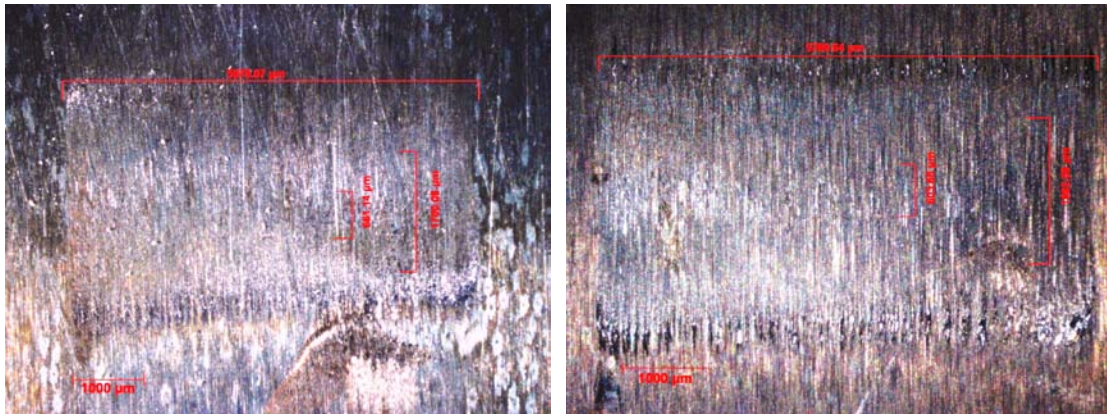
Figure B.3 - Left and right fretting pads, test 3
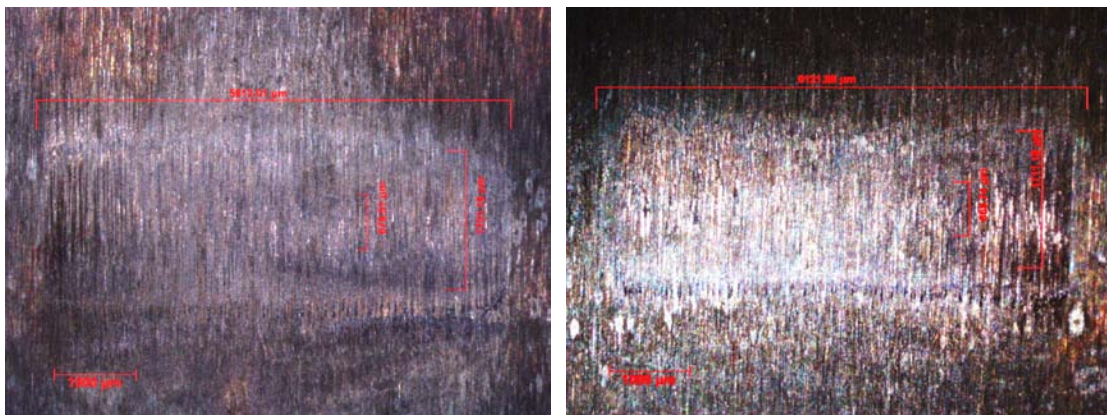
Figure B.4 - Left and right fretting pads, test 4
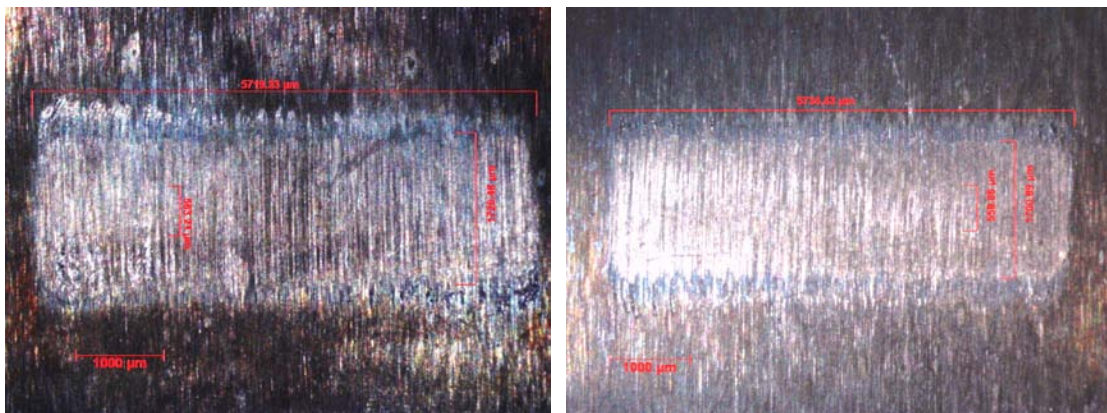
Figure B.5 - Left and right fretting pads, test 5
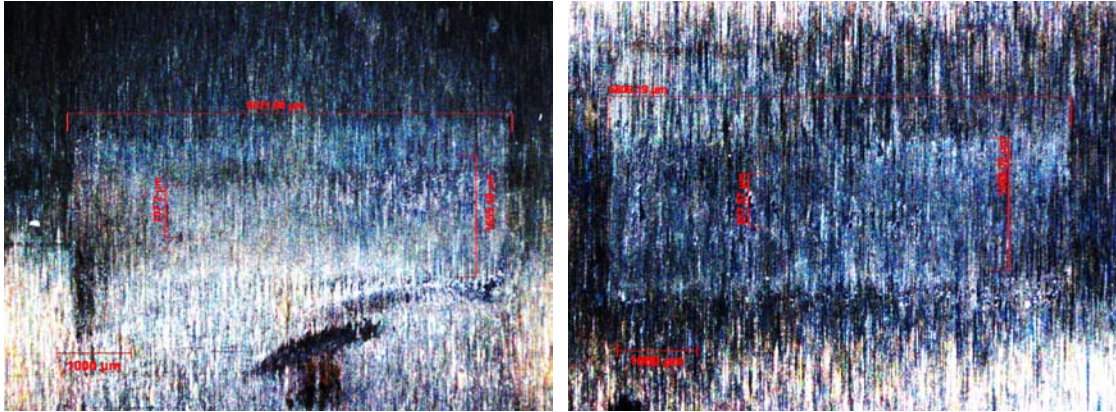
Figure B.6 – Left and right of fretting pads, test 6
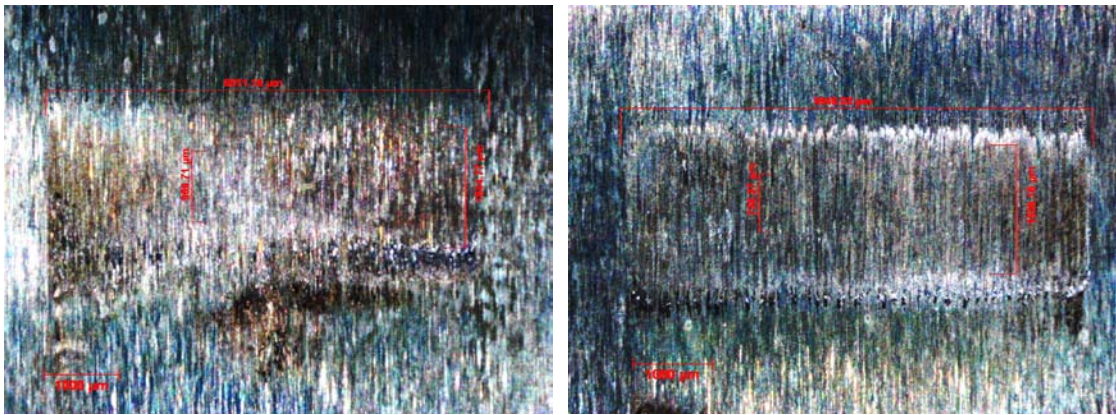
Figure B.7 – Left and right of fretting pads, test 7
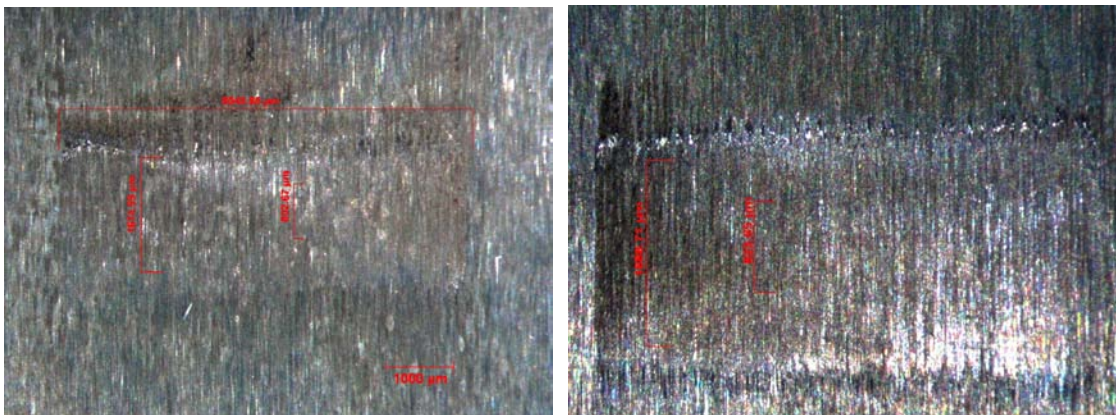
Figure B.8 – Left and right of fretting pads, test 8
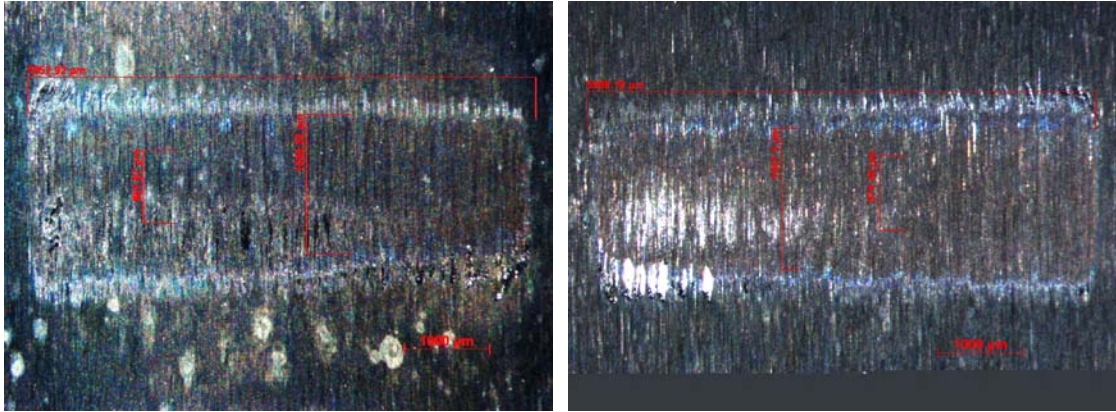
Figure B.9 – Left and right of fretting pads, test 9
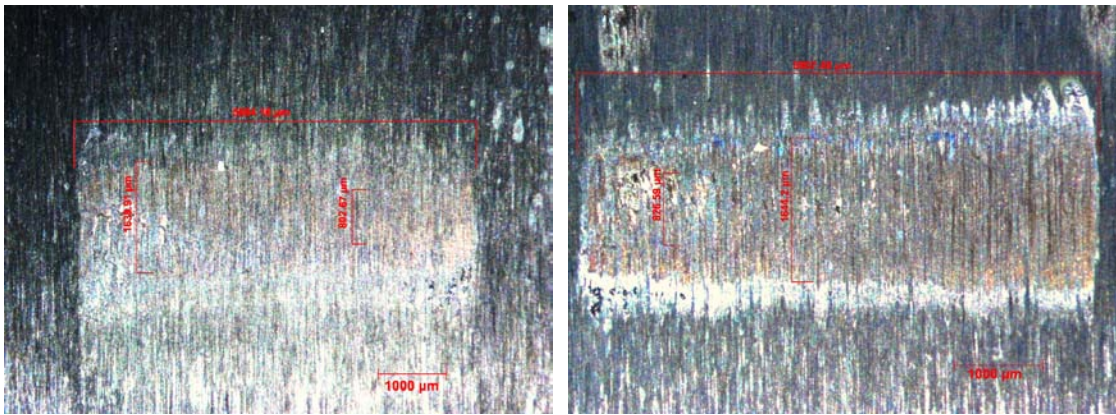
Figure B.10 – Left and right of fretting pads, test 10
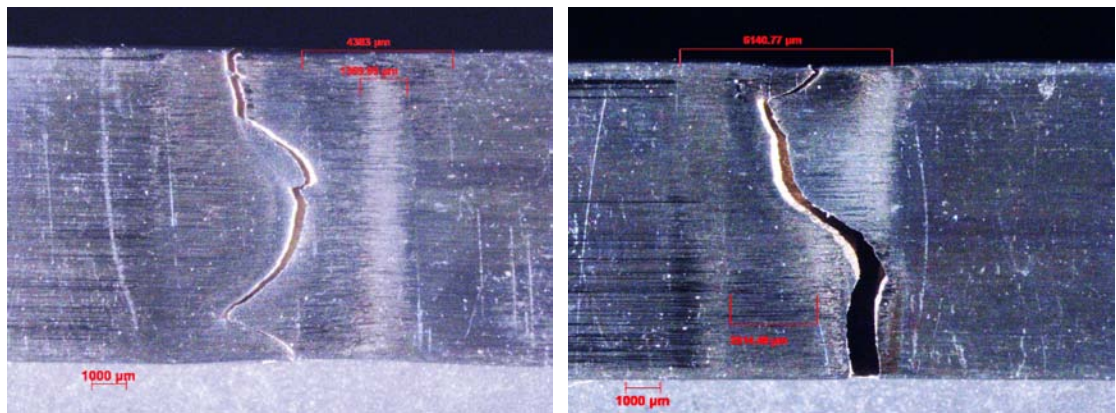
Figure B.11 – Left and right of specimen 1
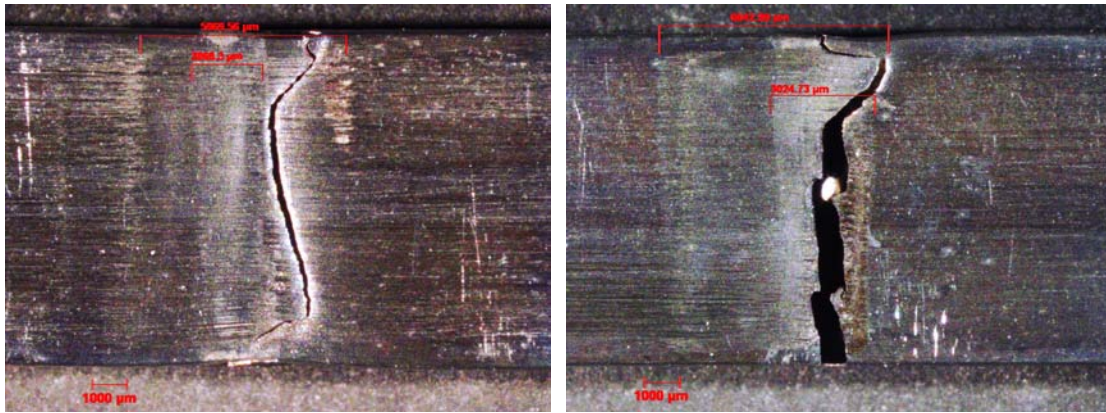
Figure B.12 – Left and right of specimen 2
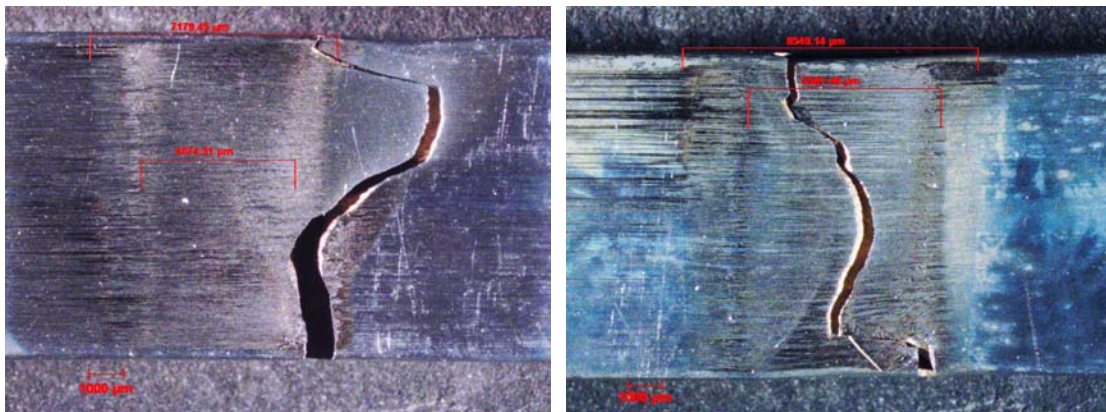
Figure B.13 – Left and right of specimen 3
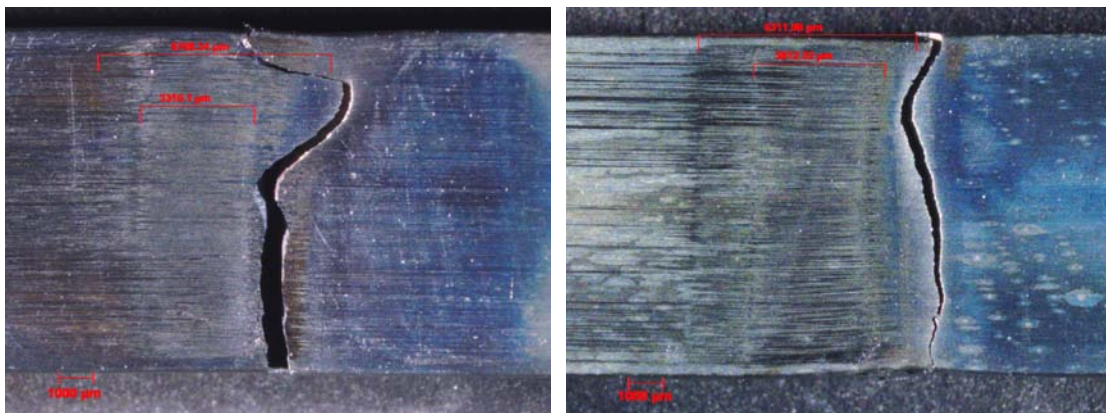
Figure B.14 – Left and right of specimen 4
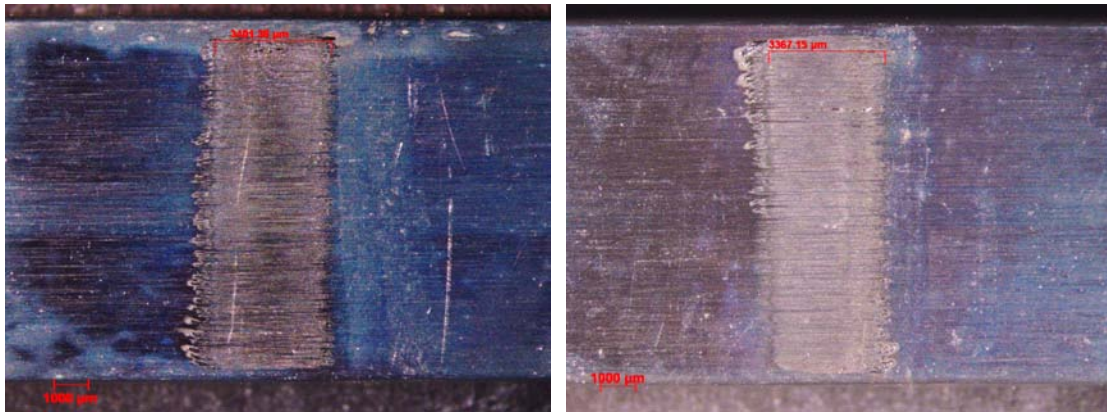
Figure B.15 – Left and right of specimen 5
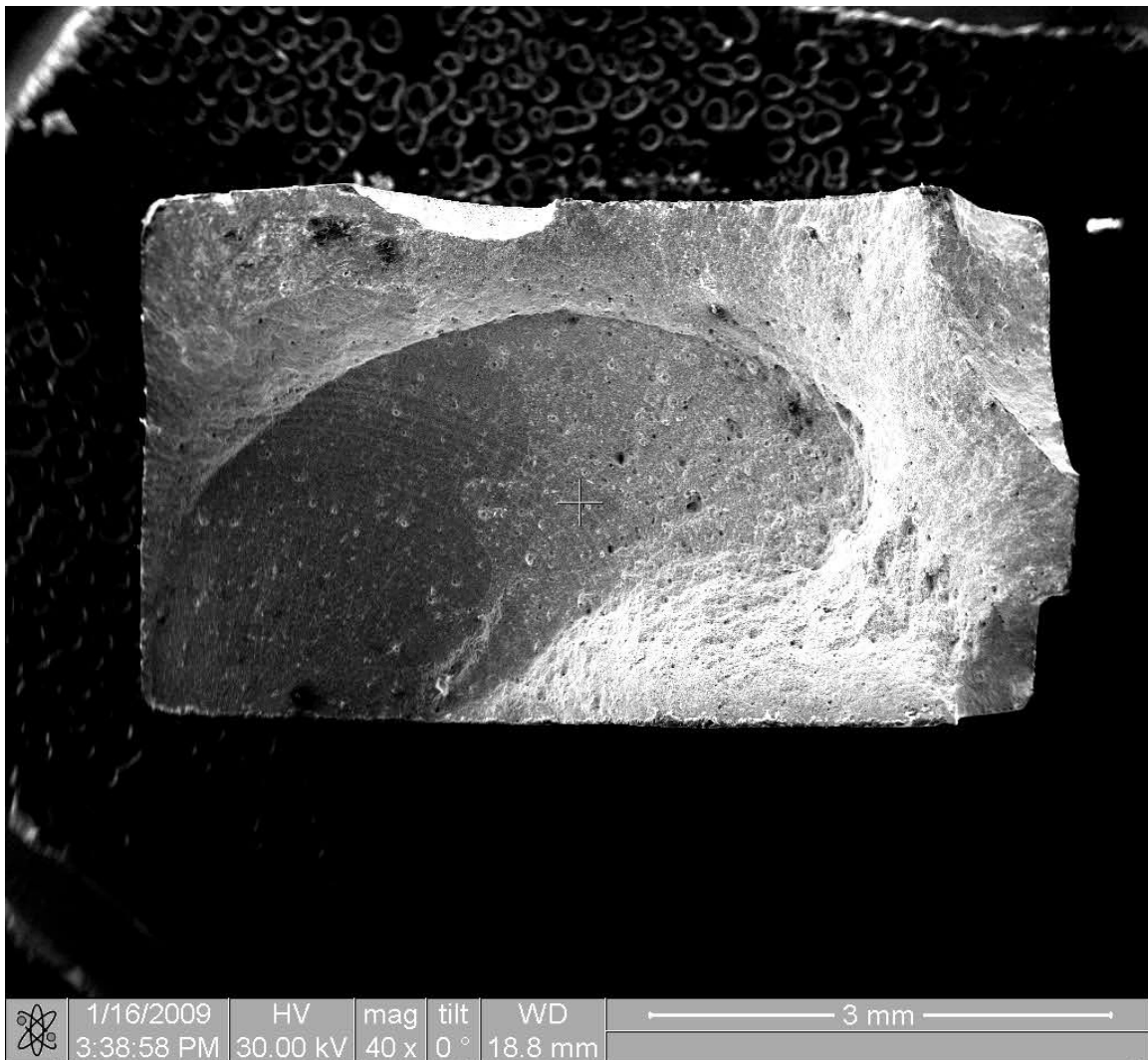
Figure B.16 – Specimen 1, fracture surface
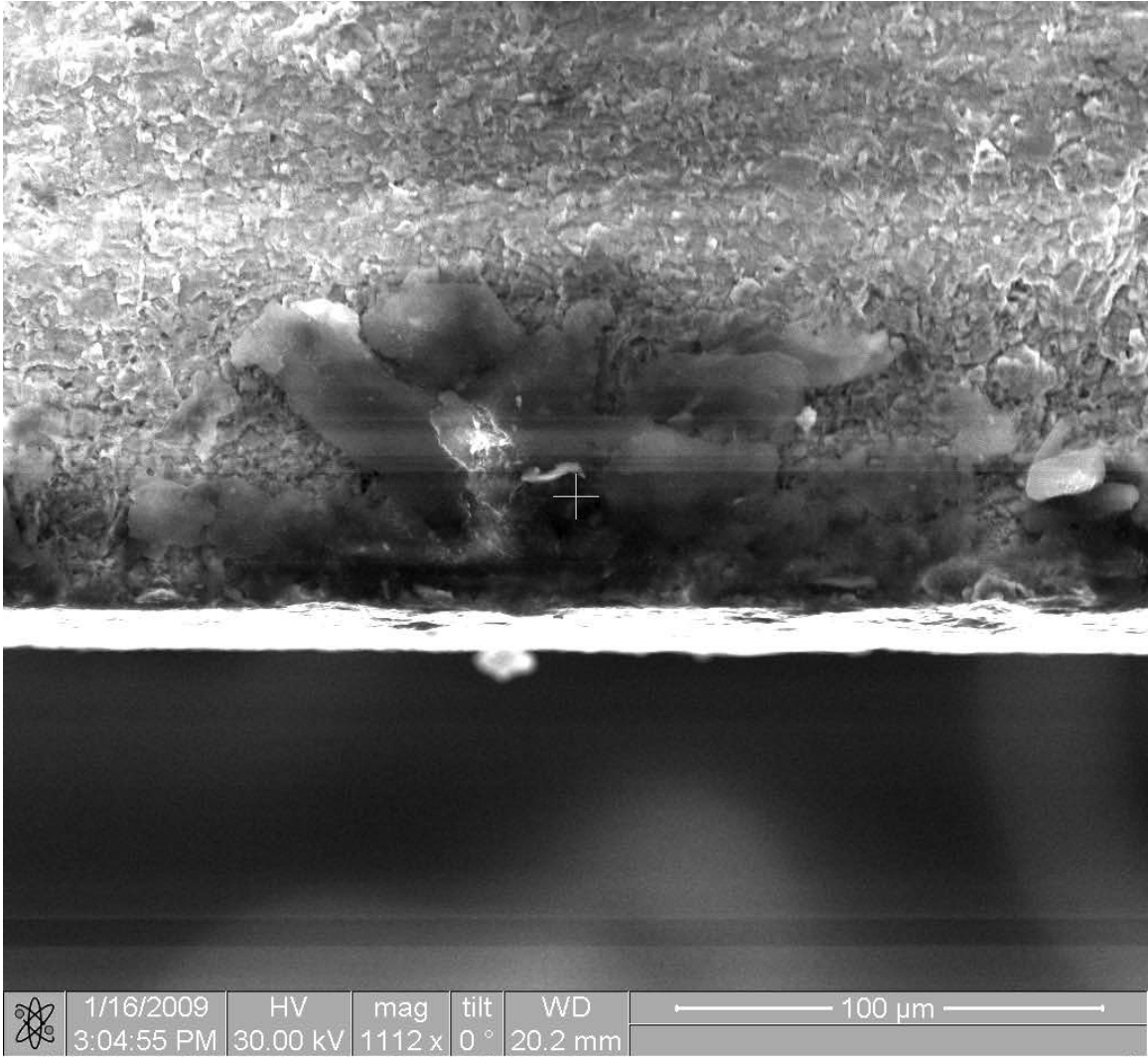
Figure B.17 – Specimen 1, crack initiation

1/16/2009 | HV | mag | tilt | WD | 4 mm
4:10:05 PM | 30.00 kV | 35 x | 0 ° | 17.1 mm
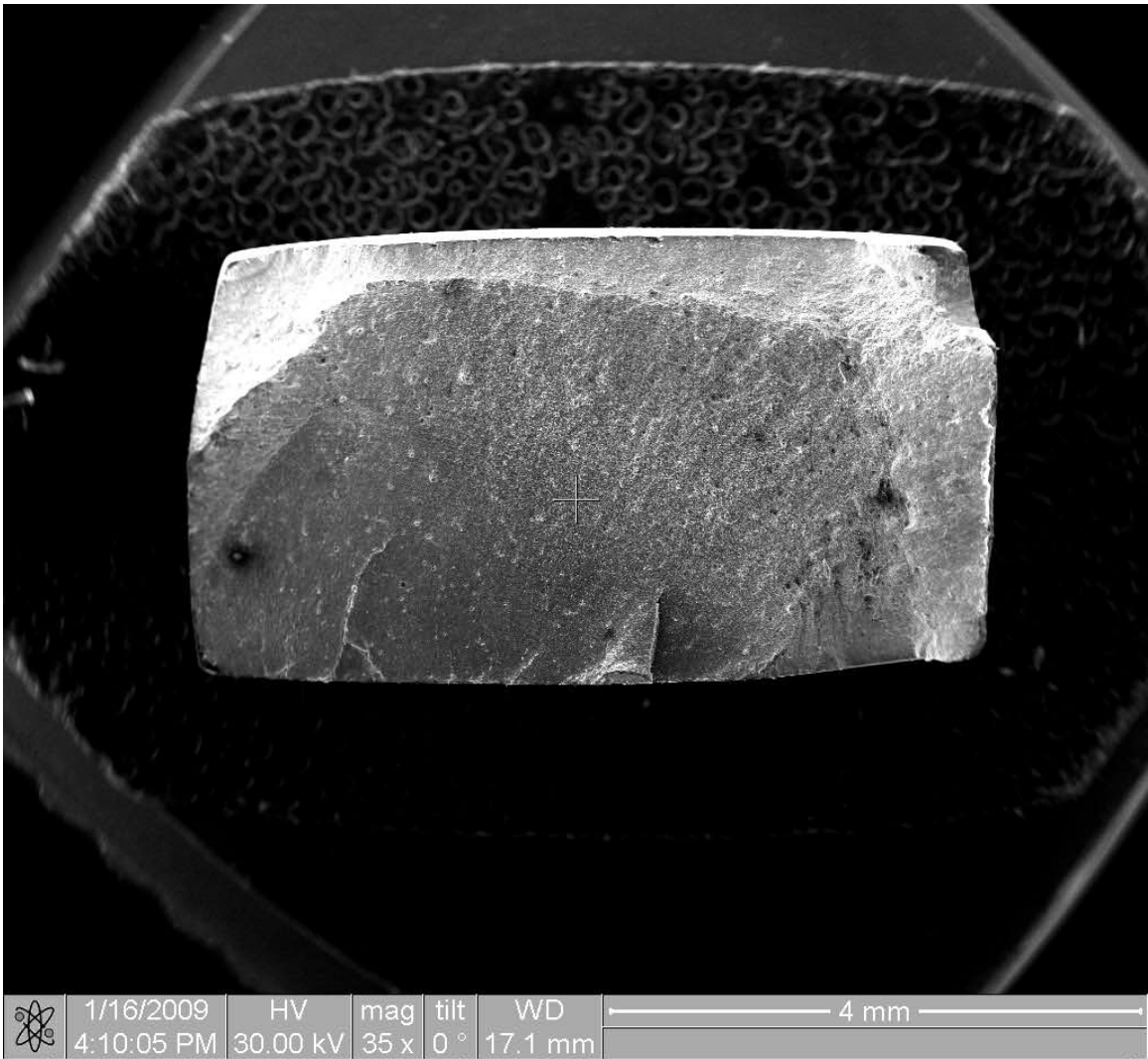
Figure B.18 – Specimen 2, fracture surface
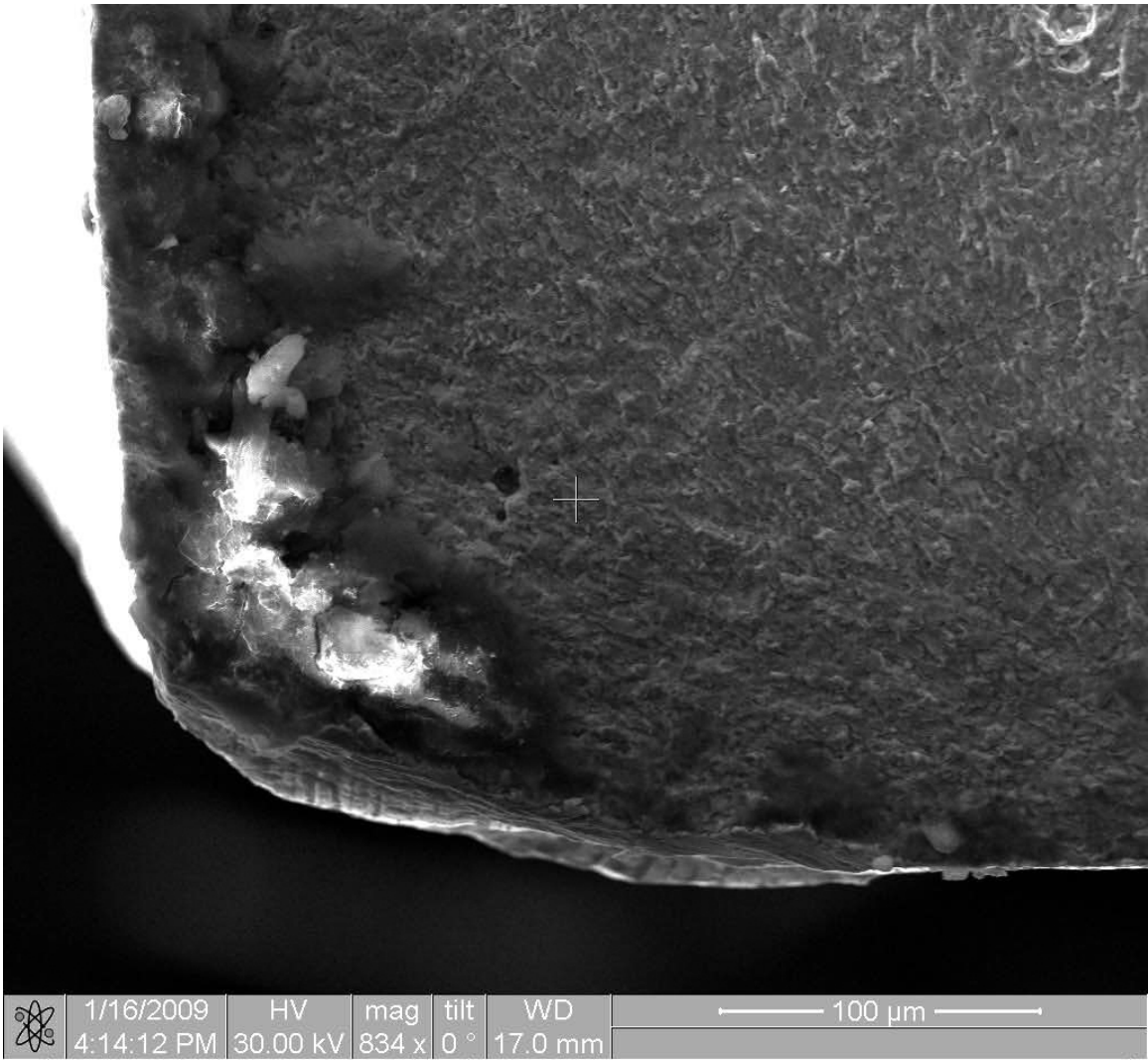
Figure B.19 – Specimen 2, crack initiation
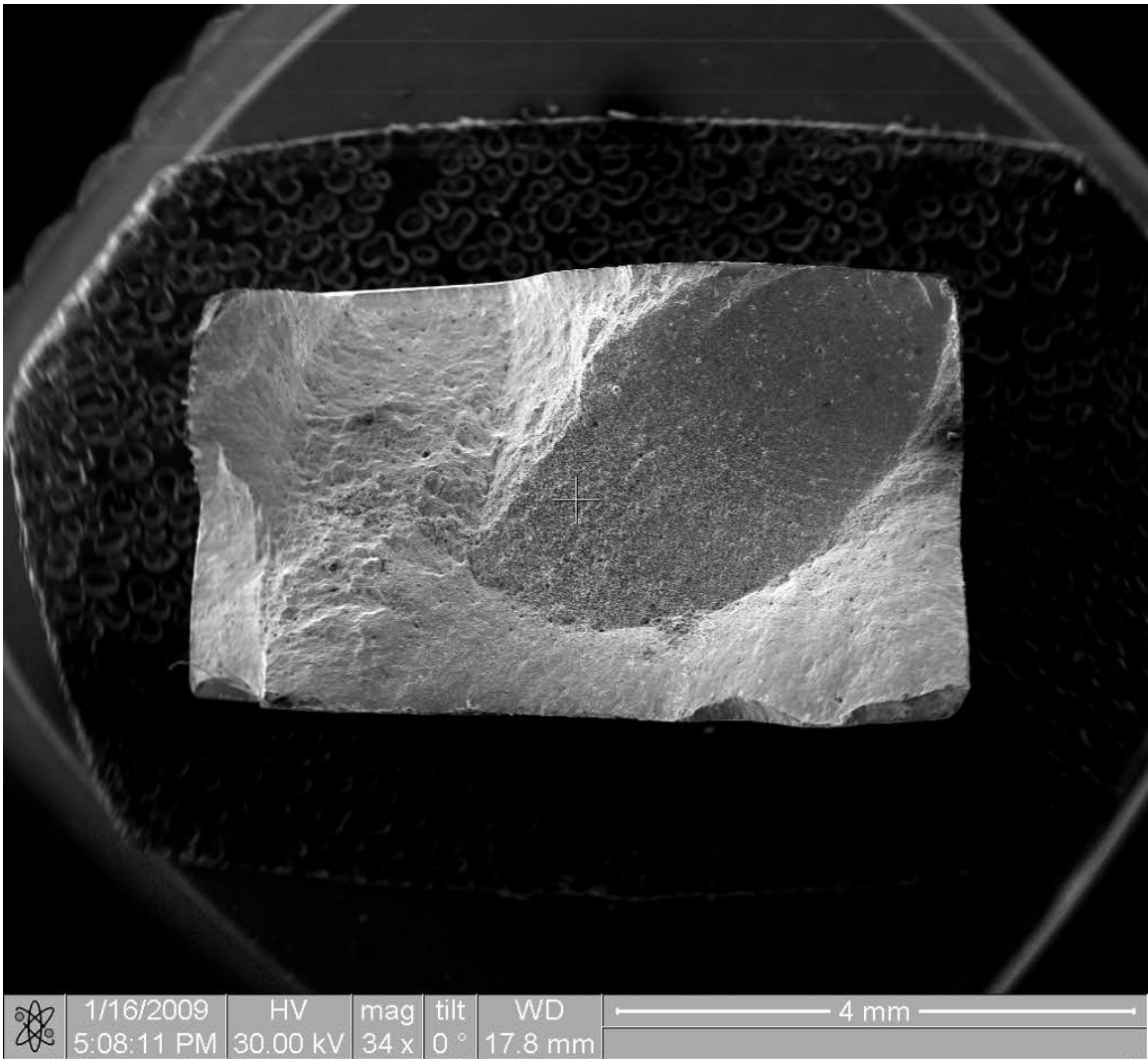
Figure B.20 – Specimen 3, fracture surface
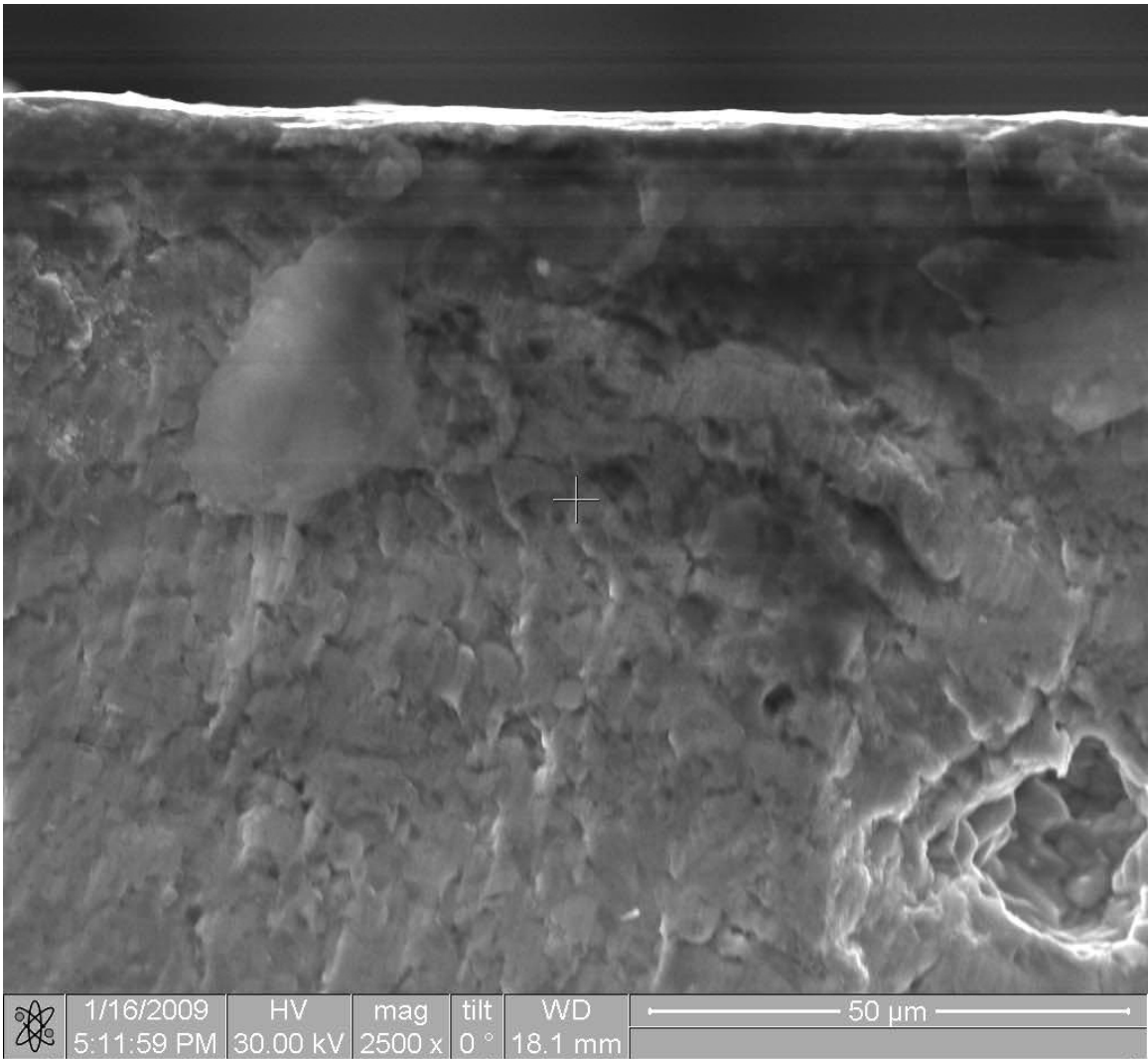
Figure B.21 – Specimen 3, crack initiation
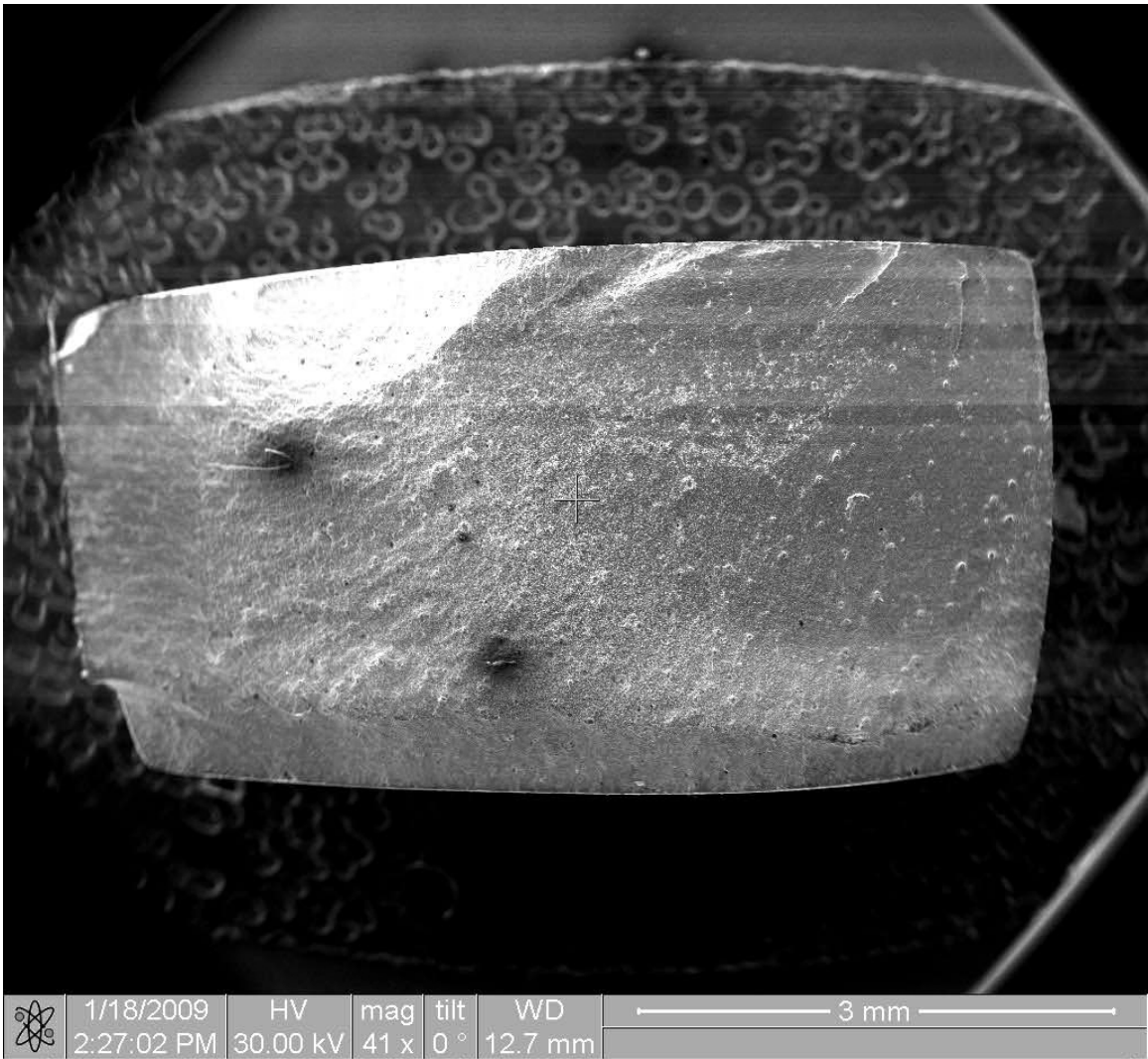
Figure B.22 – Specimen 4, fracture surface
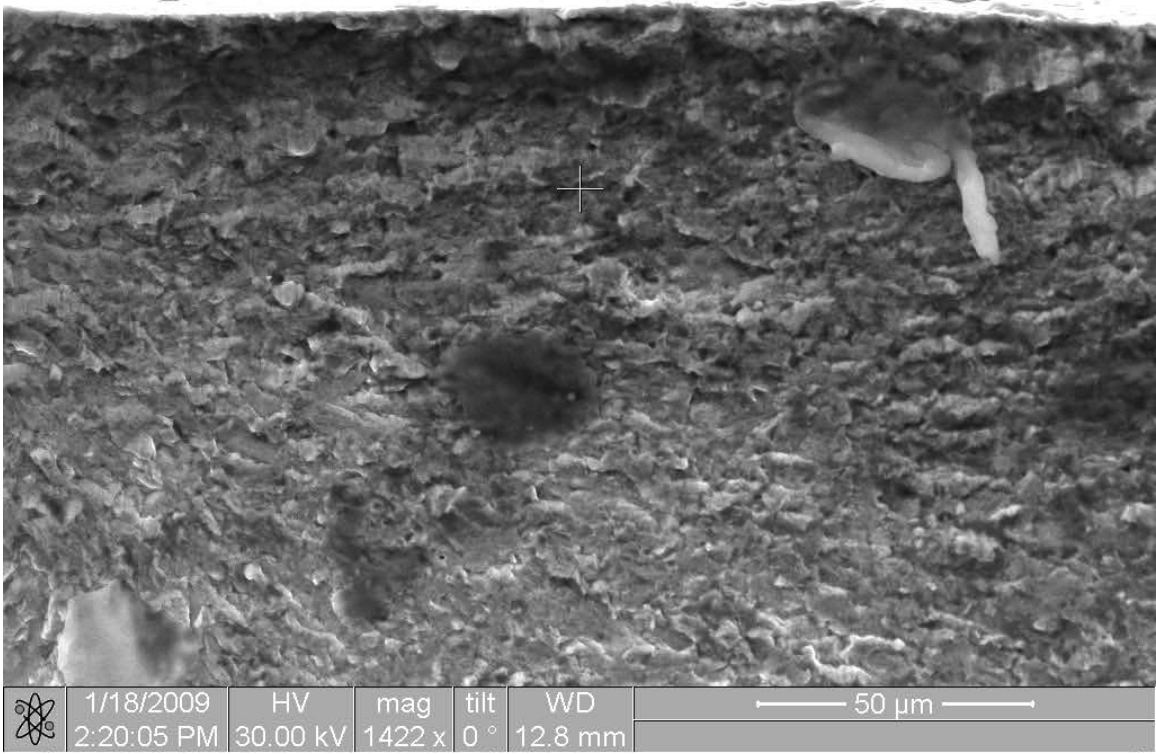
Figure B.23 - Specimen 4, Crack initiation
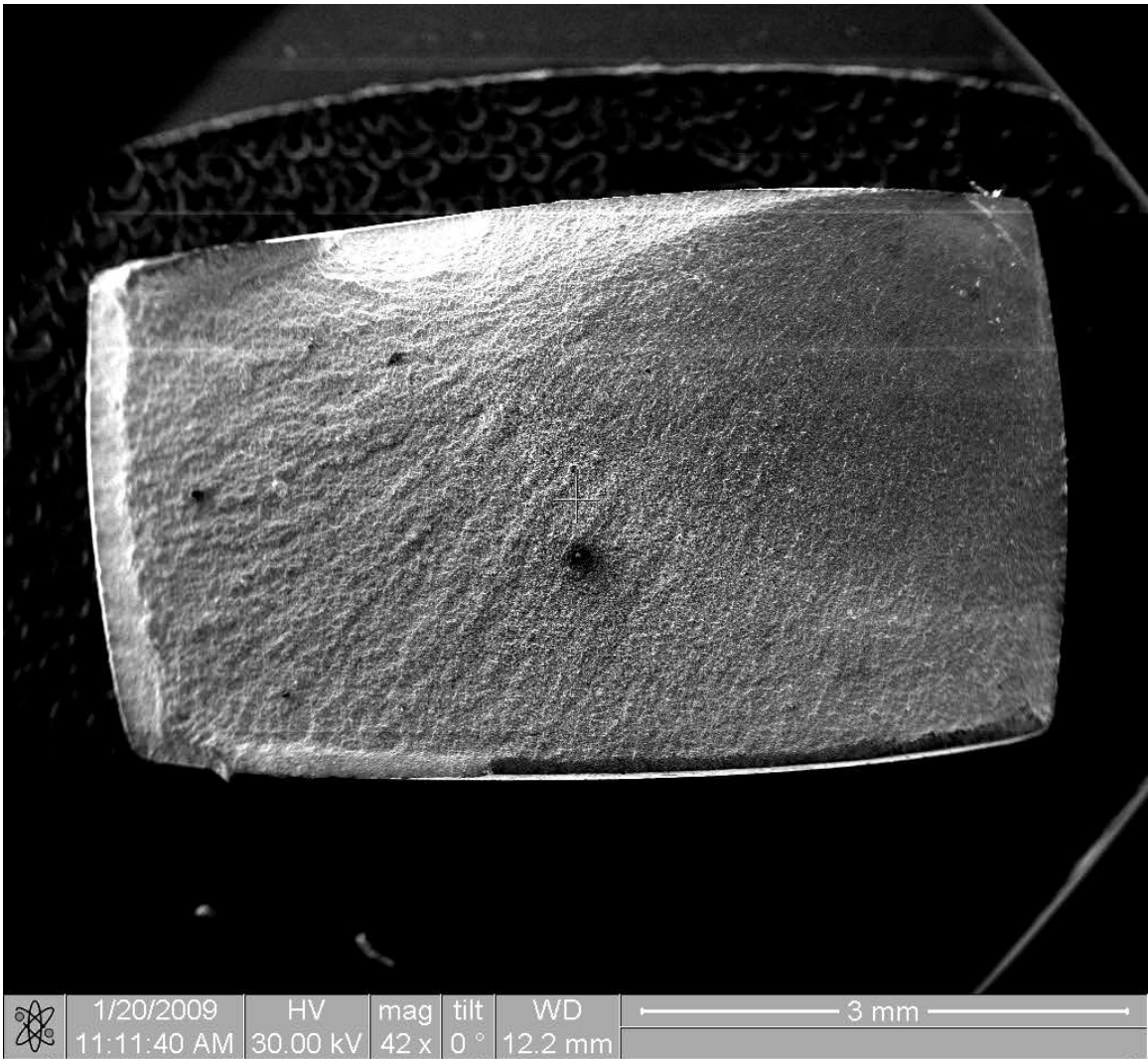
Figure B.24 – Specimen 6, fracture surface
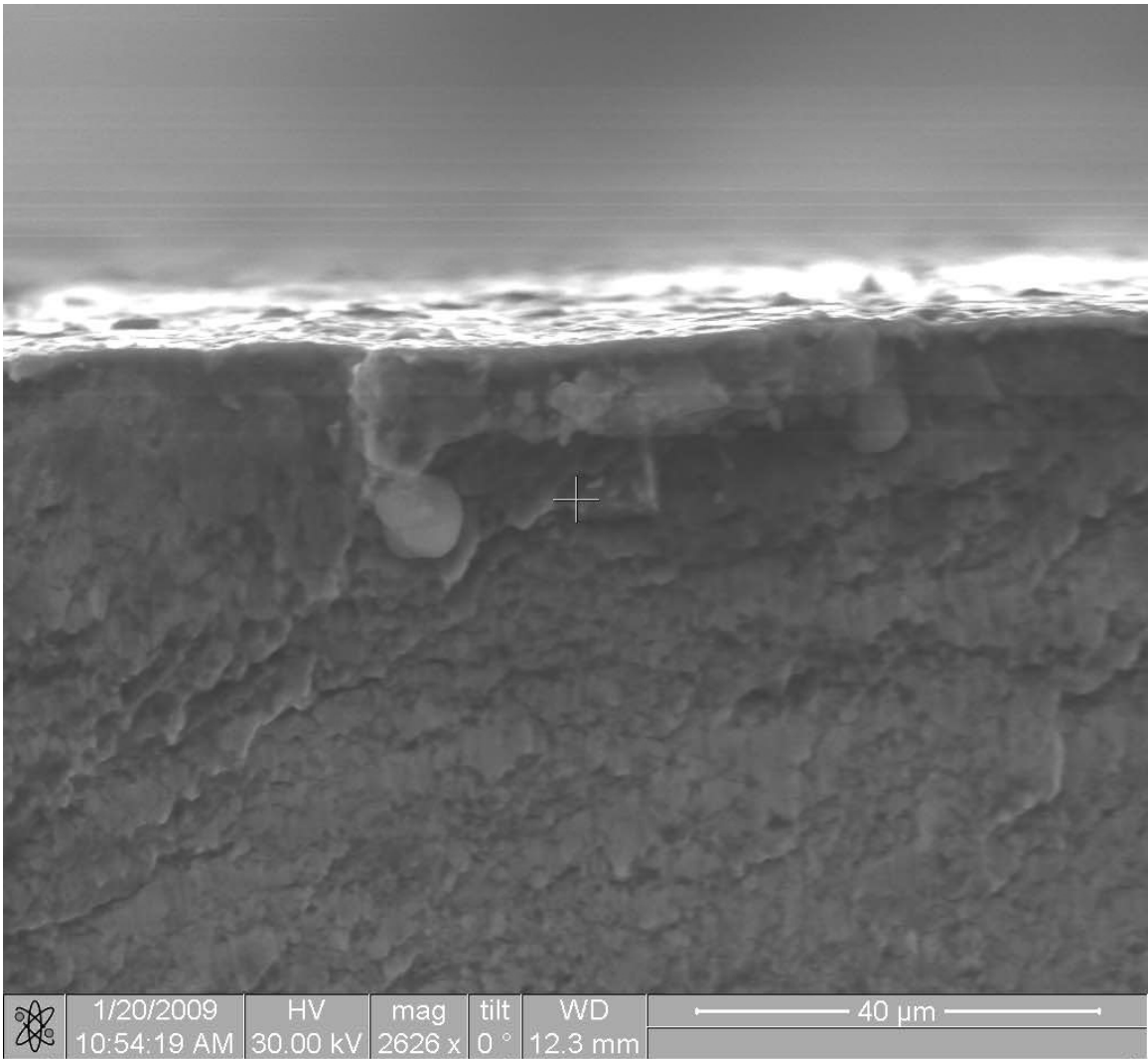
Figure B.25 – Specimen 6, crack initiation
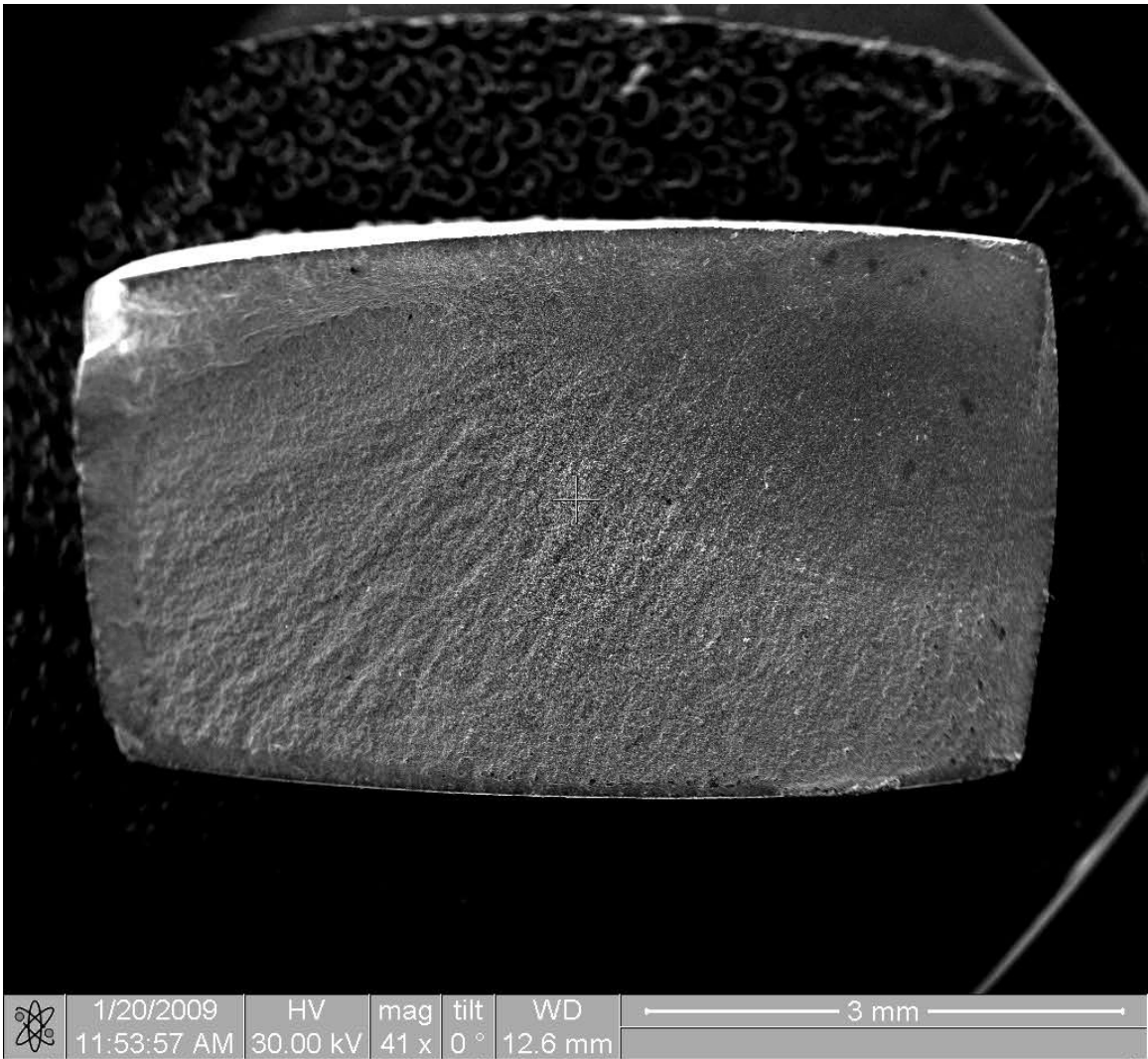
Figure B.26 – Specimen 7, fracture surface
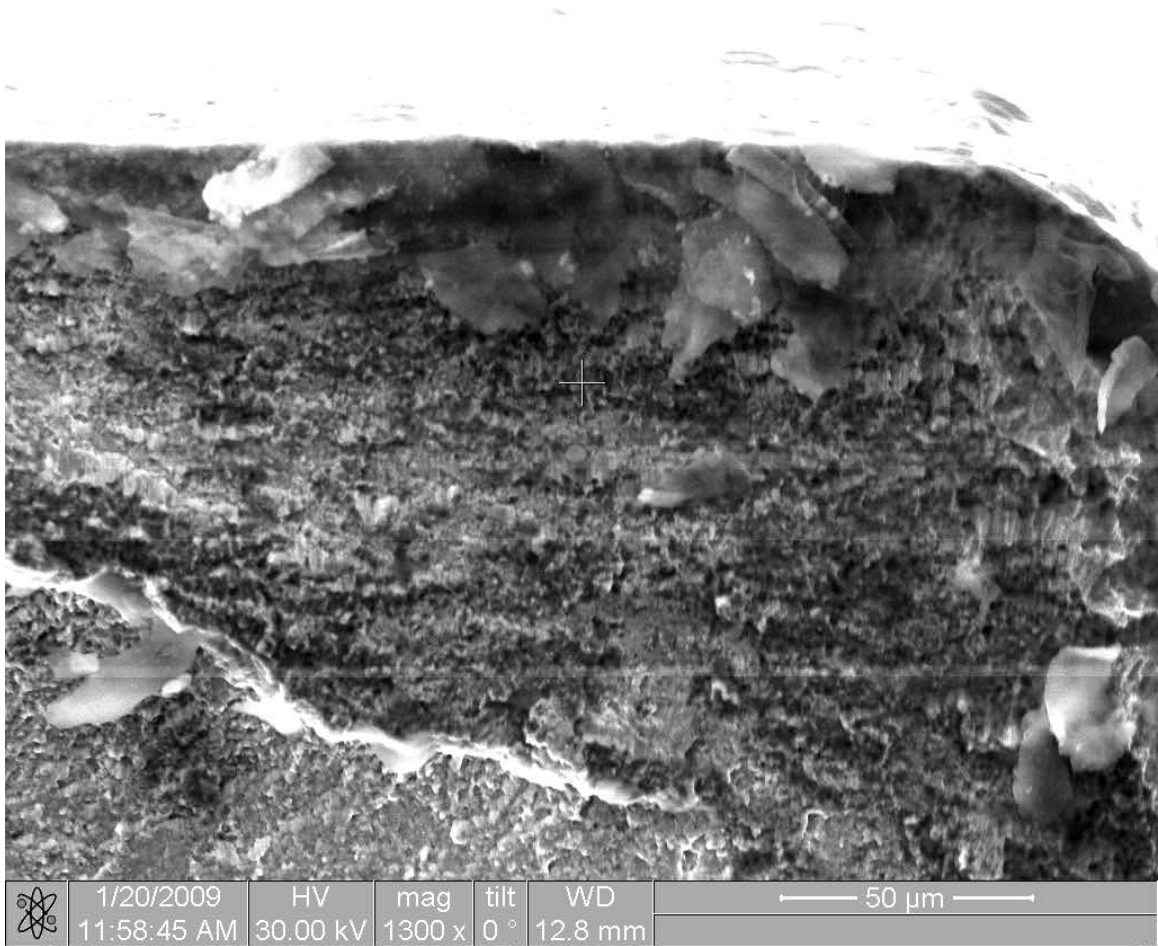
Figure B.27 – Specimen 7, crack initiation
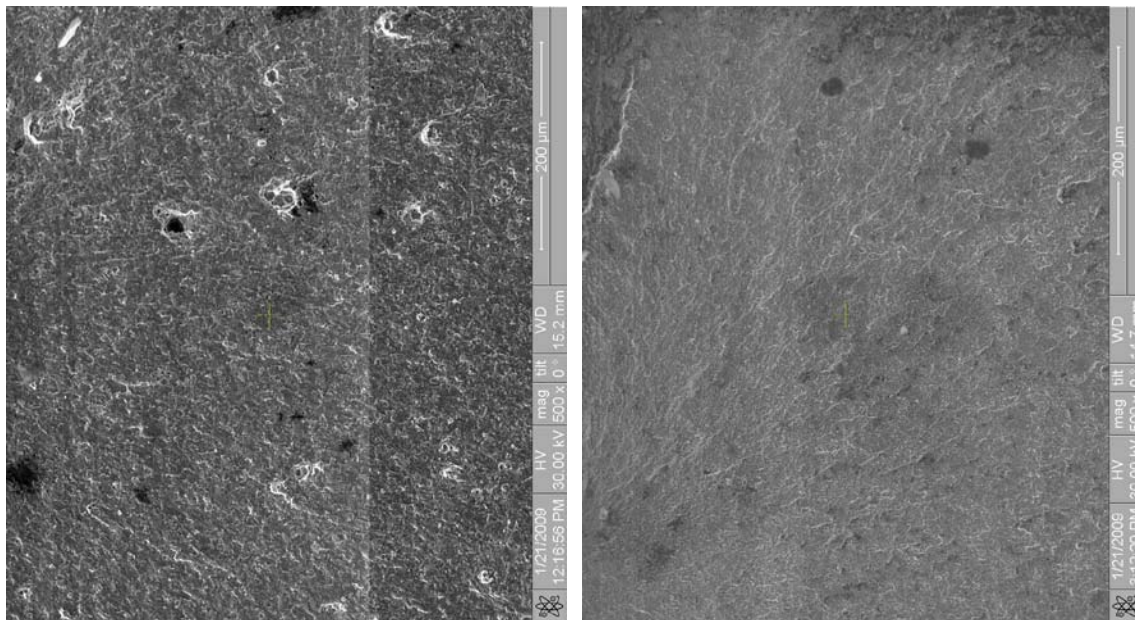
a)   b)
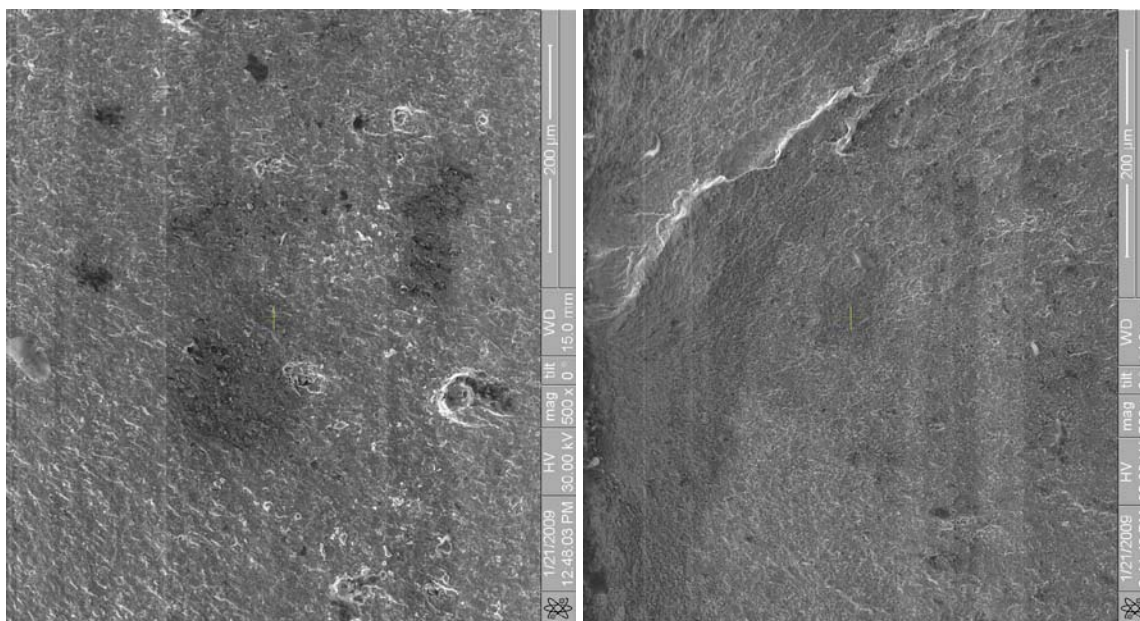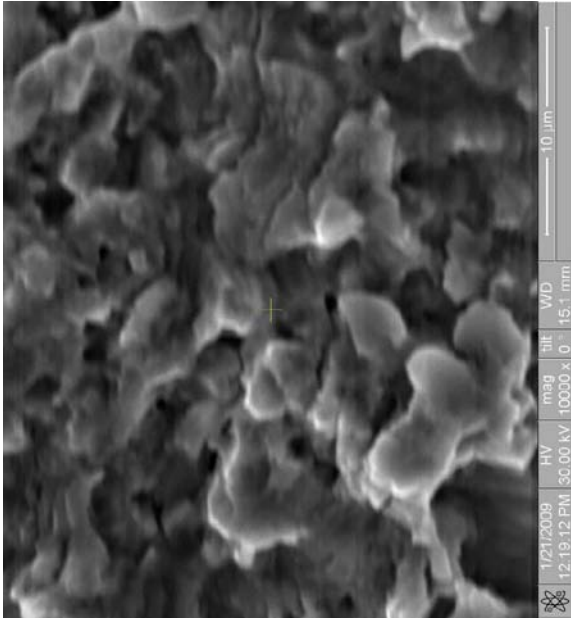
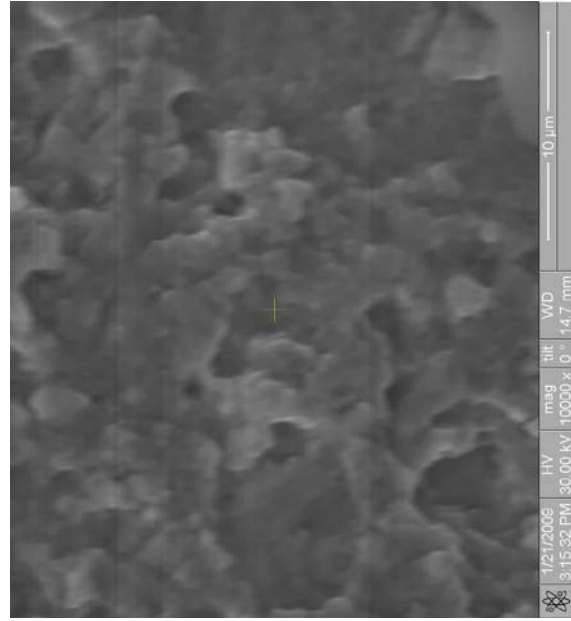c)   d)
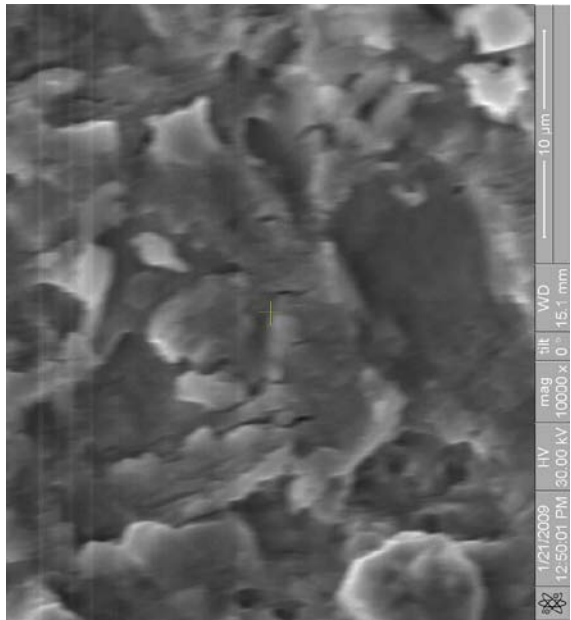
Figure B.28 – Zone I 500x magnification

a) Specimen 3, b) Specimen 7, c) Specimen 4, d) Specimen 6
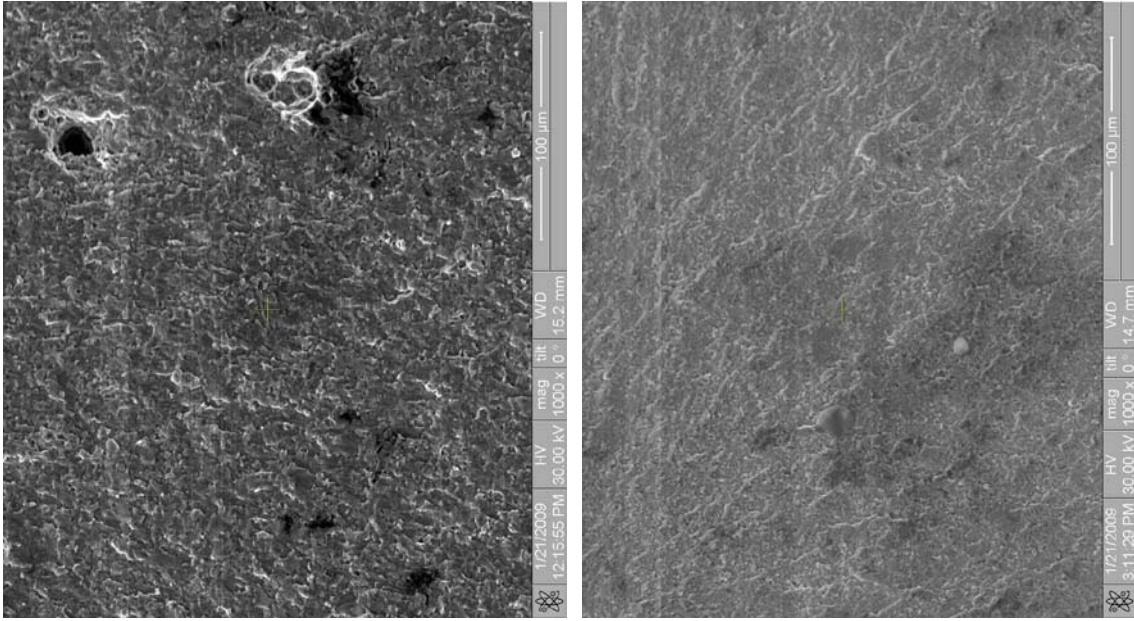
a)

b)
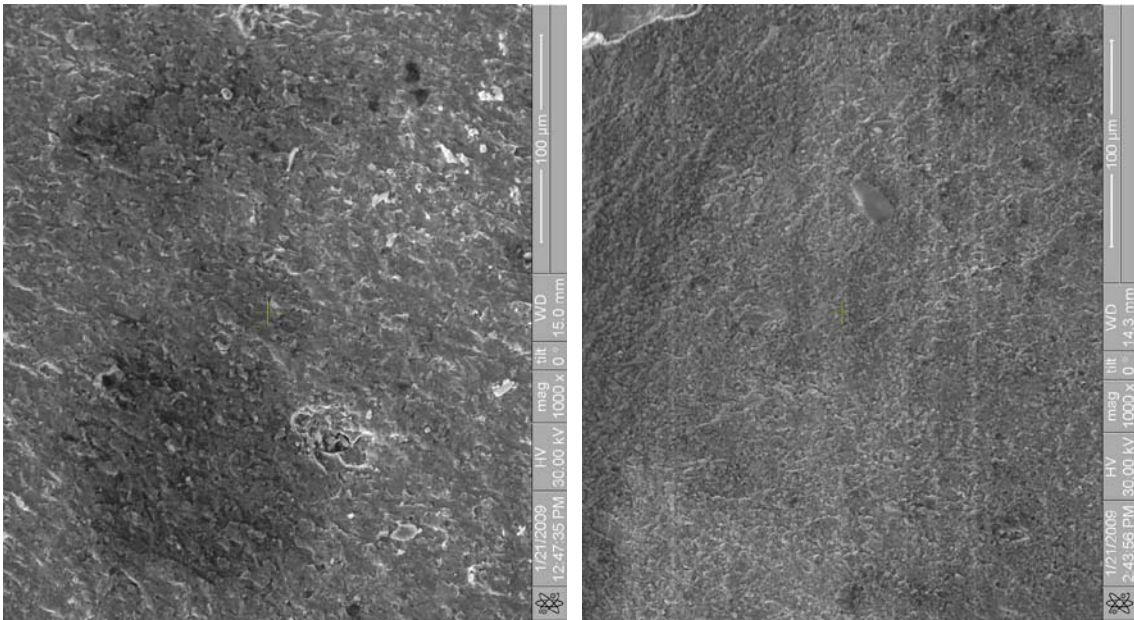
c)

d)

Figure B.29 – Zone I 1,000x magnification

a) Specimen 3, b) Specimen 7, c) Specimen 4, d) Specimen 6
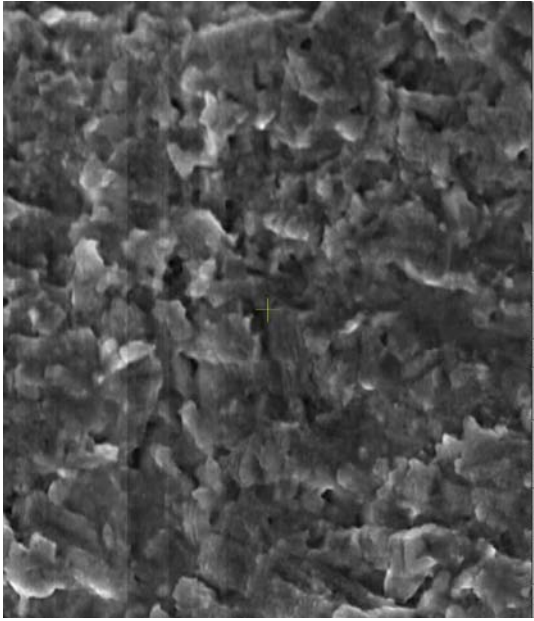
a)
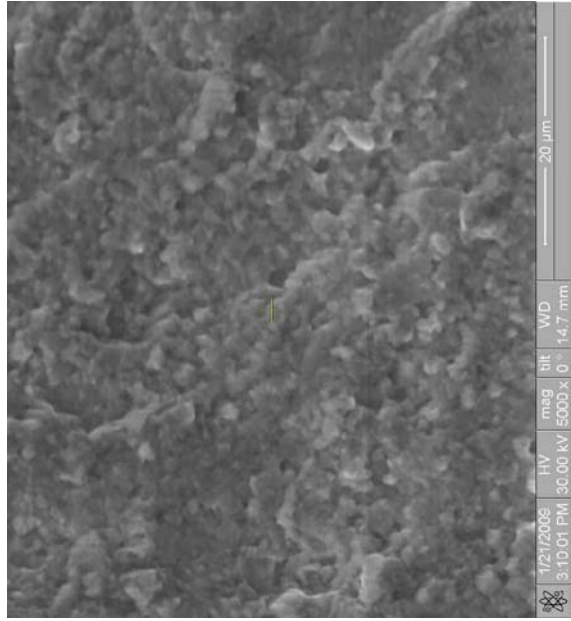
b)
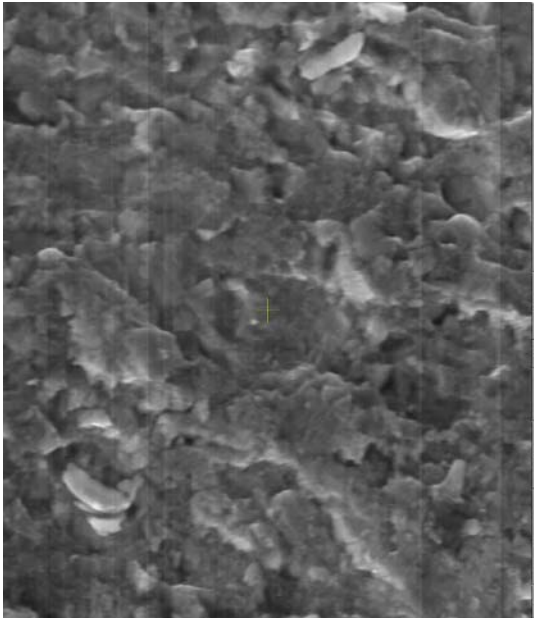
c)
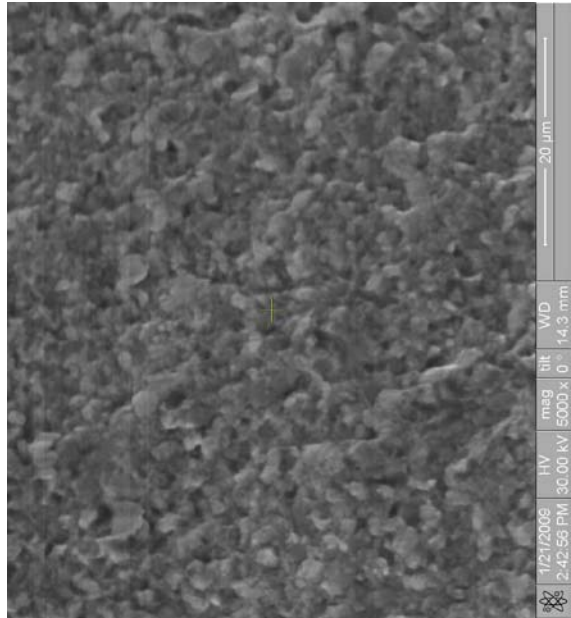
d)

Figure B.30 – Zone 1 5,000x magnification

a) Specimen 3, b) Specimen 7, c) Specimen 4, d) Specimen 6
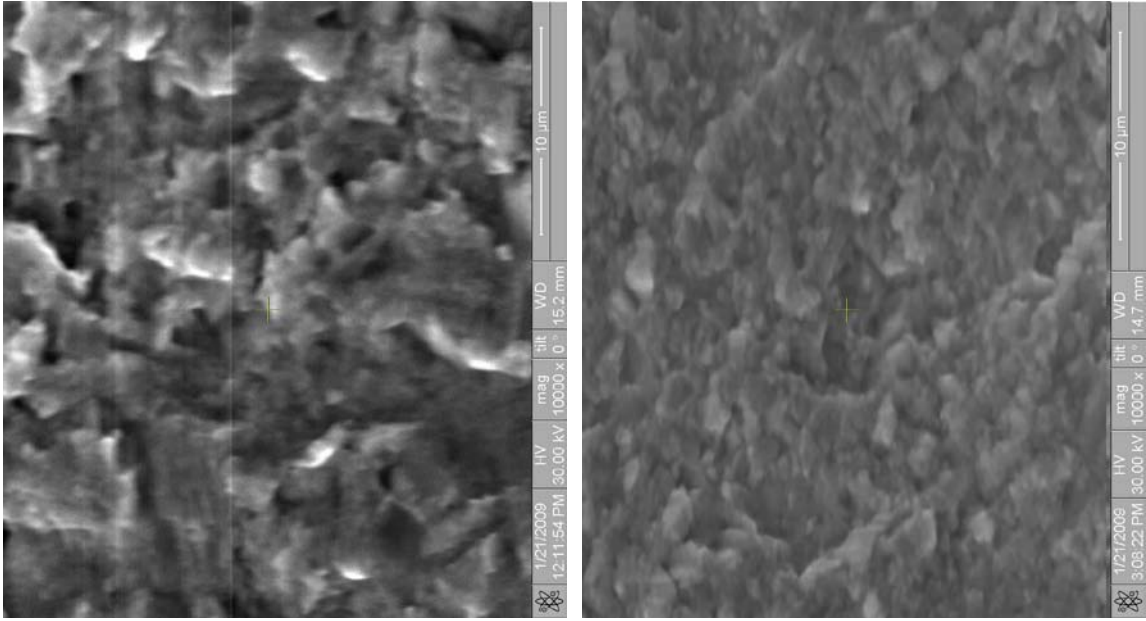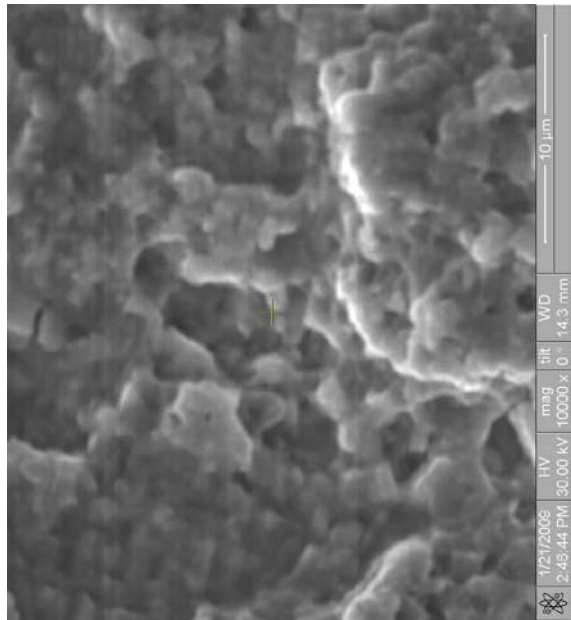
a)

b)
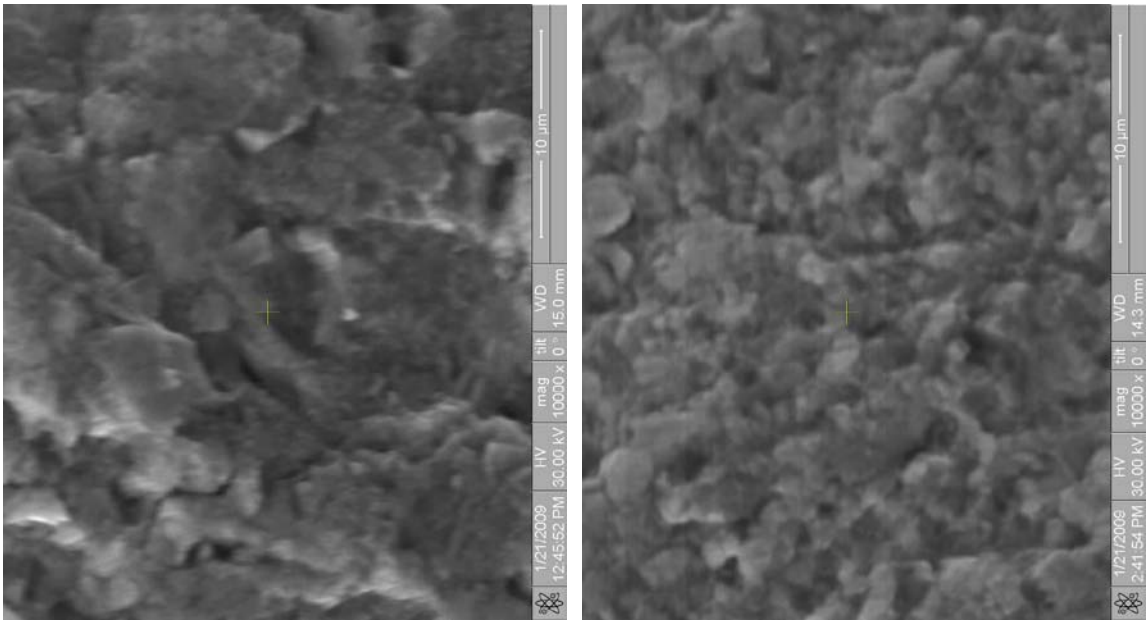
c)

d)

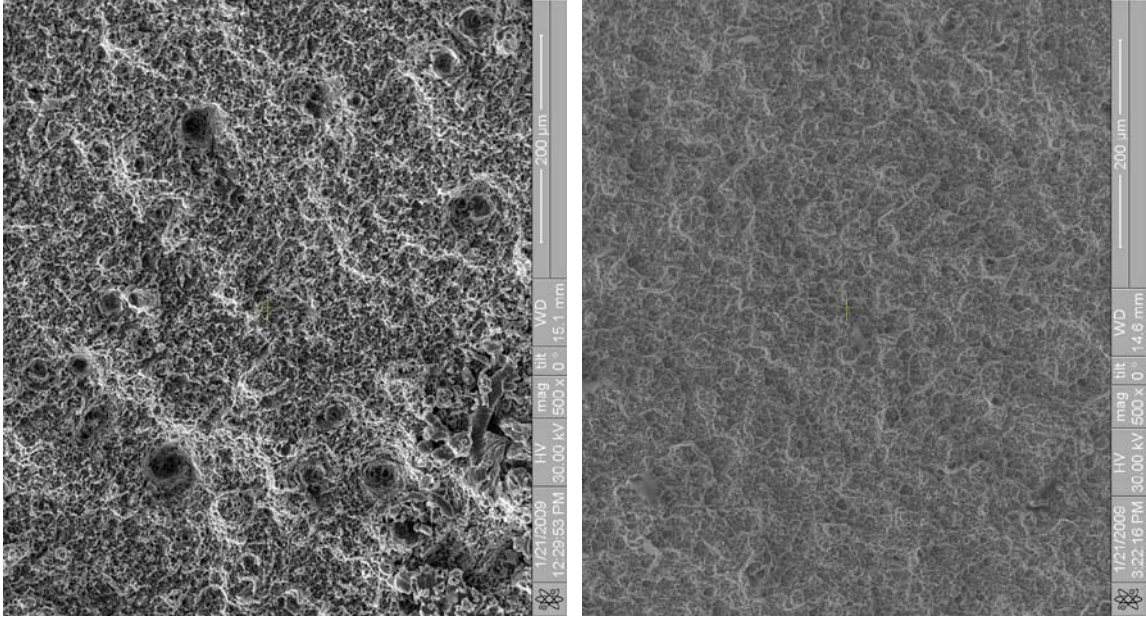Figure B.31 – Zone I 10,000x magnification

a) Specimen 3, b) Specimen 7, c) Specimen 4, d) Specimen 6
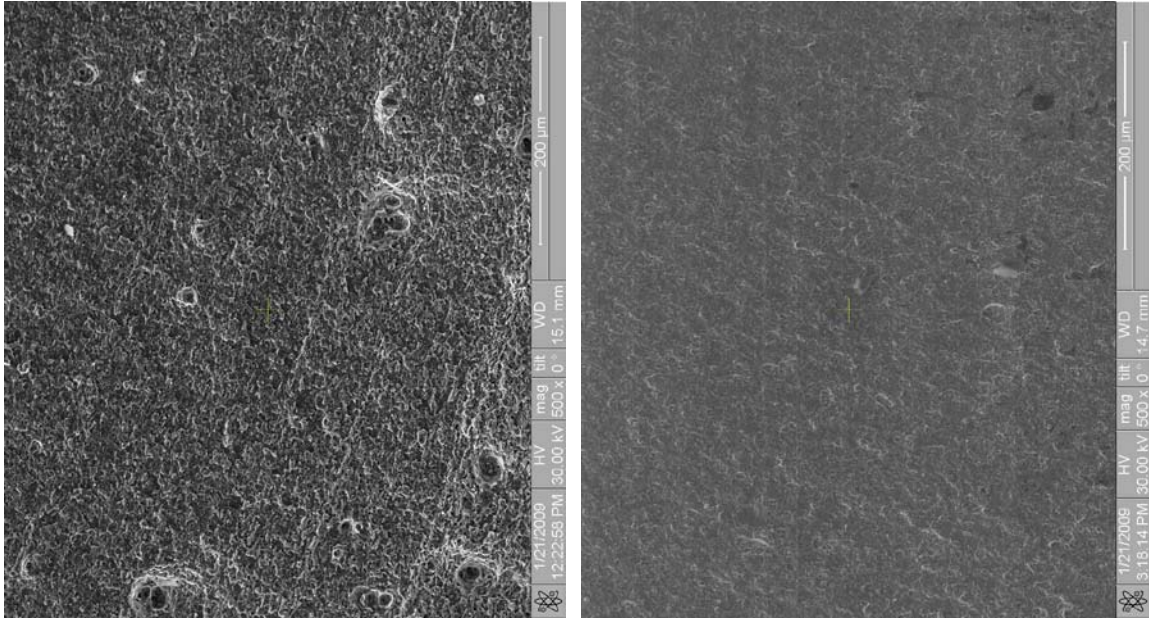
a)   b)
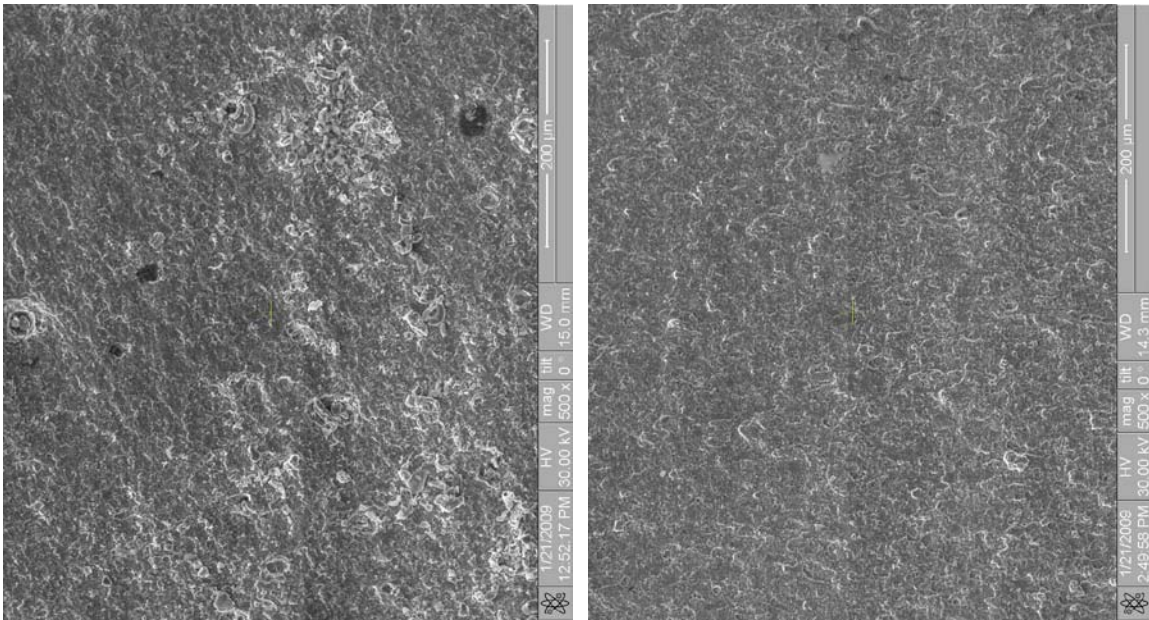
c)   d)

Figure B.32 – Zone II 500x magnification

a) Specimen 3, b) Specimen 7, c) Specimen 4, d) Specimen 6
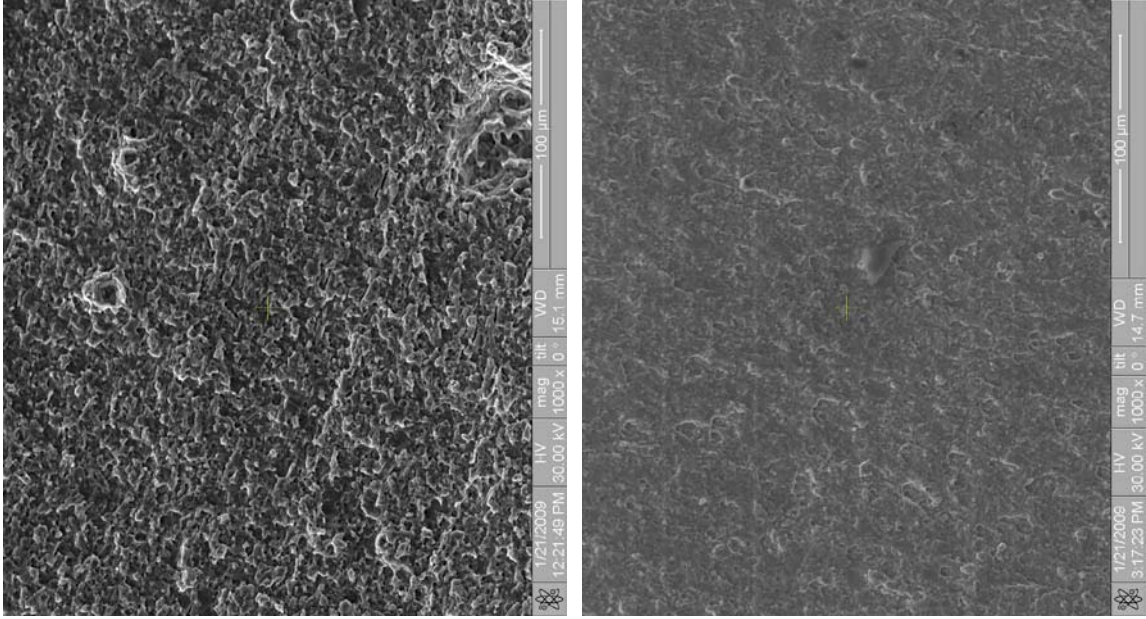
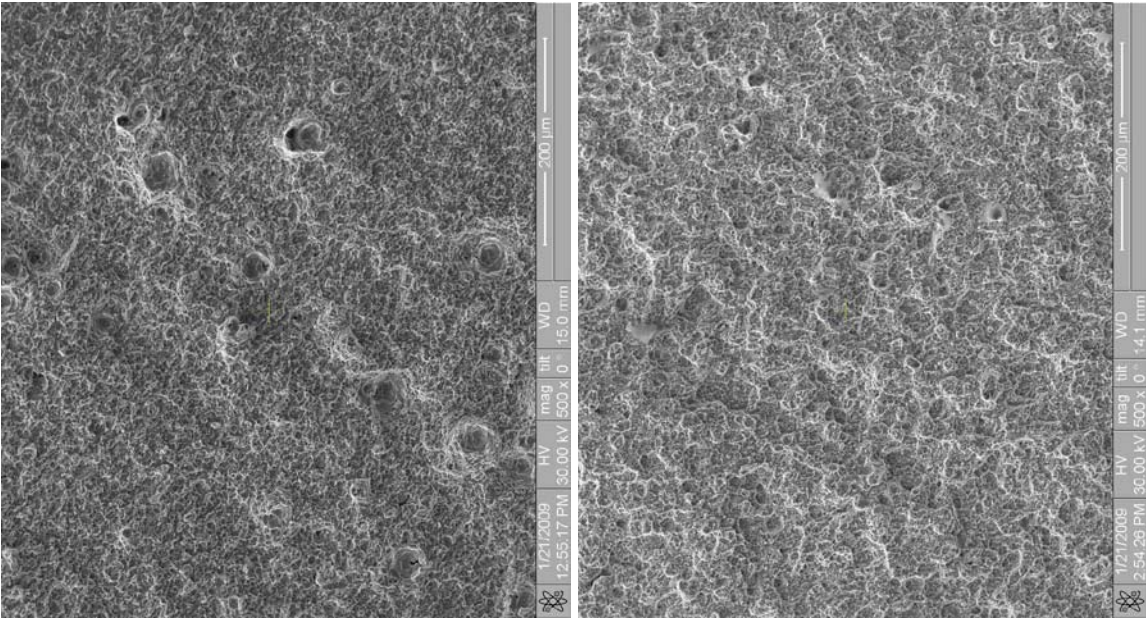a)   b)
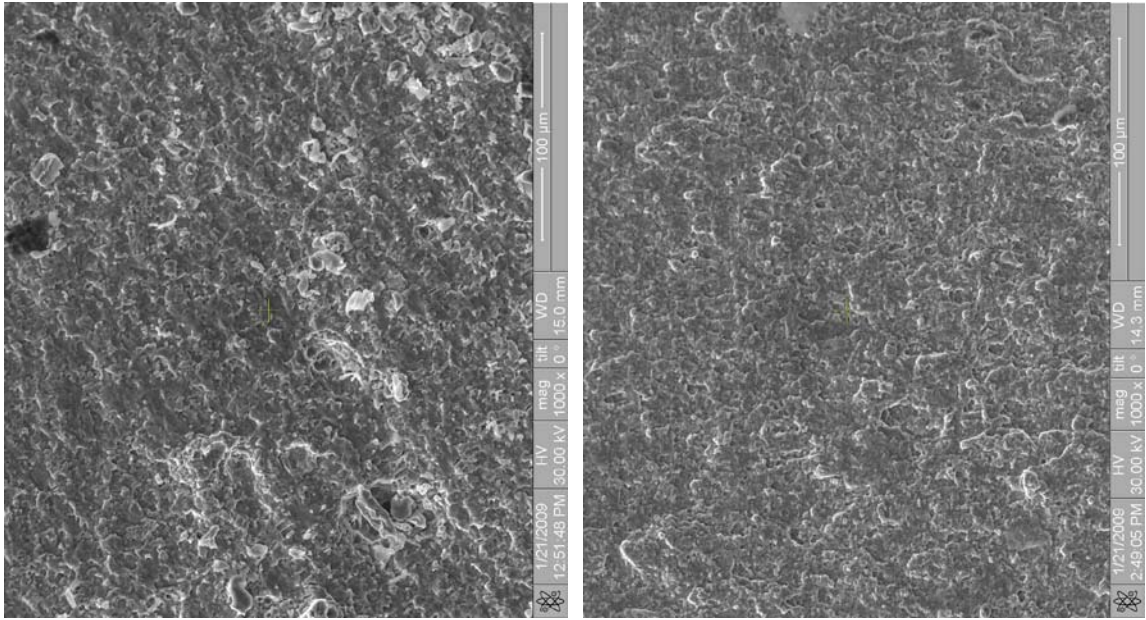
c)   d)

Figure B.33 – Zone II 1,000x magnification

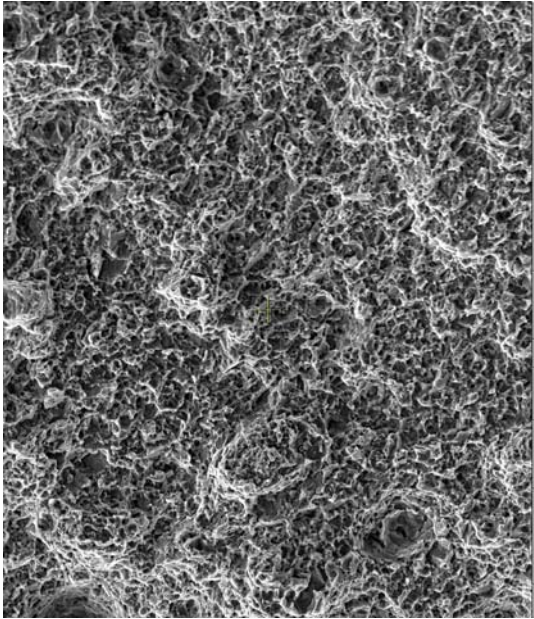a) Specimen 3, b) Specimen 7, c) Specimen 4, d) Specimen 6
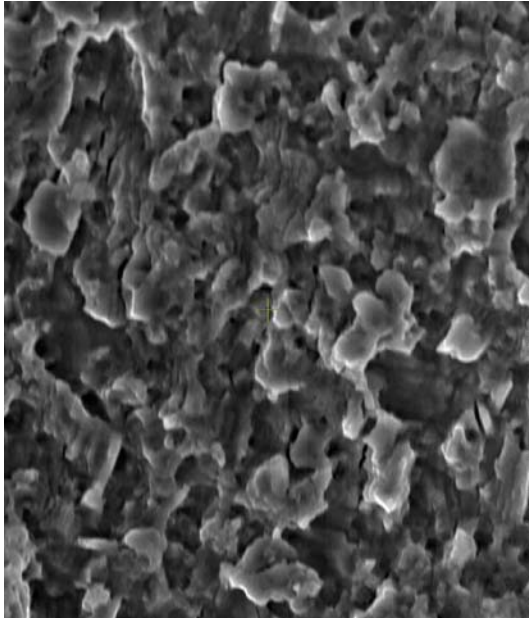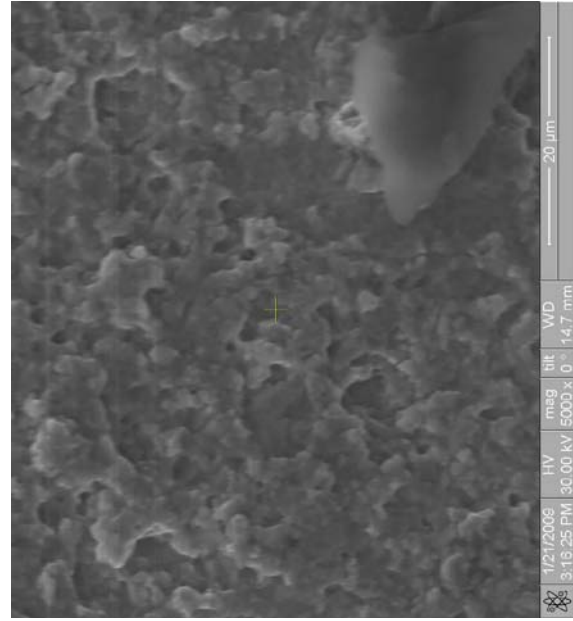
a)   b)
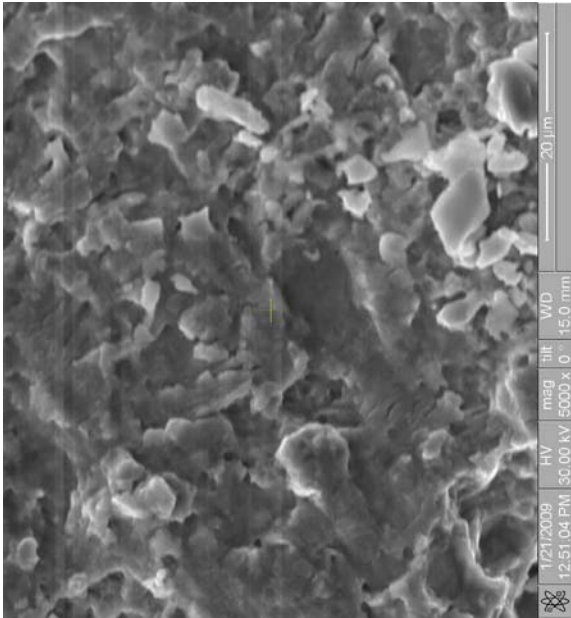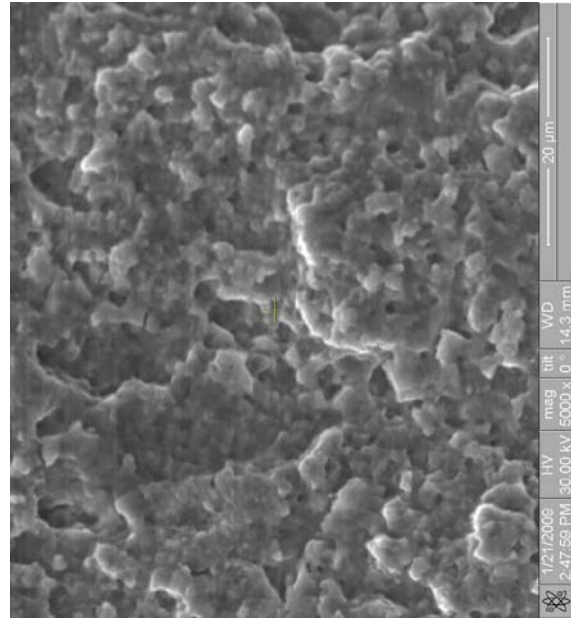
c)   d)

Figure B.34 – Zone II 5,000x magnification

a) Specimen 3, b) Specimen 7, c) Specimen 4, d) Specimen 6

a)   b)

c)   d)

Figure B.35 – Zone II 10,000x magnification

a) Specimen 3, b) Specimen 7, c) Specimen 4, d) Specimen 6
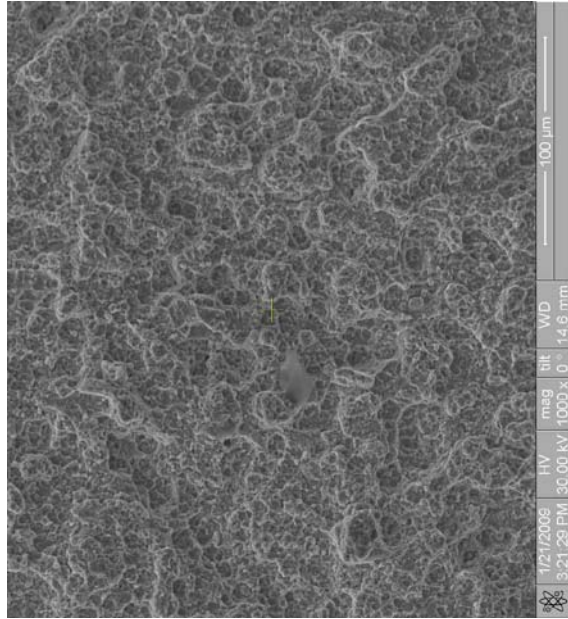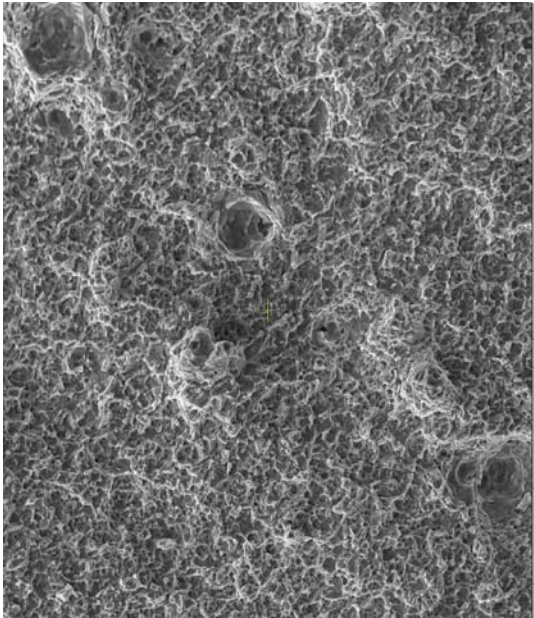
a)   b)

c)   d)

Figure B.36 – Zone III 500x magnification

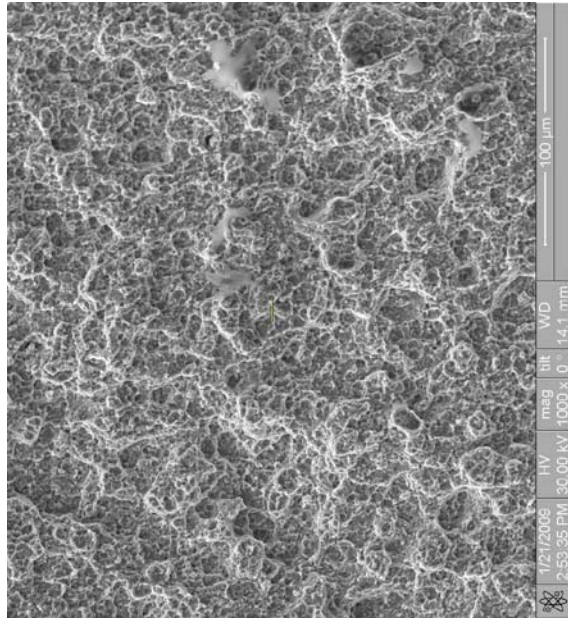a) Specimen 3, b) Specimen 7, c) Specimen 4, d) Specimen 6

a)

b)

c)

d)

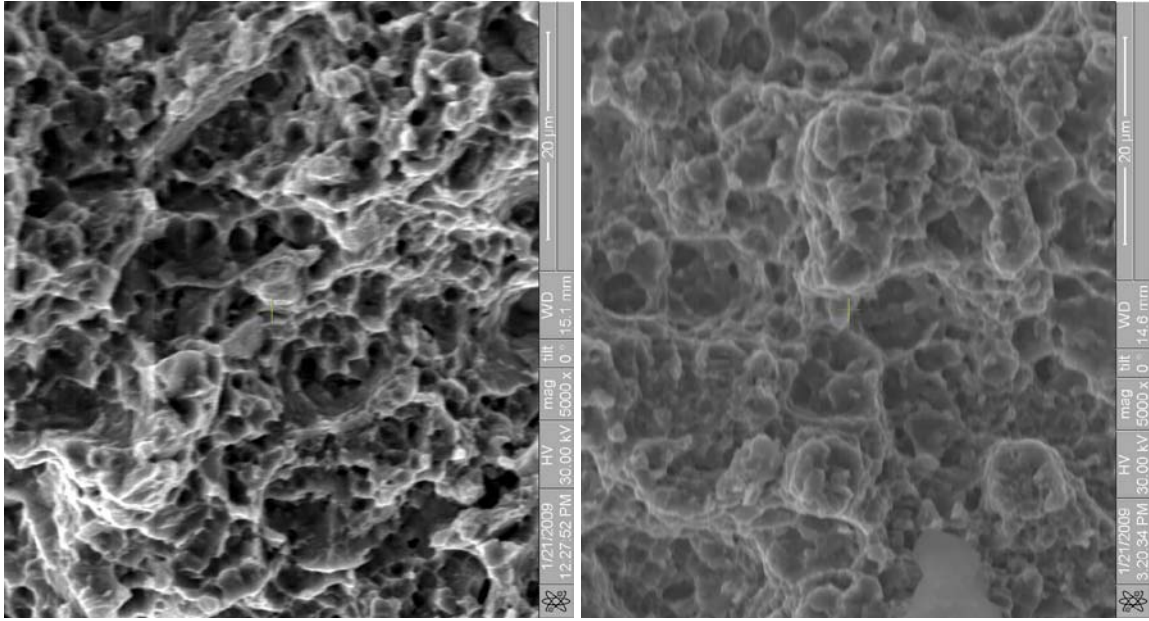Figure B.37 – Zone III 1,000x magnification

a) Specimen 3, b) Specimen 7, c) Specimen 4, d) Specimen 6

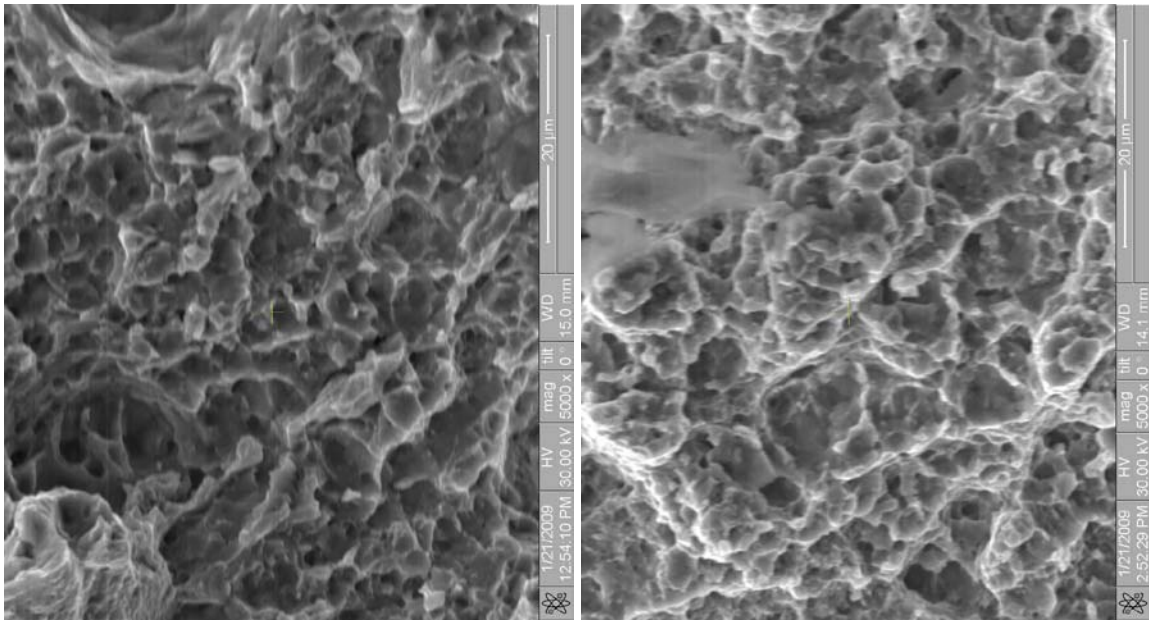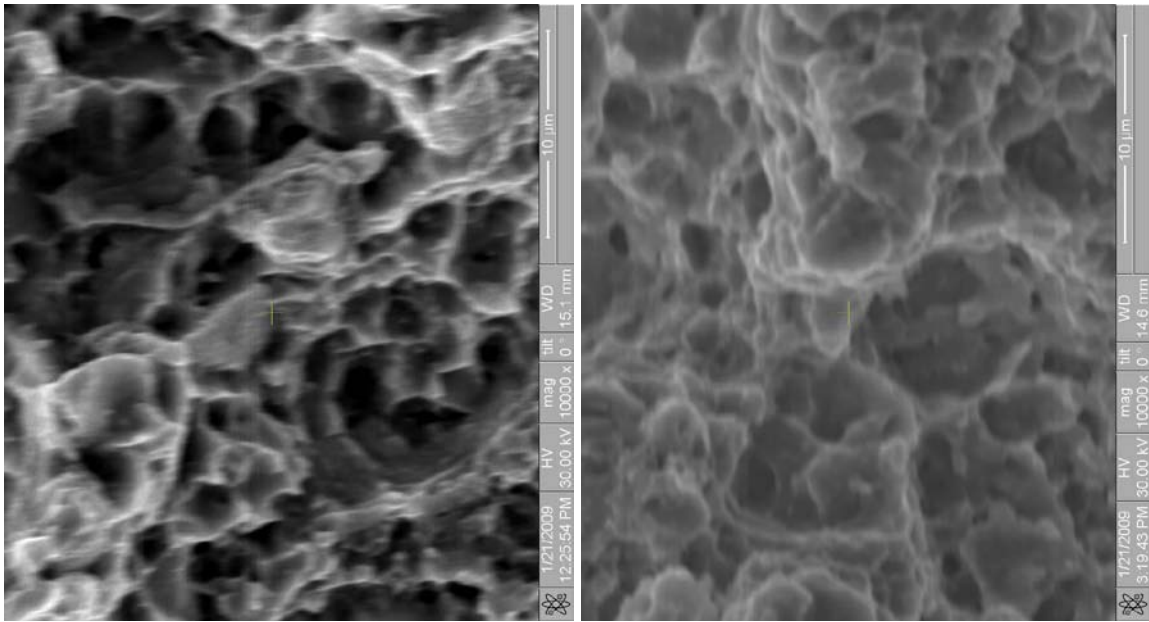a)   b)

c)   d)

Figure B.38 – Zone III 5,000x magnification

a) Specimen 3, b) Specimen 7, c) Specimen 4, d) Specimen 6

a)

b)

c)

d)

Figure B.39 – Zone III 10,000x magnification

a) Specimen 3, b) Specimen 7, c) Specimen 4, d) Specimen 6

a)　　　　　　　　　　　　　　　　b)

c)　　　　　　　　　　　　　　　　d)

Figure B.40 – Zone IV 500x magnification

a) Specimen 3, b) Specimen 7, c) Specimen 4, d) Specimen 6

a)

b)

c)

d)

Figure B.41 – Zone IV 1,000x magnification

a) Specimen 3, b) Specimen 7, c) Specimen 4, d) Specimen 6

145

a)   b)
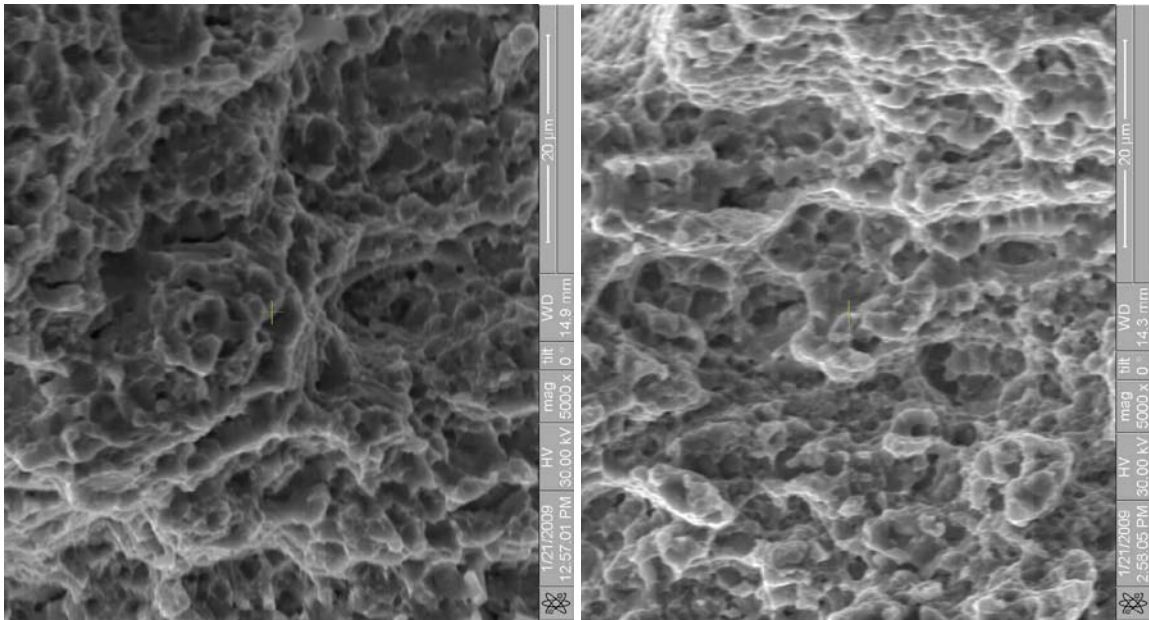
c)   d)

Figure B.42 – Zone IV 5,000x magnification
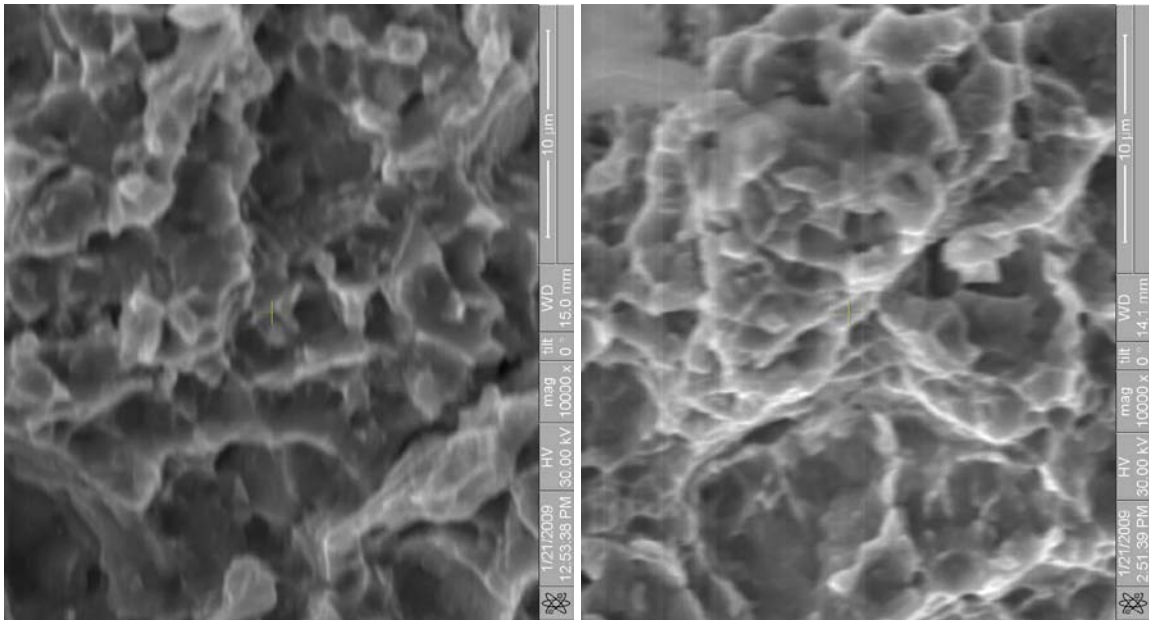
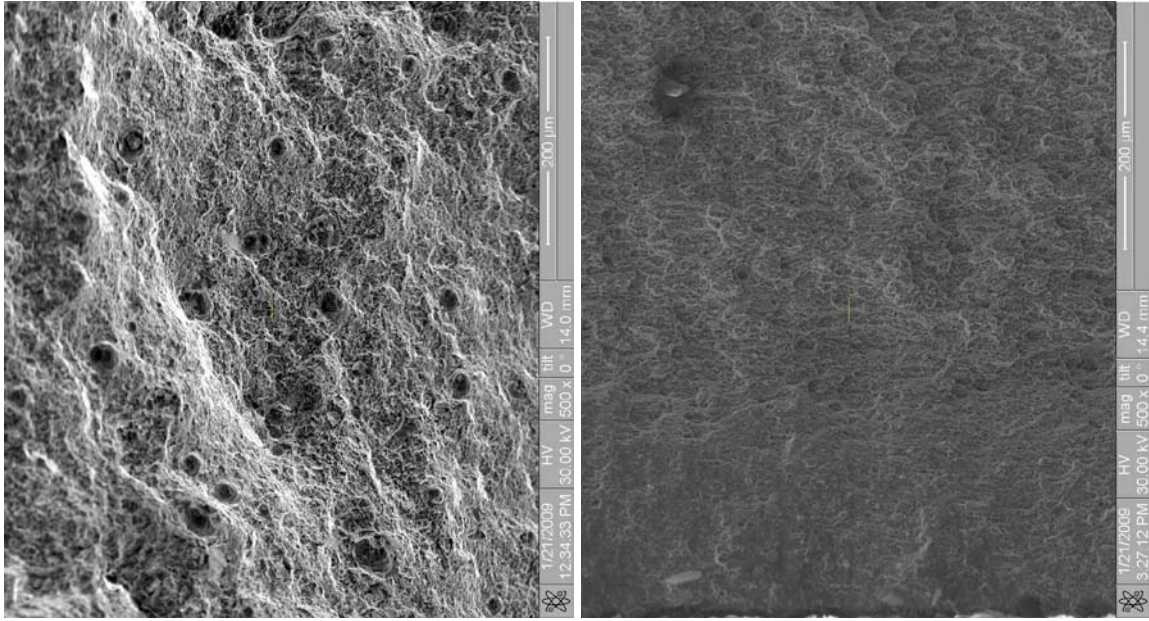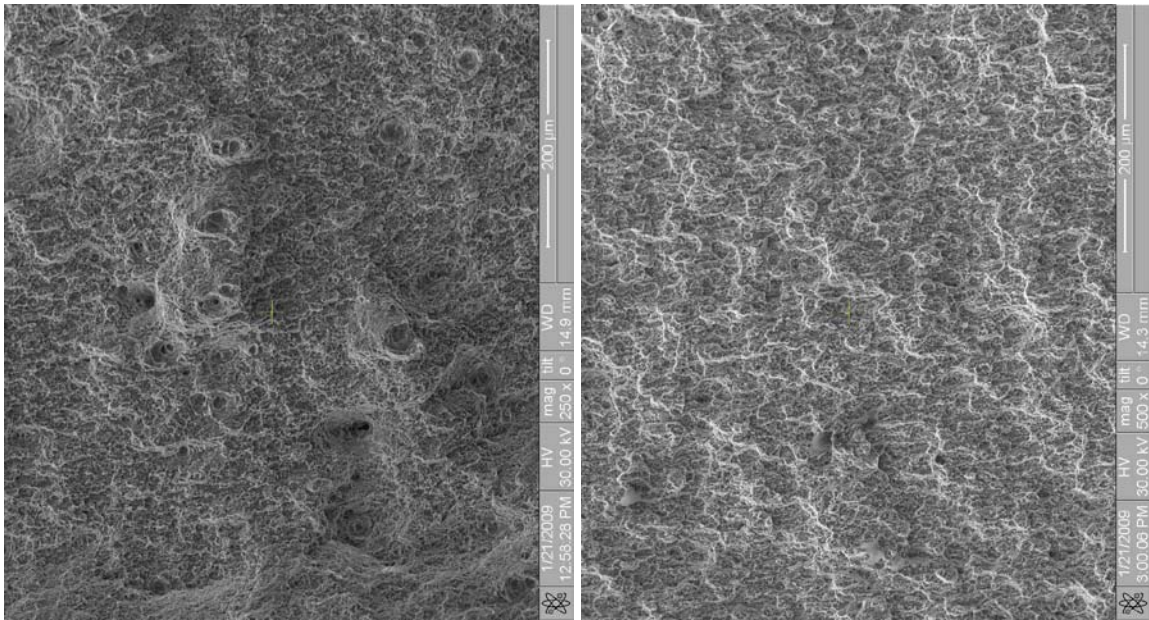a) Specimen 3, b) Specimen 7, c) Specimen 4, d) Specimen 6
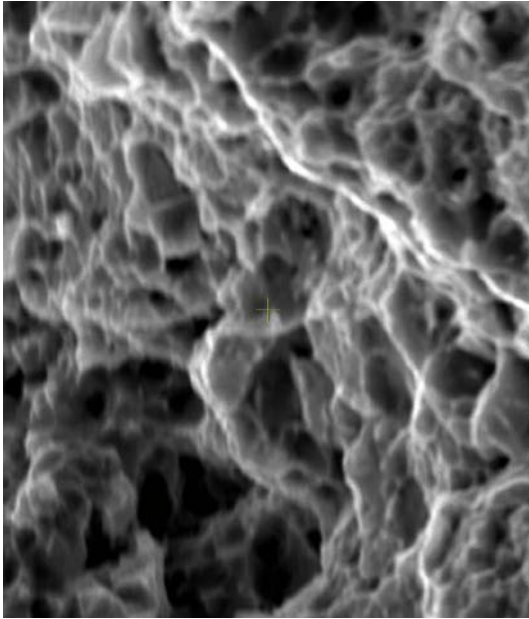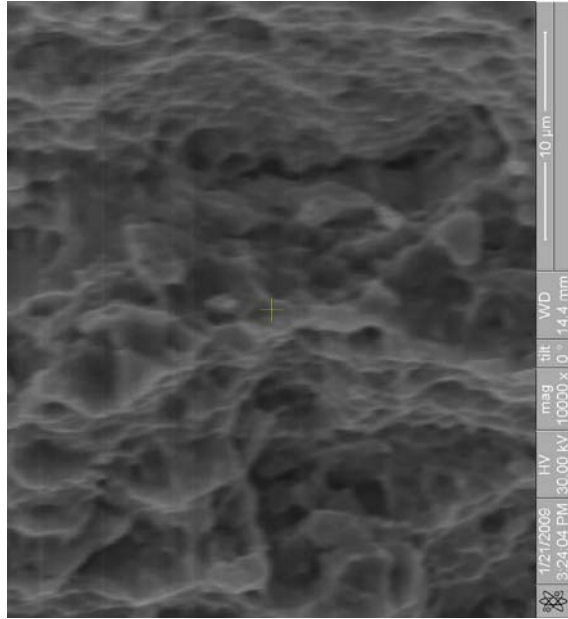
a)   b)
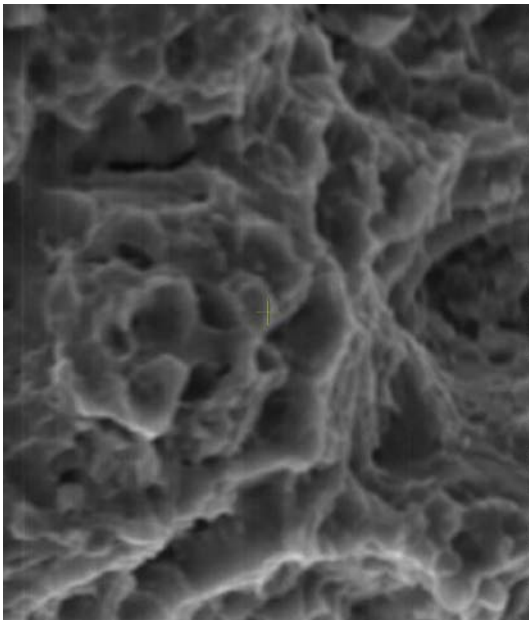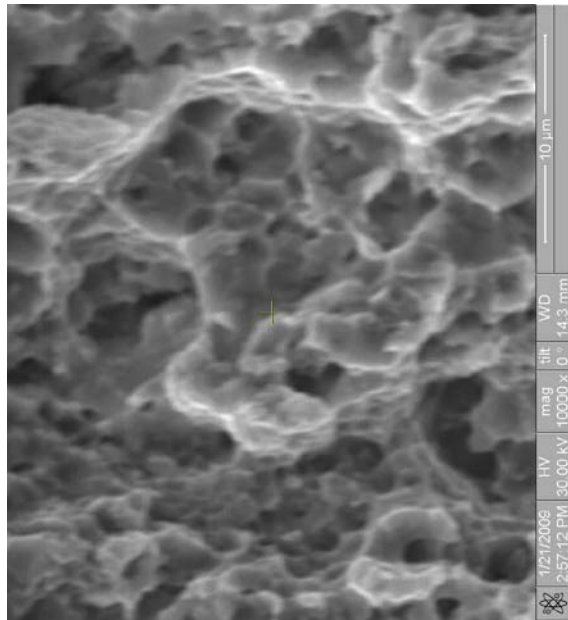
c)   d)

Figure B.43 – Zone IV 10,000x magnification

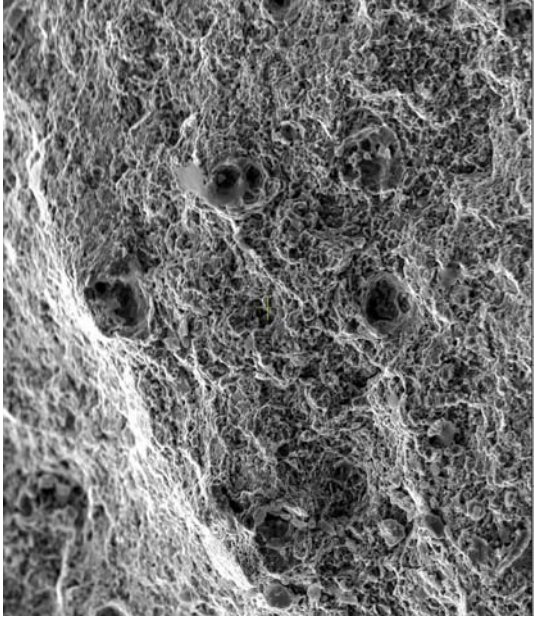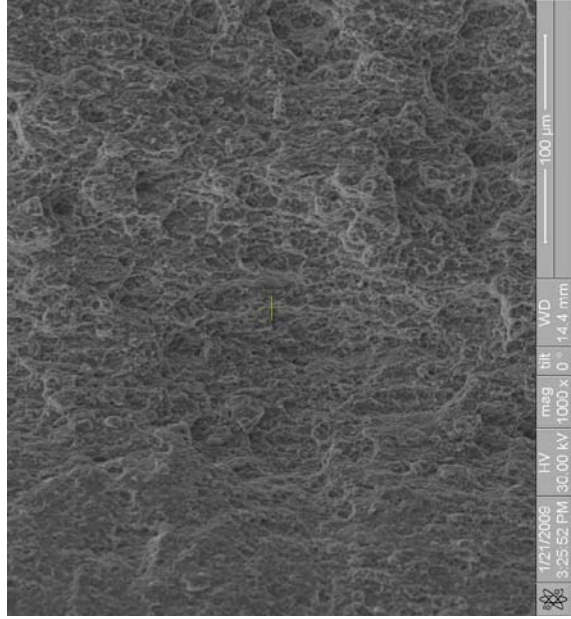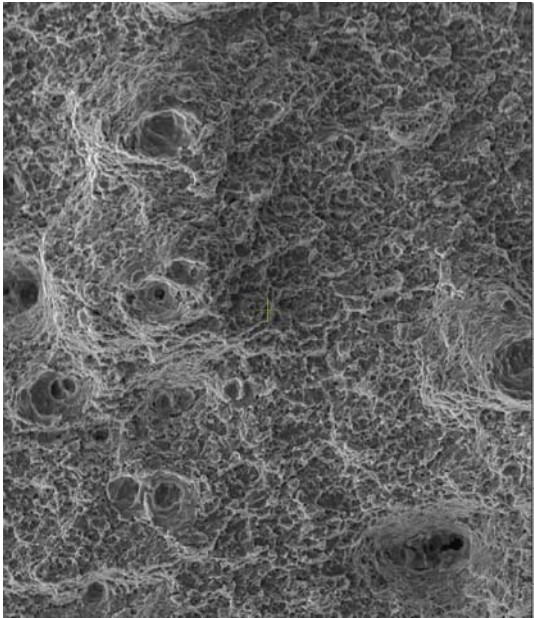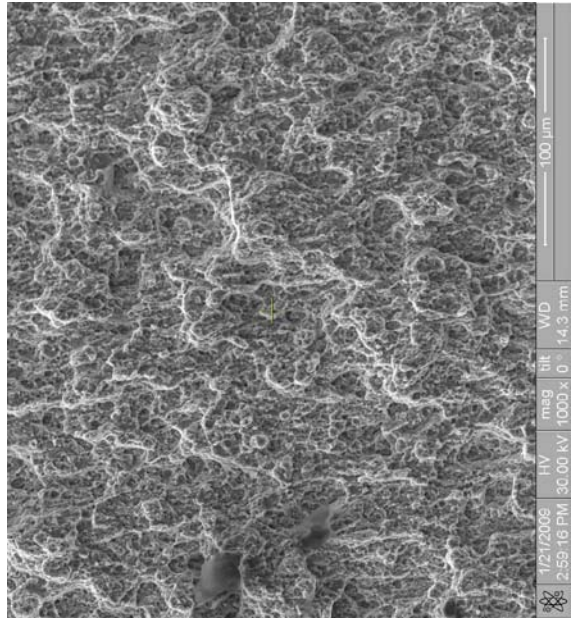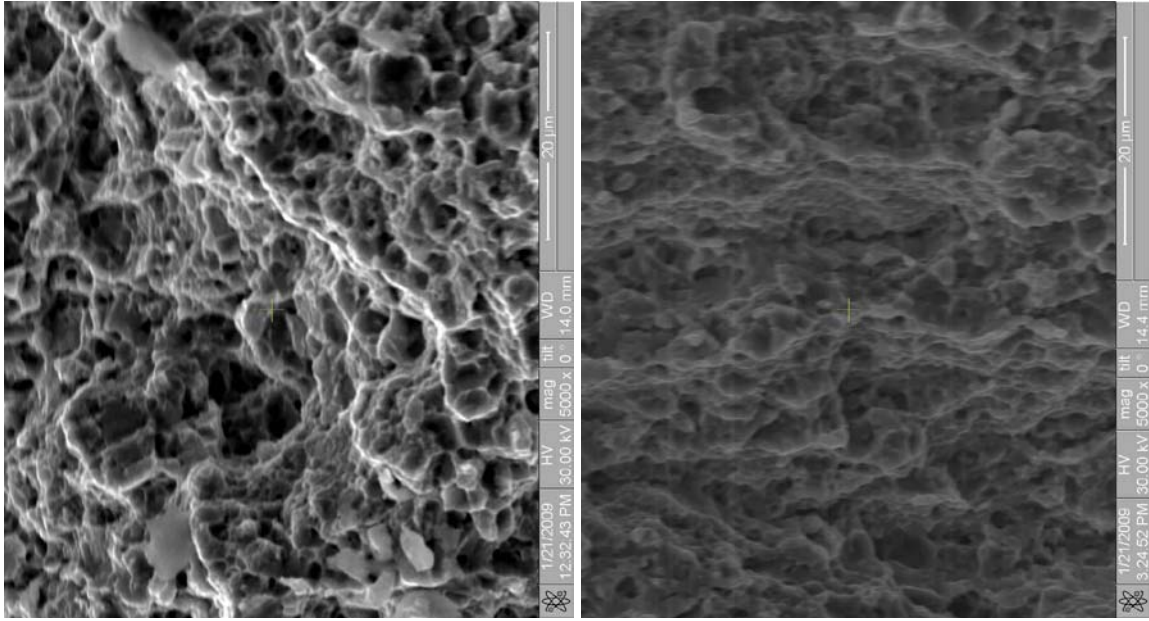a) Specimen 3, b) Specimen 7, c) Specimen 4, d) Specimen 6
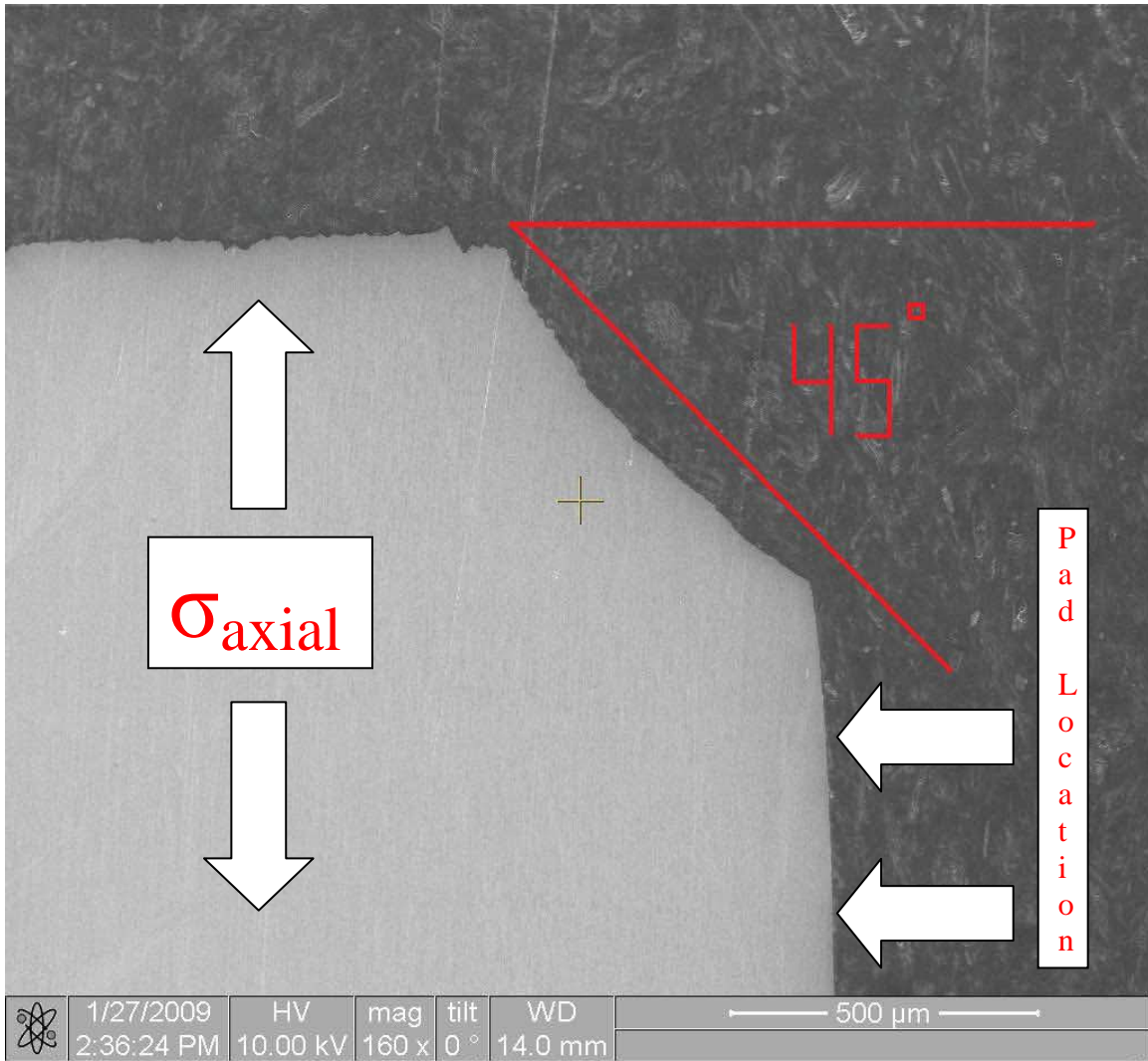
Figure B.44 – Specimen 2, crack initiation angle

Appendix C. Determination of Young's Modulus

The Young's Modulus of IN-100 has been previously determined by Mahdi [12]. Mahdi calculated this material property as 103.15 GPa at room temperature. This study will determine the Young's Modulus of IN-100 at 600°C in order to properly characterize this material property at high temperature. In order to do so, a specimen will be subject to various applied stresses at 600 °C. The corresponding strains will be calculated using $\varepsilon = \dfrac{\Delta l}{l}$. It was desired to use a strain gauge or extensometer to calculate the strains, but this was not permitted due to space limitations in the experimental setup. The results are summarized in the plot below. The Young's Modulus was experimentally determined to be 122.22 GPa.
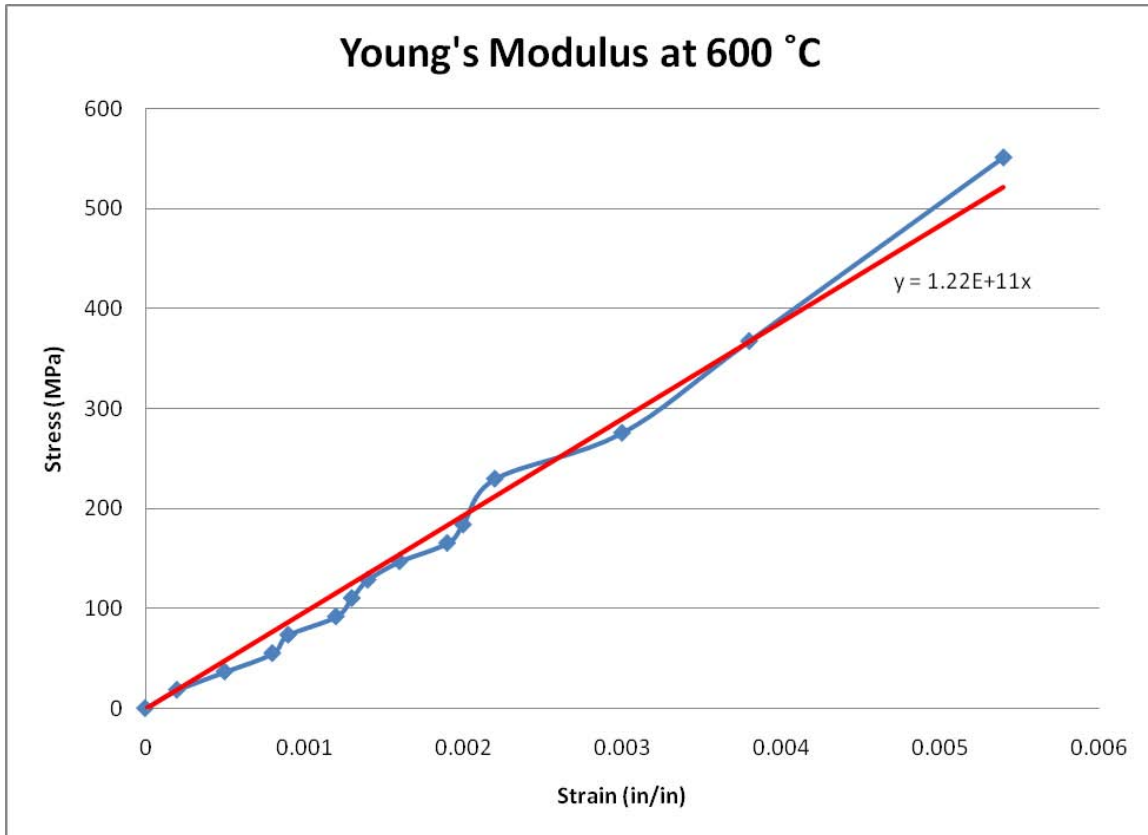
Figure C.1 – Young's Modulus

Appendix D. Determination of Coefficient of Friction

As previously noted, the studies on the effects of contact load showed that an important factor in the effect of contact load on fretting fatigue is the coefficient of friction between the fretting surfaces. It was observed that the coefficients of friction tended to stabilize at higher contact loads, causing coefficients of friction to also stabilize. It was at this point that no further effects were seen as contact loads were increased. This study calculated the coefficient of friction between two IN-100 surfaces at 600 ˚C and a contact load of 8006 N. To do this, the specimen was placed in the lower grip only and subjected to the full contact load of 8006 N. An increasing axial load was then applied to each specimen until gross slippage was observed. The coefficient of friction was then calculated using $f = \dfrac{(Q/2)}{P}$ where Q is 1799 lbf (8006 N) and P is the load where gross slippage occurs. The coefficient of friction was calculated two times, using both annealed and un-annealed specimens, and found to be an average of 0.356.

Table D.1 – Summary of Coefficients of Friction

Trial	Type	Q (lbf)	P (lbf)	f
1	Annealed	1799	2500	0.3598
2	Un-annealed	1799	2550	0.3527

Bibliography

[1] D. A. Hills, D. Nowell and J. J. O'Connor, "On the mechanics of fretting fatigue," *Wear,* vol. 125, pp. 129-146, 7. 1988.

[2] D. Koshal, *Manufacturing Engineer's Reference Book.* Oxford, England: Butterworth-Heinemann Ltd, 1993.

[3] M. J. Donachie and S. J. Donachie, *Handbook of Materials and Selection.* New York, New York: John Wiley & Sons, Inc., 2002.

[4] S. Adibnazari and D. W. Hoeppner, "Study of fretting fatigue crack nucleation in 7075-T6 aluminum alloy," *Wear,* vol. 159, pp. 257-264, 12/1. 1992.

[5] C. D. Lykins, "An investigation of Fretting Fatigue Crack Initiation Behavior of the Titanium alloy Ti-6Al-4V," 2004.

[6] A. R. Kallmeyer, A. Krgo and P. Kurath, "Evaluation of multiaxial fatigue life prediction methodologies for Ti-6Al-4V," *J Eng Mater Technol Trans ASME,* vol. 124, pp. 229-237, 2002.

[7] S. A. NAMJOSHI, S. MALL, V. K. JAIN and O. JIN, "Fretting fatigue crack initiation mechanism in Ti–6Al–4V," *Fatigue & Fracture of Engineering Materials & Structures,* vol. 25, pp. 955-964, 10. 2002.

[8] H. I. Yuksel, "Effects of Shot-Peening on High Cycle Fretting Fatigue Behavior of Ti-6Al-4V," March 2002. 2002.

[9] S. Mall, S. A. Namjoshi and W. J. Porter, "Effects of microstructure on fretting fatigue crack initiation behavior of Ti-6Al-4V," *Materials Science and Engineering A,* vol. 383, pp. 334-340, 10/15. 2004.

[10] M.P Szolwinski, J.F. Matlik and T.N. Farris, "Effects of HCF loading on fretting fatigue crack nucleation," International Journal of Fatigue, vol. 21, pp. 671-677, 1999.

[11] J. Ownby, "The effect of elevated temperature on the fretting fatigue behavior of nickel alloy IN-100," April 2008. 2008.

[12] E. Madhi, "Fretting Fatigue Behavior of Nickel Alloy IN-100," March 2006. 2006.

[13] E. Saladin, "The Effect of Microstructure on Fretting Fatigue Behavior of Nickel Alloy IN-100," March 2007. 2007.

[14] R. S. Magaziner, "Examination of Contact Width on Fretting Fatigue," March 2002. 2002.

[15] D. Nowell and D. A. Hills, "Crack initiation criteria in fretting fatigue," *Wear,* vol. 136, pp. 329-343, 3. 1990.

[16] P. T. Rajeev, H. Murthy and T. N. Farris, "Load History Effects on Fretting Contacts of Isotropic Materials," *J. Eng. Gas Turbines Power,* vol. 126, pp. 385-390, April 2004. 2004.

[17] A. Sackfield, A. Mugadu and D. A. Hills, "The influence of an edge radius on the local stress field at the edge of a complete fretting contact," *International Journal of Solids and Structures,* vol. 39, pp. 4407-4420, 8. 2002.

[18] H. Murthy, D. B. Garcia, J. F. Matlik and T. N. Farris, "Fretting fatigue of single crystal/polycrystalline nickel subjected to blade/disk contact loading," *Acta Astronautica,* vol. 57, pp. 1-9, 7. 2005.

[19] A. Shyam and W. W. Milligan, "Effects of deformation behavior on fatigue fracture surface morphology in a nickel-base superalloy," *Acta Materialia,* vol. 52, pp. 1503-1513, 4/5. 2004.

[20] A. Shyam and W. W. Milligan, "A model for slip irreversibility, and its effect on the fatigue crack propagation threshold in a nickel-base superalloy," *Acta Materialia,* vol. 53, pp. 835-844, 2. 2005.

[21] J. S. Wan and Z. F. Yue, "A low-cycle fatigue life model of nickel-based single crystal superalloys under multiaxial stress state," *Materials Science and Engineering A,* vol. 392, pp. 145-149, 2/15. 2005.

[22] H. Murthy, G. Gao and T. N. Farris, "Fretting fatigue of single crystal nickel at 600 °C," *Tribology International,* vol. 39, pp. 1227-1240, 10. 2006.

[23] N. Kawagoishi, Q. Chen and H. Nisitani, "Fatigue strength of Inconel 718 at elevated temperatures," *Fatigue & Fracture of Engineering Materials & Structures,* vol. 23, pp. 209-16, 03. 2000.

[24] J. F. Matlik and T. N. Farris, "Fretting of single crystal/polycrystalline nickel contacts at elevated frequency and temperature," in *; 6th AIAA Non-Deterministic Approaches Forum; 5th AIAA Gossamer Spacecraft Forum,* 2004, pp. 451-460.

[25] S. Albinali, "Effects of Temperature and Shot-Peening Intensity on Fretting Fatigue Behavior of Titanium Alloy Ti-6Al-4V," March 2005. 2005.

[26] J. Kohout, "Temperature dependence of stress-lifetime fatigue curves," *Fatigue & Fracture of Engineering Materials & Structures,* vol. 23, pp. 969-77, 12. 2000.

[27] D. A. Hills and D. Nowell, *Mechanics of Fretting Fatigue.* ,1st ed.Dordrecht, The Netherlands: Kluwer Academic Publishers, 1994,

[28] L. J. Fellows, D. Nowell and D. A. Hills, "Contact stresses in a moderately thin strip (with particular reference to fretting experiments)," *Wear,* vol. 185, pp. 235-238, 6. 1995.

[29] K. Chan and Y. Lee, ""Ruiz Program"," 1998.

[30] G. Venkataraman, Y. Chung, Y. Nakasone and T. Mura, "Free energy formulation of fatigue crack initiation along persistent slip bands: calculation of S-N curves and crack depths," *Acta Metallurgica Et Materialia,* vol. 38, pp. 31-41. 1990.

[31] J.G. Antonopoulos, L.M. Brown and A.T. Winter, "Vacancy dipoles in fatigued Copper," *Philosophical Magazine*, vol. 34, pp. 549. 1976.

[32] M. P. Szolwinski and T. N. Farris, "Mechanics of fretting fatigue crack formation," *Wear,* vol. 198, pp. 93-107, 10. 1996.

[33] L. J. Fellows, D. Nowell and D. A. Hills, "On the initiation of fretting fatigue cracks," *Wear,* vol. 205, pp. 120-129, 4. 1997.

[34] T. Hattori and T. Watanabe, "Fretting fatigue strength estimation considering the fretting wear process," *Tribology International*, vol. 39, pp. 1100-1105. 2006.

[35] T. Hattori and M. Nakamura, "Initiation and propagation behavior of fretting fatigue cracks," in *Proceedings of the 1997 3rd International Conference on Contact Mechanics,* 1997, pp. 183-192.

[36] K. Iyer and S. Mall, "Effects of cyclic frequency and contact pressure on fretting fatigue under two-level block loading," *Fatigue & Fracture of Engineering Materials & Structures,* vol. 23, pp. 335-346, 04. 2000.

[37] K. Walker, "The effect of stress relaxation during crack propagation ad fatigue for 2024-Y3 and7075-T6 aluminum," in *Subcommittee E-9 Winter Meeting,* 1969,

[38] C. D. Lykins, S. Mall and V. Jain, "A shear stress-based parameter for fretting fatigue crack initiation," *Fatigue & Fracture of Engineering Materials & Structures,* vol. 24, pp. 461-473, 07. 2001.

[39] V. Sabelkin, S. A. Martinez, S. Mall, S. Sathish and M. P. Blodgett, "Effects of shot-peening intensity on fretting fatigue crack-initiation behaviour of Ti–6Al–4V," *Fatigue & Fracture of Engineering Materials & Structures,* vol. 28, pp. 321-332, 03. 2005.

[40] S. K. Sondhi, B. F. Dyson and M. McLean, "Tension–compression creep asymmetry in a turbine disc superalloy: roles of internal stress and thermal ageing," *Acta Materialia,* vol. 52, pp. 1761-1772, 4/19. 2004.

[41] M. M. Hamdy and R. B. Waterhouse, "The fretting fatigue behaviour of Ti-6Al-4V at temperatures up to 600 °C," *Wear,* vol. 56, pp. 1-8, 9. 1979.

[42] O. Jin, S. Mall and O. Sahan, "Fretting fatigue behavior of Ti–6Al–4V at elevated temperature," *International Journal of Fatigue,* vol. 27, pp. 395-401, 4. 2005.

[43] M. C. Gean and T. N. Farris, "Fretting fatigue testing of Ti-17 at elevated temperatures," in *47th AIAA/ASME/ASCE/AHS/ASC Structures, Structural Dynamics, and Materials Conference,* 2006,

[44] V. Brien and B. Décamps, "Low cycle fatigue of a nickel based superalloy at high temperature: deformation microstructures," *Materials Science and Engineering A,* vol. 316, pp. 18-31, 11/15. 2001.

[45] V. Brien, L. P. Kubin and B. Decamps, "Low-cycle fatigue of a nickel-based superalloy at high temperature: Simplified micromechanical modelling," *Philosophical Magazine A,* vol. 81, pp. 2285, 2001.

[46] A. Piard, D. Gamby, C. Carbou and J. Mendez, "A numerical simulation of creep–fatigue crack growth in nickel-base superalloys," *Engineering Fracture Mechanics,* vol. 71, pp. 2299-2317, 11. 2004.

[47] P. J. Golden, "Development of a Dovetail Fretting Fatigue Fixture for Turbine Engine Materials," 2007.

[48] M. M. Hamdy and R. B. Waterhouse, "The fretting-fatigue behavior of a nickel based alloy (Inconel 718) at elevated temperatures," *Wear,* pp. 351-355, 1979.

[49] M.M. Hamdy and R.B. Waterhouse, "The fretting wear of Ti-6Al-4V and aged Inconel 718 at elevated temperature," *Wear*, vol. 71, pp. 237-248. 1981.

[50] H. Murthy and T. N. Farris, "Elevated temperature fretting of turbine materials subjected to engine type-loading," in *44th AIAA/ASME/ASCE/AHS/ASC Structures, Structural Dynamics, and Materials Conference,* 2003, pp. 1148-1158.

[51] H. Murthy, T. N. Farris and M. Okane, "Investigation of fretting characteristics of turbine materials at higher temperatures," in *43rd Structures, Structural Dynamics and Materials Conference,* 2002, pp. 2577-2585.

[52] R.B. Waterhouse, "Fretting at high temperatures," *Tribology International*, vol. 14, pp. 203-207, 1981.

[53] R. Sadeler, "Influence of contact pressure on fretting fatigue behavior of AA 2014 alloy with dissimilar mating material," *Fatigue and Fract. Engng. Mater. Struct.*, vol. 29, pp. 1039-1044, 2006.

[54] S. Adibnazari and D.W. Hoeppner, "A fretting fatigue normal pressure threshold concept," *Wear*, vol. 160, pp. 33-35, 1993.

[55] K. Nakazawa, N. Maruyama and T. Hanawa, "Effect of contact pressure on fretting fatigue of austenitic stainless steel," *Tribology International*, vol. 36, pp. 79-85, 2003.

[56] N.K. Naidu and S. Raman, "Effect of contact pressure on fretting fatigue behavior of Al-Mg-Si alloy AA 6061," *International Journal of Fatigue*, vol. 27, pp. 283-291, 2005.

[57] W.D. Callister, Jr., *Materials Science and Engineering, An Introduction*. New York, New York: John Wiley & Sons, Inc., 2007.

Vita

1st Lieutenant Alfred Traylor graduated from South River High School in Edgewater, Maryland in May 2001. He entered undergraduate studies at the United States Naval Academy where he graduated with a Bachelors of Science degree in Physics with a minor in French. At the Naval Academy, he was a member of Sigma Pi Sigma physics honor society. Upon graduation, he cross-commissioned into the United States Air Force as a 2ndLieutenant.

His first assignment was at Wright-Patterson Air Force Base, Ohio as a physicist at the National Air & Space Intelligence Center. Here he served as an infra-red intelligence analyst and as an operations and maintenance program manager for spaced-based intelligence assets. In March 2007, he entered the Graduate School of Engineering & Management, Air Force Institute of Technology. Here he was inducted into Sigma Gamma Tau, the National Honor Society for Aerospace Engineering. Upon graduation, he will be assigned to the Air Force Research Laboratory's Materials & Manufacturing Directorate at Tyndall Air Force Base, Florida.

.

REPORT DOCUMENTATION PAGE				Form Approved OMB No. 074-0188

The public reporting burden for this collection of information is estimated to average 1 hour per response, including the time for reviewing instructions, searching existing data sources, gathering and maintaining the data needed, and completing and reviewing the collection of information. Send comments regarding this burden estimate or any other aspect of the collection of information, including suggestions for reducing this burden to Department of Defense, Washington Headquarters Services, Directorate for Information Operations and Reports (0704-0188), 1215 Jefferson Davis Highway, Suite 1204, Arlington, VA 22202-4302. Respondents should be aware that notwithstanding any other provision of law, no person shall be subject to an penalty for failing to comply with a collection of information if it does not display a currently valid OMB control number. **PLEASE DO NOT RETURN YOUR FORM TO THE ABOVE ADDRESS.**

1. REPORT DATE (DD-MM-YYYY) 26-03-2009	2. REPORT TYPE Master's Thesis	3. DATES COVERED (From – To) 20 March 2007 – 26 March 2009

4. TITLE AND SUBTITLE	5a. CONTRACT NUMBER
Effects of Contact Load on the Fretting Fatigue Behavior of IN-100 at Elevated Temperature	5b. GRANT NUMBER
	5c. PROGRAM ELEMENT NUMBER
6. AUTHOR(S)	5d. PROJECT NUMBER
Traylor II, Alfred, G., 1st Lieutenant, USAF	5e. TASK NUMBER
	5f. WORK UNIT NUMBER

7. PERFORMING ORGANIZATION NAMES(S) AND ADDRESS(S) Air Force Institute of Technology Graduate School of Engineering and Management (AFIT/EN) 2950 Hobson Way WPAFB OH 45433-7765	8. PERFORMING ORGANIZATION REPORT NUMBER AFIT/GMS/ENY/09-M04
9. SPONSORING/MONITORING AGENCY NAME(S) AND ADDRESS(ES) This Space Intentionally Left Blank	10. SPONSOR/MONITOR'S ACRONYM(S)
	11. SPONSOR/MONITOR'S REPORT NUMBER(S)

12. DISTRIBUTION/AVAILABILITY STATEMENT
APPROVED FOR PUBLIC RELEASE; DISTRIBUTION UNLIMITED.

13. SUPPLEMENTARY NOTES

14. ABSTRACT
This thesis studied the effects of contact load of 8006 N on the fretting fatigue behavior of IN-100 at an elevated temperature of 600 ˚C. First, S-N curves were created for a range of applied axial stresses at an identical stress ratio of 0.03 at 8006 N. A condition of partial slip condition necessary to fretting fatigue was verified by generating hysteresis loops, plotting shear force against axial stress. The half-contact width and the crack initiation location were determined for all of the fretting specimens using optical and scanning electron microscopes. The contact widths were consistent with expected analytical values and the crack initiation location was at the trailing edge of contact for all fretting specimens at a mean angle of 45˚. This study compared the fretting results at higher contact load (8006 N) to similar results from previous studies of IN-100 at lower contact load (4003 N) with an identical microstructure at an elevated temperature of 600˚C as well as to previous room temperature testing. It was found that fretting fatigue at higher contact load drastically reduces the cycles to failure compared to fretting fatigue at elevated temperature with a lesser contact load. While the higher temperature environment allowed a longer initiation and crack propagation time, this was quickly negated by the increase in the contact load. The development of glaze oxide films and temperature induced softening or plasticity were both found to act as crack closure mechanisms in another nickel-based superalloy, IN-718, when fatigued in the high temperature environment. This glaze oxide reduces the coefficient of friction between contact surfaces, an important factor in fretting fatigue, and is also observed to be present in high temperature studies of IN-100. It was also found that a difference exists between the fretting fatigue lives of specimens that were annealed when compared to those specimens that were not annealed. These findings were slightly different than other studies at increased contact load which used various alloys of aluminum and steels.

15. SUBJECT TERMS
Fretting Fatigue, Nickel-based Superalloys, IN-100, Contact Load

16. SECURITY CLASSIFICATION OF:			17. LIMITATION OF ABSTRACT	18. NUMBER OF PAGES	19a. NAME OF RESPONSIBLE PERSON Dr. Shankar Mall
REPORT U	ABSTRACT U	c. THIS PAGE U	UU	173	19b. TELEPHONE NUMBER (Include area code) (937) 255-3636, ext 4587; e-mail: shankar.mall@afit.edu